IRON-RELATED IMMUNE CELL FUNCTION IN SEPSIS

by

Taylor Victoria Thorburn

Submitted in partial fulfillment of the requirements
for the degree of Master of Science

at

Dalhousie University
Halifax, Nova Scotia
July 2018

DEDICATION PAGE

I dedicate this thesis to my beloved aunt, Jane.

TABLE OF CONTENTS

LIST OF TABLES

LIST OF FIGURES

ABSTRACT

Sepsis is characterized by a dysregulated immune response to infection, causing damage to tissues and organs. As part of the inflammatory response, iron catalyzes the generation of reactive oxygen species (ROS). In the present study, we sought to evaluate the anti-inflammatory effects of a novel iron chelator, DIBI, *in vitro* and in two murine models of sepsis *in vivo*. *In vitro,* we found that DIBI reduced ROS production by innate immune cells. *In vivo* immune cell activation was evaluated in the intestinal microcirculation using intravital microscopy. In both sepsis models, anti-inflammatory actions were observed upon administration of DIBI, whereby DIBI reduced sepsis-induced leukocyte adhesion and preserved capillary perfusion in the intestinal microvasculature. Therefore, our data presents a promising role for iron chelation as a therapeutic option for sepsis, in which DIBI reduces ROS generation by binding iron.

LIST OF ABBREVIATIONS USED

ACCP	American College of Chest Physicians
BMDM	Bone marrow derived macrophage
CACF	Carleton Animal Care Facility
CASP	Colon ascendens stent peritonitis
CBC	Complete blood count
CFU	Colony forming units
CLP	Cecal ligation and puncture
CLR	C-type lectin receptors
CM-DCFDA	Chloromethyl 2',7'-dichlorodihydrofluorescein diacetate
CRP	C-reactive protein
DAMP	Danger-associated molecular pattern
DFO	Deferoxamine
DFP	Deferiprone
DFX	Deferasirox
DMEM	Dulbecco's modified eagle media
DMSO	Dimethyl sulfoxide
DMT1	Divalent metal transporter 1
EDTA	Ethylene diamine tetraacetic acid
ETC	Electron transport chain
FACS	Fluorescence-activated cell sorting
FBS	Fetal bovine serum
FCD	Functional capillary density

FITC-BSA	Fluorescein isothiocyanate-bovine serum albumin
GSH	Glutathione
HES	Hydroxyethyl starch
H_2O_2	Hydrogen peroxide
HOCl	Hypochlorous acid
HRP	Horseradish peroxidase
ICAM-1	Intercellular adhesion molecule 1
ICU	Intensive care unit
IEC	Intestinal epithelial cell
IFN-γ	Interferon-gamma
IL-1β	Interleukin-1 beta
IL-2	Interleukin-2
IL-4	Interleukin-4
IL-6	Interleukin-6
IL-10	Interleukin-10
IL-12p70	Interleukin-12
IL-17A	Interleukin-17A
iNOS	Inducible nitric oxide synthase
i.p.	Intraperitoneal
i.v.	Intravenous
IVM	Intravital microscopy
JAM	Junctional adhesion molecule
LEI	Leukocyte endothelial interaction

LFA-1	Lymphocyte function-associated antigen 1
LPS	Lipopolysaccharide
LTA	Lipoteichoic acid
Mac-1	Macrophage-1 antigen
MAHMP	3-hydroxy-1-(β-methacrylamidoethyl)-2-methyl-4(1 H)-pyridinone
MAP	Mean arterial pressure
M-CSF	Macrophage colony-stimulating factor
MODS	Multiple organ dysfunction syndrome
NaCl	Sodium chloride
NLR	NOD-like receptors
NO	Nitric oxide
NOS	Nitric oxide synthase
Nox	NADPH oxidase complex
n.s.	Not significant
O_2^-	Superoxide radical
OH	Hydroxyl radical
$ONOO^-$	Peroxynitrite
PAMP	Pathogen associated molecular pattern
PBS	Phosphate buffered saline
PECAM-1	Platelet endothelial cell adhesion molecule-1
PLF	Peritoneal lavage fluid
PRR	Pattern recognition receptor
PSGL-1	P-selectin Glycoprotein Ligand 1

PVP	Polyvinylpyrrolidone
qSOFA	Quick sepsis-related organ failure assessment
RNS	Reactive nitrogen species
ROS	Reactive oxygen species
RPMI	Roswell Park Memorial Institute
SCCM	Society of Critical Care Medicine
s.c.	Subcutaneous
SF	Serum free
SIRS	Systemic inflammatory response syndrome
SOD	Superoxide dismutase
SOFA	Sepsis-related organ failure assessment
TLR	Toll-like receptors
TNF-α	Tumour necrosis factor alpha
TSA	Tryptic soy agar
US	United States
V1	Submucosal collecting venules
V3	Post capillary venules
VCAM-1	Vascular cell adhesion molecule-1
VLA-4	Very Late Antigen-4

ACKNOWLEDGEMENTS

I started this degree with only a basic understanding of immunology and a drive to learn more. After two challenging, but rewarding years, I am leaving with not just a better understanding of immunology, but with a greater appreciation for what I can achieve with a little (or a lot) of hard work. I could not have made the progress I have without the support and guidance of my supervisors, Dr. Christian Lehmann and Dr. David Hoskin. Their enthusiasm and coaching kept me motivated during hard times, and created a supportive environment where I felt comfortable reaching out whenever I had questions. I would also like to thank Dr. Juan Zhou for her patience when teaching me the surgical skills required for my project, as well as providing me with insight for various aspects of my research.

I would also like to thank my committee members Dr. Andrew Stadnyk and Dr. Bruce Holbein for their expertise and guidance throughout my degree.

Research can be difficult at times but having such friendly and supportive lab mates makes a world of a difference. Whether it be helping run an experiment, or just being there to talk to during a stressful day, I would like to thank all members of the Lehmann lab for helping me through my masters. Additional thanks to Maral and Ian who were there for me from the beginning. I would also like to thank everyone in the Hoskin lab. Even though I wasn't around as much, you all always made me feel welcome. Special thanks to Javad, Wasu, and Alicia for guiding me through experiments and always being there if I needed help. I am truly lucky to have been a part of both these wonderful labs. I don't know how I could have gotten through my degree without all of the help and support over these past years.

Of course, I also have to thank all my friends and family. This was the most difficult chapter of my life thus far and I couldn't have done it without your continual reassurance. Your love and support means so much to me.

Finally, I would like to thank all the mice that were sacrificed during this work. They are easily overlooked as just a tool required for research, but every life, whether big or small has value.

CHAPTER 1: INTRODUCTION

1.1 Sepsis

1.1.1 Sepsis Definition, Epidemiology and Outcomes

Sepsis and septic shock are a major public health concern with worldwide importance. It is a leading cause of mortality in surgical intensive care units worldwide, exceeding deaths from HIV, breast cancer or stroke (1). In the United States (US), there are more than 1.5 million cases of sepsis and 250,000 deaths annually (2). In Canada, recent epidemiology studies showed 1 in 18 deaths involved sepsis and that sepsis contributes to more than half of all deaths from infectious illnesses (3). In the US, sepsis is the most significant cost of hospitalization, draining more than 24 billion dollars (6.2%) of total US hospital costs per year (4,5). These costs are associated with weeks or months-long stays in intensive care units (ICUs) and poor long-term outcomes of sepsis survivors, who frequently require hospital re-admission (6,7).

Hippocrates first coined the term "sepsis" in medical literature, deriving the term from Greek roots meaning decay or decomposition (8). Hippocrates described sepsis as a disease that arose from harmful products derived from the colon, which continued to be used by other famous philosophers such as Galen and Aristotle (8,9). Based on many years of clinical research and experimental evidence we can define sepsis with more confidence and scientific foundations. In 1992, experts from the American College of Chest Physicians (ACCP) and the Society of Critical Care Medicine (SCCM) developed the first definition of sepsis, stating that sepsis resulted from a host's systemic inflammatory response syndrome (SIRS) to infection (10). This definition focused solely

on the hyper-inflammatory response of sepsis, with standards for diagnosing sepsis requiring that a patient meets 2 or more SIRS criteria (11):

- Temperature of ≥ 38°C or ≤36°C
- Heart rate ≥90 beats/min
- Respiratory rate ≥20/min of $PaCO_2$ ≤32mmHg
- White blood cell count >12000/mm^3 or <4000mm^3 or >10% immature forms

As part of this consensus, sepsis complicated by organ dysfunction was termed severe sepsis, progressing to septic shock if hypotension persisted despite fluid resuscitation (12,13). In 2001, these diagnostic criteria were revisited and expanded on; however, nothing was significantly altered due to a lack of knowledge and supporting evidence.

Between 2014 and 2015, a task force made up of 19 experts in critical care, and sepsis-related illnesses sought to update sepsis definitions and diagnostic criteria to reflect advancements made in understanding the pathophysiology of sepsis. In 2015, the new definition of sepsis (Sepsis-3) defined sepsis as "life-threatening organ dysfunction caused by a dysregulated host response to infection" (12). This definition recognized the pro- and anti-inflammatory responses present during the course of sepsis, emphasized the non-homeostatic host response to infection and distinguished sepsis from uncomplicated infection. The term severe sepsis was discarded and septic shock was redefined as "a subset of sepsis in which underlying circulatory and cellular metabolism abnormalities are profound enough to substantially increase mortality" (12).

The Sepsis-3 definition incorporated new clinical diagnostic criteria that addressed the concept of the dysregulated host response and largely replaced the SIRS scoring system. There are various scoring systems to assess organ dysfunction; however, the sepsis-related organ failure assessment (SOFA) score was suggested to be predominant diagnostic measurement for sepsis as part of the Sepsis-3 definition (14). This scoring system assesses abnormalities in respiratory, cardiovascular, nervous, renal, circulatory and digestive systems, with a higher score predicting a higher chance of mortality (15). The scoring system ranges from 0-4. Patients without any known pre-existing organ dysfunction have a baseline score of 0. A change in a baseline SOFA score of ≥ 2 represents organ dysfunction, which in combination with a suspected or documented infection meets diagnostic criteria for sepsis. Septic shock is identified in patients presenting with sepsis criteria in combination with the need for vasopressor therapy to elevate mean arterial pressure (MAP) ≥ 65mmHg and hyperlactatemia >2 mmol/L despite volume resuscitation (12).

In a retrospective cohort study by Kumar *et al.* (16), it was determined that the probability of death from septic shock increases by 8% every hour antibiotic treatment is delayed after initial determination of hypotension. Due to the need for timely recognition of sepsis, a simplified measurement for bed-side screening was developed and termed quick SOFA (qSOFA) (17). The score ranges from 0-3 and the presence of ≥2 qSOFA points with infection indicate a patient is more likely to have sepsis than an uncomplicated infection (12). The qSOFA score was developed to be a quick prompt used outside the intensive care unit (ICU) without the need for blood tests, to quickly assess the likelihood of sepsis.

Sepsis is not a specific illness, but rather a complex clinical syndrome. At present, no validated diagnostic test, x-ray, or clinical evaluation can conclude that a patient has sepsis. Since the implementation of the first consensus sepsis definition in 1992, incidence rates of sepsis have increased; however, the probability of death from sepsis has declined (18). These findings are likely due to effective implementation of sepsis recognition techniques such as SOFA or qSOFA and timely administration of antibiotics, oxygen, and fluid resuscitation (12,16,19). In spite of a declining trend in sepsis mortality, it is still high, ranging from 20-50% and up to 80% for septic shock (1). Even if a patient survives the initial sepsis insult, their quality of life will remain affected. Sepsis survivors are frequently disabled by cognitive dysfunction, neuropathies, immunological dysfunction and other complications (6). The occurrence of sepsis and sepsis-related deaths is projected to increase due to an aging population and a rise in antibiotic resistance (10). Continuing advancements in therapeutic options and recognition techniques is crucial for early diagnosis and improving outcomes in sepsis survivors.

1.1.2 General Sepsis Pathophysiology

In the past decades, considerable advancements have been made in our understanding of the pathophysiology of sepsis. The Sepsis-3 definition now acknowledges that the clinical manifestations of sepsis are due to complex changes in immune modulating mechanisms, contrasting the previous theory that suggested sepsis resulted from an uncontrolled hyper-inflammatory response.

During acute infection, the initial appropriate response of the host's innate immune system is activated. The pathophysiologic cascade of sepsis develops when this response is amplified and dysregulated (20,21). The insult is most commonly bacterial, but there have been increasing incidences of viral, fungal and parasitic causes of sepsis (1). Sepsis can originate from multiple potential sites. However, respiratory infections are the most common cause of sepsis, making up about half of all sepsis cases, followed by genitourinary and abdominal infections, which are other major causes of sepsis (22,23). Although the etiology of disease may differ, the clinical aspects of sepsis are often similar, regardless of the source of infection. This is likely due to the fact that it is the dysregulated immune response that cause sepsis pathologies (23).

During infection, the homeostasis of the immune response is regulated by opposing, yet complementary pro- and anti-inflammatory responses (24). In sepsis, this balance is dysregulated, resulting in two major states of the immune system. Most frequently, sepsis is characterized by initial hyper-inflammation, i.e. hyper-activation of mechanisms aimed at eliminating invading pathogens. Although this is a physiological reaction to infection in the body, in sepsis, there is an exaggerated systemic release of pro-inflammatory mediators resulting in a 'cytokine storm' (9,22,25). This may lead to cardiovascular dysfunction, hypotension, and tissue hypoperfusion, which if persistent lead to organ dysfunction, failure and death (9,20,26). In the course of sepsis, frequently the immune response shifts to a hypo-inflammatory state (so-called immunoparalysis) with increased production of anti-inflammatory cytokines such as IL-10 (26). During local infection, this phase is used to diminish inflammation and allow for tissue repair (22). However, in sepsis, immune cells are exhausted during this state (23). This leads to

an inability to neutralize pathogens and leaves the host vulnerable to secondary infections (22,26).

Beyond the complex changes occurring in the immune system, sepsis is further complicated by the heterogenous nature of the disease (27). Factors such as age, pre-existing immune status, comorbidities, and the type of infection can greatly influence the progression of disease and cause pathophysiologic variances among individuals (28). For instance, patients with pre-existing conditions like HIV, diabetes, and cancer already have an altered immune system and will be at a higher risk for developing severe sepsis, as well as present with a different sepsis profile than a previously healthy individual (3) (Figure 1). The case-fatality rate of sepsis was 55% greater in cancer patients than noncancer septic patients (29). Additionally, patients on immunosuppressive therapies for conditions such as arthritis, multiple sclerosis, and lupus, may completely bypass the hyper-inflammatory phase and go straight to the immunosuppressive phase.

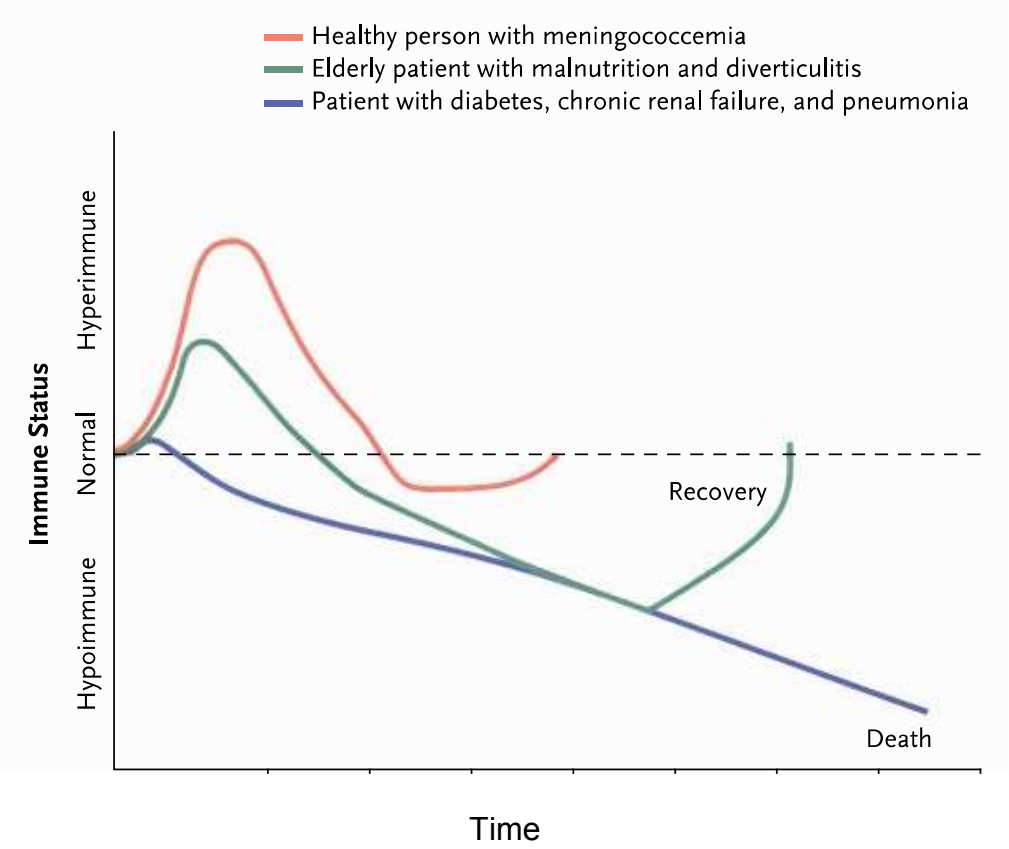

Figure 1. The heterogenous nature of temporal changes in the immune status of sepsis varying immune status'. Modified from Hotchkiss et al. (28)

1.1.3 Innate Immune Response in Sepsis

The scope of the research in this thesis focuses on the hyper-inflammatory state of sepsis, characterized by a dysregulated overwhelming response to infection. This state of sepsis mainly involves activation of the innate immune system, which can be readily mobilized within minutes of infection. Homeostasis of the innate immune response is maintained by opposing, yet complementary anti-and pro-inflammatory mediators produced by innate immune cells (24). The cells making up this system include monocytes, macrophages, dendritic cells, neutrophils, mast cells and natural killer cells.

The fast action of the innate immune system is due to quick recognition of pathogen-associated molecular patterns (PAMPs) on invading microbes by pattern recognition receptors (PRRs) on immune cells. Some PRRs include Toll-like receptors (TLRs), NOD-like receptors (NLRs) and C-type lectin receptors (CLRs) (30). Peptidoglycan and lipoteichoic acid (LTA) are common PAMPs of Gram-positive bacteria, but the endotoxin lipopolysaccharide (LPS), which makes up a component of Gram-negative bacteria, is one of the most well recognized and studied PAMP. Recognition of LPS by TLR4 results in phagocytosis of the invading pathogen and activation of the innate cell by the intracellular signaling cascade, NF-κB, which leads to the transcription of genes coding for cytokines including TNF-α, IL-1β, IL-6, IL-2 and IFN-γ (25). This cytokine storm causes an array of bodily responses including, but not limited to, enhanced phagocytic activity, leukocyte chemotaxis, activation of the coagulation system, microvasculature injury, and synthesis of acute phase proteins from the liver (25,31).

During sepsis, an overproduction of cytokines induces excessive inflammation and an overproduction of inflammatory mediators, such as reactive oxygen species (ROS). These inflammatory mediators are aimed at eliminating invading pathogens; however, they act indiscriminately and can start to destroy host tissues (32,33). The combined effects of diminished myocardial contractility and hypotension due to systemic vasodilation result in impaired tissue perfusion with consecutive multiple organ dysfunction syndrome (MODS) and finally multiorgan failure. (24). When tissues and cells die, they produce danger-associated molecular patterns (DAMPs), which further activate immune cells and continue the cascade of sepsis (23): recognition/phagocytosis of pathogens, production of cytokines and inflammatory mediators, activation of immune cells, and production of cytokines and inflammatory mediators.

1.1.4 Leukocyte Endothelial Interactions (LEIs) in Systemic Inflammation

1.1.4.1 Basic Mechanisms

During infection, leukocytes such as neutrophils, monocytes, basophils, eosinophils, dendritic cells and lymphocytes migrate from systemic circulation to the site of infection by chemotaxis. Neutrophils account for 40-70% of leukocytes circulating in human peripheral blood, representing an essential component of the first line of defense against invading microorganisms (23). The release of anti-microbial agents from neutrophil granules is crucial for destroying pathogens, but causes damage to the host's healthy tissues as well (34,35). Additionally, extravasation of neutrophils possibly results in damage to non-infected tissue, furthering inflammation. In sepsis, systemic

inflammation may lead to excessive and inappropriate activation of leukocytes, causing injury of non-infected tissues and furthering sepsis pathology (34).

The migration of leukocytes from the blood is a multistep series of adhesion and signaling events in both leukocytes and endothelial cells. An initial inflammatory stimulus triggers leukocyte margination in which the leukocyte is drawn out of the central blood stream toward the endothelial surface (Figure 2). Leukocyte margination initiates leukocyte-endothelial interactions by close mechanical contact with endothelial cells and begins leukocyte rolling (36). Selectins are upregulated on the surface of endothelial cells during inflammation and will begin to lightly tether leukocytes (37). This process is predominately mediated by P-selectins and E-selectins expressed on activated endothelial cells bound to the glycoprotein P-selectin Glycoprotein Ligand 1 (PSGL-1) on leukocytes (38). These repeated low-affinity interactions between leukocytes and endothelial cells cause the leukocytes to slow and roll along the vessel in preparation for the next step of the leukocyte activation cascade - firm adhesion (39).

Firm adhesion of leukocytes requires the low affinity integrins present on the leukocyte surface to undergo conformational changes to gain full adhesive functions (36). Chemokines from the inflammatory environment attract leukocytes (37). The interaction of these chemokines with leukocytes cause an intercellular signaling cascade, activating integrins to a highly affinitive state (37). In neutrophils, the β2 integrins lymphocyte function-associated antigen 1 (LFA-1) and macrophage-1 antigen (Mac-1) are expressed for firm adhesion by binding to the endothelial counter receptor intercellular adhesion molecule-1 (ICAM-1) (Figure 2). In contrast, lymphocytes and monocytes express the β1-integrin Very Late Antigen-4 (VLA-4), which is bound by vascular cell adhesion

molecule-1 (VCAM-1) on endothelial surfaces (40–42). Firm adhesion of leukocytes to the endothelial surface allows for the final step of leukocyte migration, leukocyte transmigration.

Upon firm adhesion of leukocytes to the endothelium, leukocytes migrate across the endothelial barrier through a paracellular or transcellular manner. The manner of transmigration can vary depending on the location in the body, but it is well accepted that leukocytes cross endothelial cells between cell borders (paracellular) (36,37). A wide variety of junctional molecules, such as platelet endothelial cell adhesion molecule-1 (PECAM-1) and the junctional adhesion molecules (JAMs) assist in paracellular leukocyte migration. However, the mechanism of leukocyte transmigration is not completely understood (36). Some observations suggest PECAM-1 guides leukocytes through the paracellular space by cell signaling (43). Studies have shown that inhibiting PECAM-1's binding domain by blocking antibodies impedes transmigration (36). Additionally, JAMs, such as JAM-C have been found to bind Mac-1 on neutrophils. Antibodies against JAM-C were found to block neutrophil transmigration through endothelial cells (44). Once leukocytes have migrated across endothelial barriers, they will move into a chemoattractant gradient toward the inflamed tissue (41).

1.1.4.2 LEI Effects on Microcirculation

The microcirculation is the circulation of blood within the microvasculature of organ tissues. Microcirculatory impairments represent a key event in sepsis pathophysiology causing tissue hypoperfusion and tissue hypoxia (45). Microcirculatory disturbances can arise due to underlying factors such as changes in blood viscosity, leukocyte activation, red blood cell aggregation and, edema externally compressing the

microvessels (46). Leukocyte activation leads to the release of antimicrobial agents, such as ROS and nitric oxide (NO), which can cause direct damage to the endothelial cells lining the microvasculature (47). Increased leukocyte transmigration to tissue can also enhance tissue inflammation and promote edema by endothelial damage, all of which contribute to microcirculatory disturbances (48). Several studies using various microcirculation imaging techniques reported impaired and dysregulated microcirculatory perfusion in patients with severe sepsis (49–51). These impairments included decreased vascular density, increased flow heterogeneity and a reduced proportion of perfused small vessels (50). A study by Sakr *et al.* (49) found that microcirculatory disturbances were more severe in sepsis nonsurvivors than survivors. Both groups presented similar microcirculatory measurements within 24 hours of sepsis; in survivors, capillary perfusion increased over time, but did not in those who did not survive the illness. Interestingly, in those who survived, microcirculatory disturbances failed to normalize to that of healthy subjects or ICU controls, suggesting endothelial alteration is still ongoing even after signs of inflammation have normalized. This could account for the ongoing complications sepsis survivors face.

1.1.4.3 LEI in the Intestine

Unlike most organs, the intestine is in constant contact with an abundance of environmental stimuli including food antigens, commensal microbiota and potentially dangerous pathogens. When functioning normally, an anatomical barrier of intestinal epithelial cells (IECs) allows physiologic movement of fluids and nutrients, but prevents the entry of potentially dangerous pathogens (52,53). As an additional defense mechanism, the intestine is equipped with an abundance of highly specialized cells to

defend against invaders. In the event of pathogen invasion, dendritic cells are likely among the first cells to act since they reside in high numbers directly below IECs. Their main role is to activate and mobilize innate immune defenses, which primarily involves assembling neutrophils and other leukocytes (54).

Disruptions in the intestinal mucosa barrier due to tissue ischemia is important in the pathogenesis of sepsis and may lead to the translocation of additional pathogens into the systemic circulation (24,55). Increased bacterial translocation across the intestinal barrier causes additional leukocyte activation, and generation of inflammatory mediators in the intestinal microcirculation. Pathogens derived from the gut can cause secondary infections, and further enhance the septic condition. For this reason, the intestinal microcirculation has been suggested to be the 'motor' of multiple organ failure due to its role in the progression of sepsis and is a crucial target in the early septic cascade (53,56). Therefore, in these studies the focus was on the intestinal microcirculation.

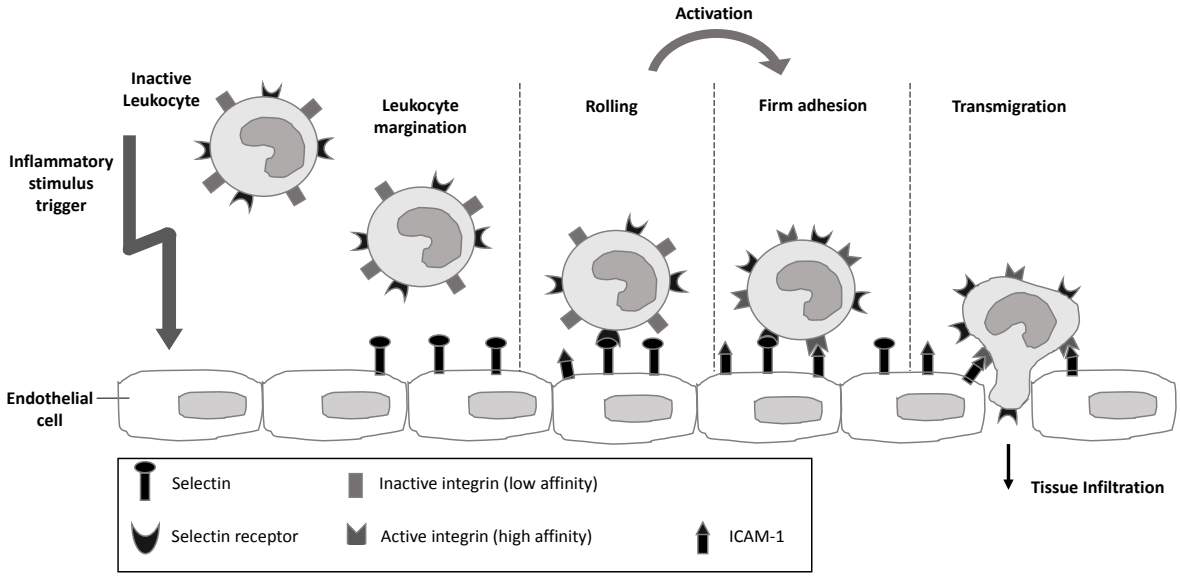

Figure 2. Leukocyte activation cascade. Leukocytes interact with endothelial cells by tethering to selectins and rolling along the endothelial layer. Firm adhesion is mediated by integrins binding to ICAM-1 on endothelial cells. Modified from Thorburn et al. (45)

1.1.5 Current Therapeutic Options

There are currently no specific anti-sepsis drugs on the market (57). Beyond antibiotic administration to kill invading pathogens and possible surgical intervention to remove infected tissue, therapeutic options generally consist of maintaining vital organ functions, including fluid resuscitation and mechanical ventilation (27). Since it was determined that it is the host's immune response attempting to fight the infection that may cause the fatal outcome, there have been a large repertoire of immune modulating drugs that have been tested experimentally to treat sepsis. However, so far none of these treatments have had significant improvements in the outcome of sepsis, likely related to the wrong timing of the drugs due to a lack of biomarkers to assess the condition of the patient (57,58).

Due to the dynamic nature of sepsis, accurate and timely assessment of the patients' immune status must be done for the success of anti-sepsis treatments. Currently, complete blood count (CBC) and C-reactive protein (CRP) remain the standard for assessing the immune status in the patient, but these tests lack sensitivity and specificity (59). Fluorescence-activated cell sorting (FACS) has recently been found useful in determining septic state by characterizing leukocyte phenotypes, activation, function and cytokine production in no more time than a obtaining a CBC measurement (60,61).

Continuing advancements in sepsis biomarkers and protocols to effectively determine the septic state of a patient are crucial for confident treatment of patients. However, at present, there is no evidence that these biomarkers or protocols will be ready in the near future and sepsis continues to affect millions each year. Nonetheless,

experimental approaches attempting to treat sepsis continue to be studied, including a potential therapeutic option discussed in this thesis by use of iron chelation.

1.2 Iron in Sepsis

1.2.1 Physiology of Iron

Iron is the fourth most common element on the planet and is essential to life. Its biological relevance comes from its ability to donate or accept electrons, thereby functioning as a cofactor in various biochemical reactions. In our bodies, iron is present in the ferric (III) and ferrous (II) state. We cannot produce iron, so it must be provided from our food. Iron absorption happens at the brush border of enterocytes in the duodenum and upper jejunum of the intestinal tract (62). Iron is transported into enterocytes by the divalent metal transporter 1 (DMT1) and can then either be used in cellular processes, bound to ferritin and stored, or transported out of the cell by the iron exporter, ferroportin (63,64). Once iron leaves the cell, it is transported bound to transferrin, an iron transporter protein. From this point, the fate of iron depends on the body's cellular needs, some of which include the synthesis of oxygen transport proteins, DNA synthesis, and hematopoiesis (64).

Due to the vital functions of iron, a balanced iron homeostasis is crucial in human physiology. Due to the redox potential of iron, it is a choice catalyst in many biological reactions, including harmful ones, such as free radical generation (65,66). Dysregulation of iron homeostasis is often associated with inflammatory and degenerative disorders (67). Therefore, iron levels are tightly regulated to maintain iron homeostasis.

Despite the potential toxic capacity of excessive iron, our bodies do not possess an iron excretion mechanism. Instead, the regulatory protein hepcidin is the main player in the coordinated response to reduce systemic iron levels (68,69). Hepcidin is synthesized by hepatocytes in the liver and acts as a negative regulator of iron absorption in response to high dietary iron, high iron stores, and during inflammation (70). Bioactive hepcidin binds to ferroportin on the cell surface, which results in ferroportin's internalization and degradation. In duodenal enterocytes, this causes iron retention and subsequently down-regulates dietary iron absorption (64,71). Interestingly, ferroportin also exists on the surface of immune cells, particularly macrophages. Although hepcidin is mainly produced in response to iron overload, it is also generated during inflammation, primarily by IL-6 signaling (72). In the same manner as enterocytes, hepcidin induction results in iron retention in immune cells, referred to as the hypoferremic response (66,67,73). Hepcidin-mediated iron retention in immune cells is thought to be an evolutionary adaptation to combat invading pathogens, which require iron as a vital nutrient (71). Restricting systemic iron levels may also reduce iron's participation in the generation of harmful free radicals. Therefore, the hypoferremic response may serve as a defense strategy and benefit the host by reducing microbial growth and decreasing iron's bioavailability for harmful reactions.

1.2.2 Irons Participation in the Generation of Reactive Oxygen Species (ROS)

1.2.2.1 ROS Definition and Composition

Reactive oxygen species (ROS) are chemically reactive species containing oxygen. The term ROS includes molecules with an unpaired electron (free radicals) and

strong oxidizing agents, such as hydrogen peroxide (H_2O_2) (33). ROS are highly reactive, short-lived, and react indiscriminately by extracting electrons from other molecules. The most common ROS species include superoxide radical (O_2^-), a precursor to many ROS species; H_2O_2, hydroxyl radical (OH), and hypochlorous acid (HOCl) (32,74). Closely related to ROS are reactive nitrogen species (RNS), the by-products of nitrogen reacting with other ROS species. Example of RNS include nitric oxide (NO) and peroxynitrite ($ONOO^-$), which is formed by NO reacting with superoxide anion (33).

Our understanding of ROS has come a long way since they were first discovered in biological systems in 1954 (75). ROS were first thought to be solely involved in pathological processes and aging due to their high reactivity, but throughout the years, the understanding that ROS only have deleterious effects has changed (74). It is now accepted that ROS play many roles in the body such as combating pathogens as part of the immune response, regulation of metabolic pathways, and acting as cell signaling molecules (74,76). Despite the uncovering of various supportive functions of ROS, they remain difficult to fully understand due to their short half-life and low stability (33,74).

1.2.2.2 Generation of ROS

In eukaryotic cells, about 90% of ROS are produced as by-products during mitochondrial electron transport (74). Electrons escaping the electron transport chain (ETC) will react with oxygen to form O_2^-, which can then spontaneously form H_2O_2 or OH (77). ROS produced by mitochondrial respiration are potentially dangerous; therefore, cells possess finely regulated antioxidant systems to limit levels of ROS. This involves superoxide dismutase (SOD) catalyzing the conversion of superoxide radicals to H_2O_2 and oxygen (33,76). The enzyme catalase further detoxifies H_2O_2 by converting it

to water and oxygen (76,78). There are a number of secondary antioxidants that also contribute to this defense system including vitamin C and E. However, the most important is glutathione (GSH), which has been found to neutralize NO (74,76). Generally, this antioxidant defense effectively eliminates the threat of ROS; however, small amounts of H_2O_2 sometime escape the defense system. If free iron is present as Fe(II), it will react with H_2O_2 to form hydroxyl radicals, which are the most potent and most highly reactive ROS species. The reaction between Fe(II) and H_2O_2 is known as the Fenton reaction (69). This reaction produces Fe(III), which cannot participate to form more hydroxyl radicals; however, if superoxide is present, Fe(III) can be converted back to Fe(II) by reaction with the superoxide radical. This cycle is known as the Haber-Weiss reaction (69). There are no known enzymatic systems to neutralize hydroxyl radicals so these radicals can go on to cause cell damage (74).

During microbial killing by phagocytic cells, ROS is produced by a process known as the 'respiratory burst'. The NADPH oxidase complex (Nox) increases cellular oxygen consumption to catalyze the production of superoxide radical and hydrogen peroxide (78,79). Components of Nox are dormant in resting cells and can assemble on either the plasma membrane of cells, or inside the phagosome, depending on the nature of the stimulus (80). When PRRs on phagocytes recognize pathogens or other markers of an inflammation, ROS are released into the inflammatory environment (79). By contrast, phagocytosis of bacteria cause assembly of Nox components on the phagosome and intracellular release of ROS to degrade internalized microbes (79). The activated Nox complex catalyzes the transfer of electrons to oxygen to form its primary product, superoxide anion; H_2O_2 is correspondingly generated as well (32,81). While superoxide

anion and H_2O_2 can be damaging on their own, participation in the iron-mediated Fenton and Haber Weiss reactions will give rise to hydroxyl radical, an exceedingly potent radical (79). Additionally, superoxide can form NO by nitric oxide synthase (NOS), subsequently producing peroxynitrite, a potent inducer of tissue damage (82). The respiratory burst is a powerful antimicrobial weapon and is an important defense mechanism against infectious agents. However, if these antimicrobial activities become uncontrolled and the body cannot counteract their toxic effects, oxidative stress may occur.

1.2.2.3 Oxidative Stress

Under physiologic states, the generation and detoxification of ROS are well balanced to maintain stable ROS levels. However, during certain instances this balance can be disrupted, resulting in oxidative stress. Oxidative stress can be an acute event, when for some reason, ROS levels sharply increase out of the controlled range (83). During acute events, some pathological consequences may arise, but through enhanced expression of antioxidant molecules, such as SOD, catalase, and GSH, enhanced ROS will be neutralized and return levels to a steady state (83). On the other hand, in some cases, such as sepsis, high ROS levels cannot be neutralized, causing a state of 'chronic oxidative stress' (84–86).

During oxidative stress, ROS act indiscriminately to cause tissue damage, mainly through induction of lipid peroxidation (82). The unpaired electrons of ROS, particularly from OH, will readily attack unsaturated fatty acids, such as those present on the cell membrane by capturing hydrogen molecules. This leaves an unpaired electron on the carbon molecule of fatty acids, which causes a chain-reaction of fatty acid fragmentation.

Since lipid peroxidation is a self-propagating chain-reaction, oxidation of only a few lipid molecules causes significant tissue damage (87). Lipid peroxidation results in a loss of membrane integrity and release of stress signals, which propagates inflammation, and continues the cycle of oxidative stress (32). Beyond lipid peroxidation, oxidative stress disrupts the normal redox state of cells causing mitochondrial dysfunction, DNA damage and disruptions in cell signaling.

1.2.3 Iron Chelation

Although essential to the body, in excess, iron can be toxic. Individuals suffering from iron-overload disorders, such as hemochromatosis or repeated blood transfusions, can accumulate iron in organs such as the heart and liver, leading to cellular damage due to iron catalyzing ROS-generating reactions (64). Additionally, these patients have an increased risk of infection possibly from iron-promoting microbial growth (88–91). Currently, iron-overload disorders are managed with chelation therapy, in which iron chelators are administered to remove excess iron from the body (71).

Iron chelators are small molecules that bind tightly to iron, neutralizing its ability to catalyze redox reactions. They can be produced synthetically or can be derived from biologically produced molecules, such as siderophores secreted by certain microorganisms (92). The goal of iron chelation in iron-overload disorders is to prevent iron-mediated injury to cells, as well as to possibly prevent microorganisms from accessing iron stores. Due to the damage observed by oxidative stress and the link between ROS generation and iron, removing excessive iron by iron chelation represents a potential therapeutic option in sepsis.

1.2.4 Clinically Used and Novel Iron Chelators

Currently there are 3 clinically approved iron chelators: deferoxamine (DFO), deferasirox (DFX), and deferiprone (DFP). Each of which have their advantages and disadvantages such as specificity/affinity for iron, route of administration, half-life, side effects, and cost (93,94). The studies in this thesis focused on the novel iron chelator, DIBI, produced by Chelation Partners Inc., a company based in Halifax, NS, Canada.

DIBI is a highly selective iron chelator comprised of a large polyvinylpyrrolidone (PVP) backbone with nine 3-hydroxy-1-(β-methacrylamidoethyl)-2-methyl-4(1 H)-pyridinone (MAHMP) residues (95). DIBI is non-toxic, bioavailable (i.p./i.v.), and binds iron in a 3:1 ratio, providing a compartmentalized sink for iron. Previous studies have found DIBI to be anti-inflammatory in combination with antibiotics in a poly-bacterial experimental murine sepsis model (96) and without antibiotics in a LPS-induced endotoxemia model (97). Additionally, in a study comparing the iron-chelating effects of DIBI and other clinically used iron chelators (DFO and DFP) on the growth *Candida albicans* and *Candida vini*, DIBI almost completely inhibited the growth of those fungi, while DFO and DFP minimally affected their growth (98).

1.3 Hypotheses

The general hypothesis of this project was that iron chelation during the acute hyper-inflammatory state of sepsis would reduce leukocyte recruitment, and preserve capillary blood flow, acting as an extension of the physiologic hypoferremic response that is activated during microbial invasion. Specifically, we hypothesized that by reducing the

bioavailability of iron, we would reduce its participation in Fenton and Haber-Weiss chemistry, thereby reducing the generation of ROS, which in turn would attenuate the dysregulated immune cell recruitment and other pathologies associated with oxidative stress. Additionally, we also hypothesized that iron chelation would attenuate bacterial growth in a murine poly-bacterial model of sepsis by reducing iron's bioavailability to microorganisms.

1.4 Study Objectives

The goal of this research project was to evaluate the systemic effects of iron chelation on immune cell recruitment and microcirculatory integrity in murine models of sepsis. As mentioned previously, disruptions in intestinal integrity represents a key step in the pathophysiologic cascade of sepsis, leading to the translocation of pathogens from the intestinal lumen into the systemic circulation, the development of secondary infections, and further exasperating sepsis pathologies. Measurements of leukocyte-endothelial interactions and capillary flow in the intestinal microvasculature can be used for determining the degree of inflammation with impairments indicating sepsis disease progression. Therefore, maintaining microcirculatory integrity is a therapeutic target in the early sepsis cascade. For this research project we chose to assess the intestinal microcirculatory integrity with two different experimental sepsis models in mice.

As a proof of concept, *in vitro* assays were used to determine DIBI's antioxidant functions on macrophages and neutrophils harvested from mice. These cells are both first responders during innate immune responses and are primary sources of ROS at the site of inflammation, thus making them ideal cell lines to study DIBI's antioxidant effects. The

LPS-induced endotoxemia model was used to assess DIBI's efficacy at reducing immune hyper-activation in the absence of bacteria. This model simulates a bacteremia state based on the presence of bacterial antigens from intravenous administration of the endotoxin LPS and causes a systemic pro-inflammatory immune response. For the second experimental sepsis model, we chose a clinically relevant model of poly-bacterial sepsis. The colon ascendens stent peritonitis (CASP) model simulates abdominal sepsis by surgical implantation of a stent into the intestine, causing the leakage of luminal contents into the peritoneal cavity. This model is more clinically relevant than the LPS model due to the presence of live pathogens and their inflammatory mediators. Due to the presence of live microorganisms in this model, we were also able to assess DIBI's anti-microbial effects.

CHAPTER 2: MATERIALS AND METHODS

2.1 Animals

Male C57BL/6 mice (6-8 weeks old; 20-30g) were purchased from Charles River Laboratories International Inc. (Saint-Constant, QC, Canada) and were used for *in vitro* assays, endotoxemia, and colon ascendens stent peritonitis (CASP). Animals were housed in ventilated cage racks and allowed to acclimatize for one week following arrival in the Carleton Animal Care Facility (CACF) of the Faculty of Medicine at Dalhousie University, Halifax, NS, Canada. Animals were kept on a standard 12-hour light/dark cycle and were provided a standard diet of rodent chow and water *ad libitum.* All experimental procedures were preformed following the guidelines and standards outlined by the Canadian Council on Animal Care and were approved by the University Committee on Laboratory Animals at Dalhousie University, under protocol No. 16-051.

2.2 *In vitro Experiments*

2.2.1 Immune Cell Isolation and Culture

Male C57BL/6 mice were sacrificed by cervical dislocation for collection of bone marrow from femurs and tibias and subsequent isolation of bone marrow derived macrophages (BMDMs) or neutrophils.

2.2.1.1 Mouse Macrophage Isolation

Bone marrow was flushed using a 26-G x 3/8 needle and 30ml Luer-Lok syringe filled with sterile 1xPBS. Clumps of bone marrow were broken up using a 18-G x 1 needle to create a single cell suspension. Cell suspensions were centrifuged at 350 x g for 5 min. The supernatant was discarded and cells were re-suspended in 0.6% NaCl to lyse red blood cells, followed exactly 20 sec by the addition of equal parts 1.6% NaCl, and finally equal parts sterile PBS to return cells to an isotonic solution. Cells were then centrifuged at 350 x g for 5 min, counted and plated out into 6-well plates with $1x10^6$ cells/well .

BMDMs were placed in humidified 5% CO_2 incubator maintained at 37°C where they differentiated over 7 days. They were cultured in RPMI 1640 (Roswell Park Memorial Institute 1640; Sigma-Aldrich, Oakville, ON, Canada) media supplemented with 10% FBS (Fetal bovine serum; Invitrogen, Oakville, ON, Canada) and 15% L929-conditioned DMEM (Dulbecco's Modified Eagle medium; Sigma-Aldrich, Oakville, ON, Canada) as a source of macrophage colony-stimulating factor (M-CSF). After 3 days of culture, cells were provided with fresh BMDM medium. After 6 days of culture, old media and non-adherent cells were removed and fresh BMDM media was added. On day 7, cells were ready to use in experiments.

2.2.1.2 Mouse Neutrophil Isolation

Bone marrow was flushed using a 26-G x 3/8 needle and 30ml Luer-Lok syringe filled with neutrophil medium, which consisted of 1XPBS containing 1 μM EDTA (Ethylene diamine tetraacetic acid; Anachemia, Radnor, PA, USA) and 2% FBS. Clumps of bone marrow were broken up using a 18-G x 1 needle to create a single cell suspension. Cell suspensions were centrifuged at 300 x g for 10 min, supernatants were

discarded and cells were re-suspended in neutrophil media. Neutrophils were then isolated from single cell suspensions of bone marrow by negative selection using the EasySep™ Mouse Neutrophil Enrichment Kit and EasySep™ magnet (Stemcell Technologies, Vancouver, BC, Canada) following the manufacturer's instructions. Isolated neutrophils were centrifuged, suspended in neutrophil medium, and used immediately for experiments. The EasySep murine isolation protocol routinely yields cell suspensions that are >85% pure and viable when sorted by FACS, according to manufacturer's information manual.

2.2.2 DCFDA Assay

Intracellular measurement of oxidative stress was achieved using chloromethyl 2',7'-dichlorodihydrofluorescein diacetate (CM-H_2DCFDA; Life Technologies, Oregon, USA). CM-DCFDA is light and air sensitive; therefore, it was prepared fresh each time and all work was done in the dark. Additionally, medium was prepared without phenol red and serum to prevent interferences with the channel and prevent false positive results from esterases reacting with the DCFDA compound, respectively. An initial 5000μM stock was prepared in DMSO (Dimethyl sulfoxide; Sigma-Aldrich, Oakville, ON, Canada) and working concentrations were prepared in pre-warmed medium that was free of serum and phenol red. For every treatment group, a negative control (non-CM-DCFDA stained) was added. For all experiments, fluorescence data was acquired for $1x10^4$ cell counts per sample using a FACS Calibur flow cytometer with BD CellQuest™ software (version 3.3, BD Biosciences, Mississauga, ON). FCS Express Version 3 was used to analyze the data (De Novo software, Los Angeles, CA, USA).

2.2.2.1 BMDMs

Bone marrow derived macrophages were harvested and seeded in 12 well plates with BMDM media supplemented with 10% FBS at a concentration of $5x10^5$ cells/ml and left overnight to adhere to plates. The next day, media was removed and wells were washed with 1 mL pre-warmed 1XPBS. A 10μM concentration of CM-DCFDA was prepared using warm serum free (SF), phenol red free RPMI 1640 medium and added to all positive controls, while media without CM-DCFDA was added to negative controls. Cells were left to incubate for 1 hour in the dark. CM-DCFDA stain was removed and cells were washed with 1XPBS. Treatments were added to cells in warm, phenol red-free RPMI 1640 medium supplemented with 1% FBS and left to incubate for 24 hours. After the desired treatment time, media was removed from wells and added to FACS tubes. Cells were removed from wells by adding 1 ml 10mM EDTA and incubating at 37°C for 4 minutes. Cells were collected by pipetting and added to corresponding FACS tube. Cells were centrifuged at 350 x g for 5 minutes, supernatants were removed and cells were re-suspended in 350 μl 1XPBS.

2.2.2.2 Neutrophils

Neutrophils were prepared for the DCFDA assay immediately after isolation. Cells were counted and suspended in warm, phenol red and serum free RPMI. For each treatment, $5x10^5$ cells were added to FACS tubes. A 5 μM concentration of CM-DCFDA was prepared using warm SF, phenol red free RPMI and added to all positive controls, while media without CM-DCFDA was added to negative controls. Cells were left to incubate for 30 minutes in the dark. Cells were topped up with 1 ml warm SF, phenol red

free RPMI and centrifuged at 300 x g for 10 minutes to remove stain. The supernatants were then discarded and 1 ml warm, phenol red-free RPMI supplemented with 1% FBS was added to cells, along with treatments, which were left to incubate for 2 hours. After desired treatment time, cells were centrifuged at 300 x g for 10 minutes, supernatants were discarded and cells were re-suspended in 350 µl PBS.

2.2.3 Amplex Red Assay

The Amplex red assay was used to detect hydrogen peroxide (H_2O_2) released from neutrophils. This assay uses the Amplex Red reagent (10-acetyl-3,7-dihydroxyphenoxazine; Invitrogen, California, USA) in combination with horseradish peroxidase (HRP) to detect H_2O_2 activity. Cells were added to a 96-well flat bottom plate in triplicate at a density of $1x10^6$ in 100 µl in phenol red free RPMI supplemented with 5% FBS. Treatments were added and left to incubate for 2 hours. H_2O_2 was used as a positive control (100 µM). A master mix containing Amplex red reagent and HRP was made in phenol red free RPMI supplemented with 5% FBS. Each well received 100 µl of the master mix for a final concentration per well of 25µM Amplex Red and 0.005 U/ml HRP. Plates were put in the incubator at 37°C in a humidified 5% CO_2 incubator and absorbance was measured at 570 nm using ELx800 UV universal microplate reader (BioTek Instruments, Winooski, VT, USA), Digiread Software (Biochrom, Cambridge, UK).

2.2.4 Griess Assay

The Griess assay was used to detect stable nitrite ion in solution as a means of measuring nitric oxide produced by neutrophils. Cells were first suspended to a concentration of $5x10^5$ cells/ml in phenol red free RPMI supplemented with 5% FBS. Cell suspensions were added to FACS tubes along with treatments and left to incubate for 2 hours. A standard curve was made with sodium nitrate purchased from Sigma Aldrich. The standard curve concentrations of sodium nitrate and cell supernatants were then added to a 96 well plate with an equal volume of Griess reagent. Plates were incubated in the dark at room temperature for 10 minutes. Absorbance values were obtained at 570 nm using ELx800 UV universal microplate reader (BioTek Instruments, Winooski, VT), Digiread Software, and SOFTmax PRO software (version 4.3; Molecular Devices Corp., Sunnyvale, CA, USA).

2.2.5 Chemokinesis Assay

The chemokinesis assay was used to assess the coordinated movement of a cell population. BMDMs were harvested and prepared in a cell suspension of 250,000 cells/ml. Using sterile tweezers, culture inserts (Ibidi, Martinsried, Germany) were obtained and placed into wells of a 6 well plate (2 inserts per well). Tweezers were used to press inserts down and ensure they were firmly adhered to plastic to prevent leaks. The 6 well plate was flipped upside down and the inserts were outlined using a small tipped permanent marker. Flipping the plate upside down ensured all inserts were firmly adhered to plate. Each well of inserts received 100µl of cell suspension (25,000 cells per well) and left overnight. Old media was removed from wells and treatments were added in 100µl media to each well and left to incubate for 24h. After 24h, the culture inserts were

carefully removed with sterile tweezers and treatments were added to well of 6-well plate in 2 ml media. Using an inverted microscope (Nikon Eclipse TS100-F) and image capturing device (Nikon Digital sight DS-L2), the cell-free gaps were located for each insert using the pre-traced areas as a guide. Pictures were taken of carefully selected areas of gaps with well-defined borders. Additional pictures were taken at 24h and 48h, ensuring pictures were taken at the same spot each time. Imaging software (ImageJ; National Institute of Health, USA) was used to assess the speed of gap closure for all treatment groups.

2.3 *In vivo*

2.3.1 Experimental Endotoxemia Model

2.3.1.1 Anesthesia

Mice were weighed prior to anesthesia using a commercially available weighing scale. Induction of anesthesia was accomplished by an intraperitoneal (i.p.) injection of sodium pentobarbital (90 mg/kg, 54 mg/ml; Ceva Sainte Animale, Montreal, QC, Canada) at a 50% dilution with 0.9% NaCl. Depth of anesthesia was assessed by the animals' response to toe pinch every 15 minutes during the procedure. Supplemental doses of sodium pentobarbital at a 10% dilution were delivered intravenously (i.v.) when needed. Oxygen was provided to animals if breathing became irregular.

2.3.1.2 Surgical Procedures

After mice were fully anesthetized they were placed on a heating pad in a supine position. A rectal thermometer was inserted to measure and maintain body temperature at

37°C±0.5°C (TCAT-2LV Controller; Physitemp Instruments Inc. New Jersey, USA). Temperature was recorded every 15 minutes during the experiment. The abdomen and anterior-lateral neck area were shaved and disinfected using isopropyl alcohol swabs. The mouse was taped in the preferred position and their tongues were pulled to the side using forceps to allow for a more consistent flow of oxygen. This also allowed for easy access if a buildup of mucous and/or saliva were to occur and needed to be extracted to prevent obstruction of the trachea. During the surgery, the animals breathed room air, but oxygen was provided if breathing became irregular.

Using scissors, a small, shallow incision was made on the right side of the neck, followed by blunt dissection of the surrounding tissues using curved haemostats until the jugular vein was completely cleared of connective tissue, fat and muscle. For cannulation of the right jugular vein, an approximate 5-7mm exposed region was needed. Once the vein was successfully exposed, fine tip forceps were placed underneath the vein to receive a piece of black silk thread, which was repeated to obtain 2 pieces of thread. At the superior end of the vessel, the thread was used to tie off the vessel using a surgical knot. At the inferior end of the vessel the thread was used to tie a loose knot. Using micro-dissecting scissors, a small incision was made at the superior end of the vessel just below the surgical knot. Using fine tip forceps, a catheter was placed approximately 1 cm into the vessel through the incision site. The catheter was made prior to experiment by placing non-radiopaque polyethylene tubing (PE10, Clay Adams, Sparks, MD, USA) over a 30-gauge needle and securing it with waterproof glue. Before securing the catheter in place, the catheter was tested for any obstructions or leakages by flushing a small amount of saline and observing that no saline leaked out. The catheter was then secured

by tightening the inferior knot using a triple knot, and tying an additional double knot over the superior end of the vessel and catheter tube. Successful cannulation of the jugular vein allowed for i.v. administration of endotoxins, treatment drugs, fluorochromes, anesthetics and saline.

2.3.1.3 Experimental Timeline

The experimental timeline of endotoxemia protocol begins at induction of anesthesia of the animal (Figure 3). After cannulation of the right jugular vein, endotoxemia was induced by i.v. administration of lipopolysaccharide from *Escherichia coli* (LPS (5 mg/kg); Sigma-Aldrich, Oakville, ON, Canada). LPS (5 mg/kg, 1mg/ml) was dissolved in sterile saline (0.9% sodium chloride) and was administered i.v. as a short-time infusion (over 5 minutes), representing time 0 in the experimental timeline. The rational for the timing and dosage of LPS was based on successful induction of endotoxemia in previous experiments (99). All i.v. administrations were followed by flushing a small amount of saline to ensure all the compound was infused. Treatment compounds (or saline) were given i.v. 15 minutes following LPS challenge. Endotoxemia was carried out for 2 hours before IVM. During that time, the temperature and depth of anesthesia was continuously monitored every 15 minutes. Additional sodium pentobarbital (9 mg/kg) was administered if depth of anesthesia was insufficient. Fifteen minutes prior to IVM, fluorochromes were administered i.v. and laparotomy was performed. Upon completion of IVM, whole blood and samples of the small intestine were collected for further analysis.

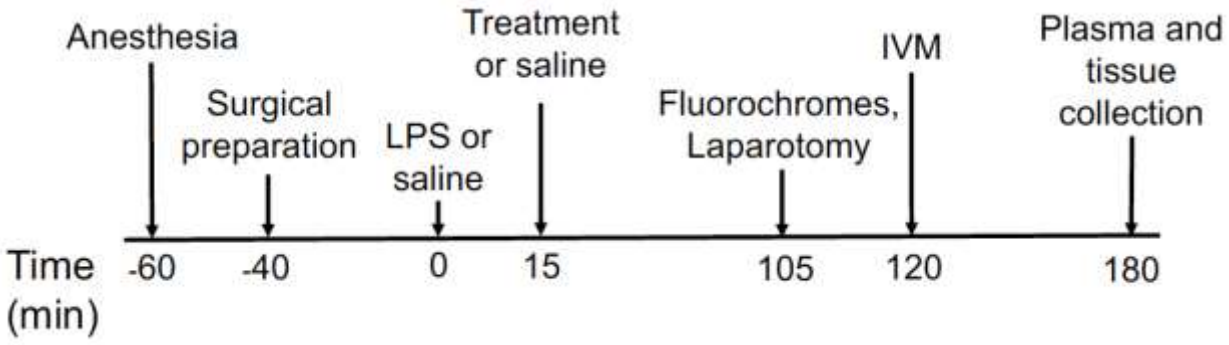

Figure 3. Experimental timeline of endotoxemia model.

2.3.1.4 Experimental Groups

A total of 6 experimental groups were tested with the endotoxemia model with 5-7 animals per group (Table 1). Group 1 (CNT) represented a healthy control group, group 2 (LPS) represented the endotoxin challenge group in which endotoxemia was induced by i.v. administration of LPS (5mg/kg) without treatment.

The remainder of the groups represented endotoxin challenge with treatments administered 15 minutes after LPS challenge. Group 3 (LPS+DIBI 10) received LPS (5 mg/kg) as well as DIBI (10 mg/kg). Group 4 (LPS+DIBI 5) received LPS (5 mg/kg) as well as DIBI (5 mg/kg). Group 5 (LPS+DIBI 2.5) received LPS (5 mg/kg) as well as DIBI (2.5 mg/kg). Group 6 (LPS+PVP) received LPS (5 mg/kg) as well as PVP (polyvinylpyrrolidone; the polymer backbone of DIBI; 10 mg/kg).

Table 1. Experimental groups for endotoxemia experiments.

Model	**Groups**	**Intervention**
Endotoxemia	Control	Saline
Endotoxemia	LPS	LPS (5mg/kg)
Endotoxemia	LPS+DIBI 10	LPS (5mg/kg) & DIBI (10mg/kg)
Endotoxemia	LPS+DIBI 5	LPS (5mg/kg) & DIBI (5mg/kg)
Endotoxemia	LPS+DIBI 2.5	LPS (5mg/kg) & DIBI (2.5mg/kg)
Endotoxemia	LPS+PVP	LPS (5mg/kg) & PVP (10mg/kg)

2.3.2 Colon Ascendens Stent Peritonitis (CASP)

2.3.2.1 Anesthesia

Anesthesia was induced by placing animals in a closed environment with a consistent flow of 4% isoflurane gas and an oxygen flow rate at 1.8L/hour until mice were sufficiently anesthetized, which was determined by an absent reaction to the toe pinch test. Depth of anesthesia was maintained by securing a cone over the nose of the mouse and providing a continuous flow of 1-2% isoflurane at an oxygen flow rate of 1.5L/hour. Buprenorphine (0.1 mg/kg, 0.03 mg/ml) was delivered subcutaneously (s.c.) before the start of surgery for post-operative analgesia.

2.3.2.2 Surgical Procedures

Once the mice were fully anesthetized they were placed in a supine position on a heating pad. The tubing from the anesthetic machine was fixed in place by use of a large saline bag, to ensure continuous flow of oxygen and isoflurane to the animal. Depth of anesthesia was assessed via the pedal pinch withdrawal test and buprenorphine (0.1mg/kg) was then given s.c.. The surgery was carried out aseptically, which was accomplished by shaving the abdominal area of the mouse with an electric shaver and performing a surgical scrub on the mouse. First, a cotton ball was soaked with hibitane (chlorhexidine gluconate) and was applied to mouse in a circular motion, starting at the incision site and working out toward the periphery; repeat x3. In the same manner hibitane was applied, isopropyl alcohol 70% solution (A) and povidone-iodine (B) were applied to disinfect the mouse further; they were applied in an alternating manner (A, B, A, B, A, B). All instruments and materials used were autoclaved or sterilely packed. The

surgeon wore sterile gloves, a surgical cap, and a mask, in accordance with Dalhousie University CACF guidelines.

A surgical drape was placed over the mouse with a small opening for the planned surgical site. Using a No. 15 scalpel, a midline incision was made longitudinally along the abdomen. Blunt forceps were used to separate the skin from the abdominal muscle layer. The non-vascularized tissue of the *linea alba* was located and a midline incision was made longitudinally along the muscle layer using scissors. During surgical procedure, saline was frequently applied to the open surgical area to ensure the area was kept moist. Saline soaked cotton tipped applicators were used to gently locate and retract the ascending colon from the abdominal cavity. An area about 1cm distal to the ileocecal valve on the ascending colon was chosen and a 7-0 polypropylene monofilament suture was fixed superficially in the colon wall with three knots. Before the catheter was inserted, forceps were used to make dents about 5 mm from the end of the catheter. This creates a place for sutures to grab when fixing the catheter in place, as well as act as a guide for how far in the catheter needs to go. A 20G 1-1/4 catheter (Jelco, Smiths Medical, Kent, UK) was inserted beside the location where the sutures were fixed and pushed into the intestinal wall up to the pre-calibrated markings; the interior needle was removed. The loose suture ends were looped around the catheter twice and fixed with three knots; repeated x2. An additional suture was fixed superficially in the colon wall on the opposite side of the first knot and as close to the catheter as possible. The same process was used to further fix the catheter in place. The loose ends of the suture were cut and the catheter tube was cut to leave 2-3mm of the tube projecting from the ascending colon. The cecum was gently massaged using wet cotton tipped applicators to milk fecal

matter out of the stent (Figure 4). This ensures the stent was placed correctly and there were no blockages. The ascending colon was then gently placed back in the abdominal cavity. The abdominal muscle layer was sutured using a 5-0 absorbable monofilament polyglyconate suture using with a running uninterrupted stitch. Just before muscle layer was completely sutured shut, treatment drugs or saline were administered i.p.. The abdominal skin layer was sutured using a 5-0 absorbable monofilament polyglyconate suture with interrupted knots.

The mouse was placed in a clean cage in the recovery room with half of the cage over a heating pad and monitored until fully conscious and mobile. The mouse was supplied with rodent chow mash and water *ad libitum*. The mice recovered in the recovery room for six hours and were then brought upstairs for the remainder of the experimental time.

Figure 4. Fecal matter was milked out of cecum using cotton tipped applicators during the CASP procedure.

2.3.2.3 Experimental Timeline

The experimental timeline of CASP begins with induction of anesthesia, surgical implantation of the stent, and administration of treatment drugs. Time 0 of the experimental timeline is marked when treatments/saline were administered i.p. to the mouse (Figure 5). The animals were allowed to recover after surgery with some animals receiving additional treatments in required experimental groups at 4 hours into the experimental timeline. Seven hours after initial treatments, the animals were anesthetized again with sodium pentobarbital (90mg/kg; 54mg/ml) at a 10% dilution with 0.9% sodium chloride in preparation for IVM. Fluorochromes FITC and rhodamine were administered i.v. via tail vein injection 30 minutes prior to IVM. 15 minutes prior to IVM, laparotomy and peritoneal lavage fluid (PLF) was collected. This was done by instilling 2 ml pre-warmed saline into the peritoneum and gently mixing the fluid inside the abdomen. Around 1.5 ml PLF was removed to assess bacterial burden and microbiome composition. Upon completion of IVM, whole blood and samples of the small intestine were collected for further analysis.

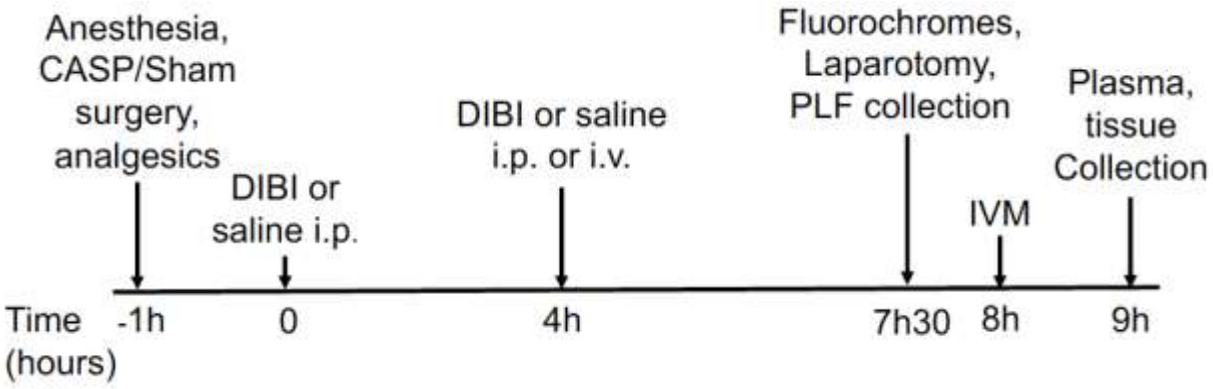

Figure 5. Experimental timeline of CASP model.

2.3.2.4 Experimental Groups

A total of 6 experimental groups were tested with the CASP poly-bacterial model with 5-6 animals per group (Table 2). Group 1 (SHAM) was a healthy control group. In this group, all animals underwent the same surgical intervention as CASP groups, but the stent did not pierce the intestine; therefore, there was no active leakage of feces into the peritoneum. Group 2 (CASP) underwent CASP surgery without any treatment interventions.

The remaining groups underwent the CASP surgeries and received 1 of 4 DIBI dosing strategies. Group 3 (CASP+DIBI (40 i.p.)) received DIBI as a prophylactic (immediately after CASP surgery; time 0) treatment (40 mg/kg; i.p.). Group 4 (CASP+DIBI (80 i.p.)) received an initial DIBI dose (80 mg/kg; i.p.) at time 0. Group 5 (CASP+DIBI (80x2 i.p.)) received an initial DIBI dose (80 mg/kg; i.p.) at time 0, and an additional dose of DIBI 4 hours after surgery completion (80 mg/kg; i.p.). Group 6 (CASP+DIBI (80 i.p.+80 i.v.)) received an initial DIBI dose (80 mg/kg; i.p.) at time 0, and an additional dose of DIBI 4 hours after surgery completion (80 mg/kg; i.v.).

Table 2. Experimental groups for CASP experiments.

Model	**Groups**	**Intervention**
CASP	SHAM	Saline
CASP	CASP	CASP (20G)
CASP	CASP+DIBI (40 i.p.)	CASP (20G) & DIBI (40mg/kg i.p.)
CASP	CASP+DIBI (80 i.p.)	CASP (20G) & DIBI (80mg/kg i.p.)
CASP	CASP+DIBI (80 i.p.x2)	CASP (20G) & DIBI (80mg/kg i.p. twice)
CASP	CASP+DIBI (80 i.p.+80 i.v.)	CASP (20G) & DIBI (80mg/kg i.p. + 80mg/kg i.v.)

2.3.3 Intravital Microscopy

Intravital microscopy (IVM) was performed in all groups in the endotoxemia model and the CASP model. In the endotoxemia model, IVM was performed 2 hours after endotoxin administration. In the CASP model, IVM was performed 8 hours after completion of the surgery. The duration of IVM lasted approximately 30-45 minutes for each experiment.

2.3.3.1 Fluorescence Staining

Fluorescence staining was carried out 15 minutes prior to IVM to observe leukocyte-endothelial interactions and evaluate the intestinal microcirculation. Fluorochromes were administered i.v. either through the catheter in the endotoxemia model, or by tail vain injection for the CASP model. Administration of 0.05% rhodamine-6G (1.5ml/kg; Sigma-Aldrich, ON, Canada) was used to stain leukocytes. To observe the intestinal microcirculation, 5% fluorescein isothiocyanate-bovine serum albumin (FITC-BSA, 1ml/kg; Sigma Aldrich, Oakville, ON, Canada) was used to observe capillary perfusion.

2.3.3.2 Laparotomy

Immediately after fluorochrome administration and ensuring the animal's depth of anesthesia was sufficient, laparotomy was performed. Using scissors, a midline incision was made on the animal's abdomen and forceps were used to separate the skin from the muscle layer below. The *linea alba* was located, and using scissors, the muscle layer was cut along the *linea alba* to expose the abdominal cavity. The *linea alba* contains primarily connective tissues; therefore, by cutting along this line bleeding is minimized.

2.3.3.3 Intravital Microscopy Setup

Saline soaked cotton tipped applicators were used to locate the caecum and subsequently a portion of the terminal ileum, which was excised. The mouse was placed on it's side on a specifically designed IVM stage (100), with the excised portion of the intestine placed on a viewing platform (Figure 6). The IVM stage was fixed on a heating pad. The exposed segment of the intestine received a continuous flow of thermostat-controlled (37°C) saline to maintain physiologic conditions. The flow of saline was controlled at 5 ml/hour and the hanging drop method was used to ensure maintenance of physiologic conditions (101). The mouse, IVM stage, and heating pad were then placed under the microscope for observation. To further ensure physiologic conditions were maintained, a warm saline pack was placed over the animal and exchanged periodically with a freshly warmed pack throughout IVM.

Figure 6. Animal set up for intravital microscopy.

2.3.3.4 Microscopy

IVM of the terminal ileum was performed using a epifluorescent microscope (Leica DMLM, Wetzlar, Germany) and a light source (LEJ EBQ 100; Carl Zeiss, Jena, Germany). Randomly chosen intestinal vessels were captured in real-time with a black and white monitor (Speco Technologies, Amityville, NY, USA) and transferred to the monitor using a digital EM-CCD camera C9100-02 with AC-adapter A3472-07 (Hamamatsu, Herrsching, Germany). Acquisition of captured images was done using Volocity software (PerkinElmer, Waltham, MA, USA) and then stored on external hard drives for offline analysis, which was done using imaging software (ImageJ; National Institute of Health, USA).

With rhodamine-6G staining the mitochondria of cells, leukocyte recruitment (number of rolling/adhering cells) was recorded in the submucosal collecting (V1) and postcapillary (V3) venules of the intestinal submucosa. With FITC staining the plasma in the blood, capillary perfusion could be visualized, allowing functional capillary density (FCD) to be measured in the intestinal muscle layers and mucosal villi.

2.3.3.5 Leukocyte Endothelial Interactions

The green excitation filter of the microscope was used to focus on and collect videos of the submucosal venules (Figure 7). Six visual fields were taken of both V1 and V3 venules; each video was recorded for 30 seconds. The V1 venules were distinguished by accompanying an adjacent arteriole, as well as being 50-100 μm in diameter. The V3 venules were distinguished as being much smaller – typically 20-40 μm, and not existing with an adjacent arteriole.

2.3.3.6 Functional Capillary Density

The blue excitation filter of the microscope was used to visualize and obtain videos of the microcirculation in the muscle layers of the small intestine and the mucosal villi (Figure 8). The microcirculation in the small intestine are arranged in circular and longitudinal patterns in the muscle layers; however, since the mouse intestine is very thin, the layers were focused on together. Six visual fields were taken of the muscle layer microcirculation; each video was recorded for 30 seconds. To observe the capillary perfusion in the mucosal villi, as the last step of IVM, a portion of the intestine was superficially cauterized lengthwise. Scissors were then used to cut along the cauterized area and open up the intestinal wall. The luminal contents were flushed out using 0.9% saline, creating a window to view the mucosal villi. The exposed area was carefully manipulated using saline soaked cotton tipped applicators to gain an optimal view of the mucosal villi. A glass slide was placed over the exposed area and the mouse was put back under the microscope. Six visual fields focusing on the capillary perfusion in the mucosal villi were taken; each video was recorded for 30 seconds.

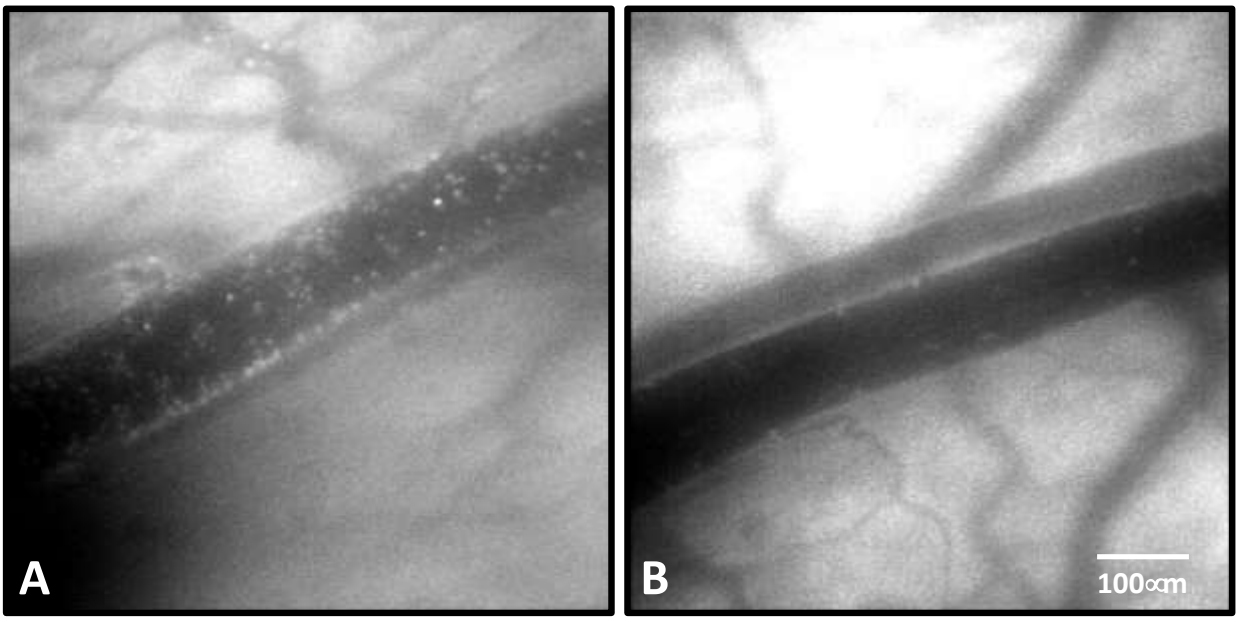

Figure 7. Intravital microscopy of the intestinal submucosal collecting venules (V1). (A) Adhering leukocytes in untreated CASP animal (B) Reduced leukocyte adherence with administration of DIBI (80 mg/kg i.p.) after CASP surgery.

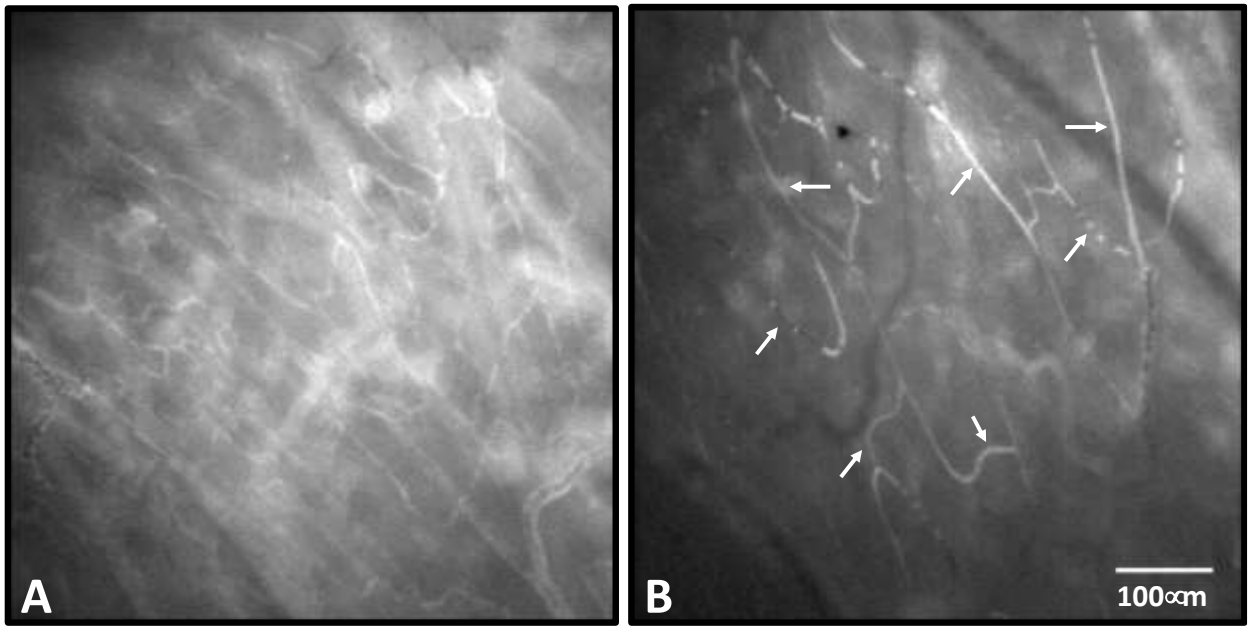

Figure 8. Intravital microscopy of capillary perfusion in the muscle layer of the intestine. (A) Healthy capillary perfusion in SHAM operated animal. (B) Unhealthy capillary perfusion in untreated CASP animal. Arrows denote non-perfused capillaries.

2.3.3.7 Video Analysis

Analysis of all video recordings were performed offline using ImageJ software in a blinded fashion. For each animal, the 4 following parameters were analyzed: leukocyte rolling, leukocyte adhesion, capillary perfusion of the muscle layer and capillary perfusion of the mucosal villi. Rolling leukocytes were classified as non-adherent leukocytes that visibly crossed a pre-measured cross-section of the vessel of interest within the 30 second recording of the video. Leukocyte adhesion was assessed by drawing an area around a large, clear section of the vessel; leukocytes that remained adhered to the endothelium in the pre-drawn area for the full 30 second video were classified as adherent leukocytes. This data allowed quantification of rolling leukocytes (cells/minute) and adherent leukocytes (cells/mm^2). To quantify capillary perfusion in the intestinal muscle layer, a rectangular area was overlain on the video and measured. The length of perfused capillaries in the pre-measured area were summed to calculate the FCD ($\mu m/\mu m^2$). To quantify capillary perfusion in the mucosal villi, 2-3 villi were randomly chosen for each video and measured. The length of perfused capillaries was measured in each pre-measured villus and the sum of the villi areas and total length of perfused capillaries were used to calculate FCD.

2.3.4 Blood & Tissue Collection

Following IVM, the mouse was taken off the IVM stage and euthanized by cardiac puncture for blood collection using a 1 ml heparin (1000 USP units/ml; Sandoz Canada Inc. Boucherville, QC, Canada) coated syringe with a 25G x 5/8 needle. On average, 0.5 ml blood was obtained. Half of the volume obtained was placed in a 1.5ml Eppendorf tube and used for bacterial counting and the other half was placed in another

1.5 ml Eppendorf tube and centrifuged at 250 x g for 10 minutes. The plasma was isolated, placed in a 1.5 ml Eppendorf tube, and stored at -80°C until further use.

2.3.5 Bacteria Counting

Analysis of bacterial load was performed for both PLF samples and blood samples in the CASP model. The following procedure is the same for PLF samples and blood; however, an initial 10 fold dilution was made with blood samples before plating. Pipette tips, Eppendorf tubes and glass beads were autoclaved prior to experiment. Tryptic soy agar (TSA) plates were also prepared a minimum of 1 day prior to experiment for adequate drying time. Six plates were laid out in preparation for spread plating containing 5-7 glass beads in the lid.

Ten-fold serial dilutions of samples were made with PBS once samples were obtained. For PLF samples, the first plate contained undiluted sample and the last plate contained a 1:100000 dilution. For blood, the first plate contained a 1:10 dilution, while the last plate contained a 1:1000000 dilution. For each dilution, 100 μl was pipetted onto its corresponding agar plate; plates were shaken to distribute samples. Once the plates were dry and the sample was fully absorbed, the glass beads were removed and the plates were incubated upside down in a 37°C incubator overnight. Colonies were counted between 16-24 hours after plating. Colony forming units/ml (CFU/ml) was calculated by multiplying the number of colonies by the dilution factor and dividing it by the volume (100 μl).

2.3.6 Microbiome Sequencing

To analyze the proportions of bacteria in PLF samples, 500 µl of PLF sample was placed in a 1.5 ml Eppendorf tube and brought to Dr. Morgan Langille's lab, located in Room 5-D of the Tupper Medical Building at Dalhousie University for microbiome sequencing. The 16S Bacteria and Archea Standard Operating Procedure was used to profile microbiome samples (102).

2.3.7 Plasma Cytokines and Adhesion Molecules

CASP plasma cytokine and chemokine levels were measured using a custom made 12-plex mouse magnetic Bio-Plex Pro™ cytokine, chemokine, and growth factor assay obtained from Bio-Rad (Mississauga, ON, Canada). The Bio-Plex Pro assays work on the principle of sandwich ELISA (Figure 9). The cytokines chosen to be measured were as follows: IFN-γ, TNF-α, IL-1β, IL-2, IL-4, IL-6, IL-10, IL-12 p70, IL-17A, P-selectin and ICAM-1. Preparation of the samples were done following the manufacturer's instructions. All samples were run in duplicate and prepared in four-fold dilutions using the Bio-Plex® sample diluent. A standard curve was generated for each analyte being tested. Before experiments were carried out, Luminex systems were calibrated following manufacturer's instructions and the wash station was primed.

Briefly, 50µl of detection antibody magnetic beads were added to each well of a flat-bottom 96 well plate and washed with buffer using the Bio-Plex Pro wash station. Standards were prepared in four-fold serial dilutions and added to plate along with the samples. The plate was incubated in the dark on a shaker at 300 rpm for 1 hour and then washed 3 times. Bio-Plex detection antibodies were added to plate and incubated in the dark on a shaker for 30 min; the plate was washed 3 times with wash buffer. Streptavidin-PE was prepared and added to wells and incubated on shaker for 10 min in the dark. The

plate was washed 3 more times and the Bio-Rad 200 luminometer with Bio-Plex manager software was used to read plate.

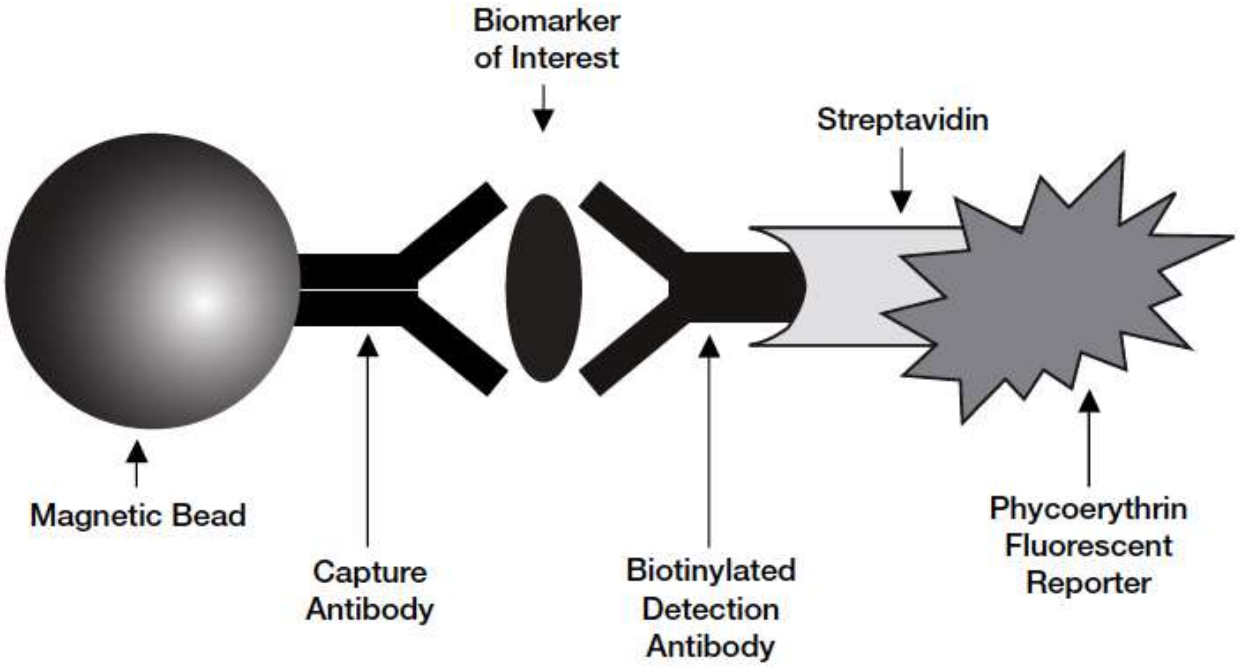

Figure 9. Bio-Plex sandwich immunoassay

2.4 Statistical Analysis

Statistical analyses were performed using GraphPad Prism 6.0 (GraphPad Software Inc, La Jolla, CA, USA). Normal distribution of all data was confirmed using the Kolmogorov-Smirnov test. *In vivo* data were then analyzed using a one-way ANOVA, followed by Newman-Keuls test for multiple comparisons. For *in vitro* data, differences between groups were compared using two-tailed unpaired t-test. All data were expressed as mean ± standard error of mean (SEM). Differences at $p < 0.05$ were considered statistically significant.

CHAPTER 3: RESULTS

3.1 *In vitro* studies

3.1.1 DCFDA Assay

Intracellular ROS production was assessed in BMDMs and neutrophils using the DCFDA assay. In this assay, cells were treated with CM-DCFDA, which gets reduced to a highly fluorescent compound when encountered by ROS species (103); the fluorescence was measured by flow cytometry. LPS (100 ng/ml) was used to stimulate ROS production in BMDMs and neutrophils and hydrogen peroxide (H_2O_2; 100 μM) was used as a positive control. In BMDMs, LPS and H_2O_2 significantly increased ($p < 0.05$) ROS production from the medium control (Figure 10) and administration of DIBI (200 μM) in combination with both stimulants significantly reduced ($p < 0.05$) intracellular ROS. Also of note, administration of DIBI alone did not significantly alter ROS production by control cells.

When the DCFDA assay was performed on neutrophils, LPS (100 ng/ml) was not able to stimulate intracellular ROS production; however, H_2O_2 (100 μM) significantly increased ($p < 0.05$) intracellular ROS production compared to control cells (Figure 11). Administration of DIBI (200 μM) in combination with H_2O_2 decreased mean intracellular ROS levels from 384% (H_2O_2) to 236% (H_2O_2 + DIBI), but this decrease was not significant. In line with findings from BMDMs, administration of DIBI alone did not significantly alter intracellular ROS production in neutrophils.

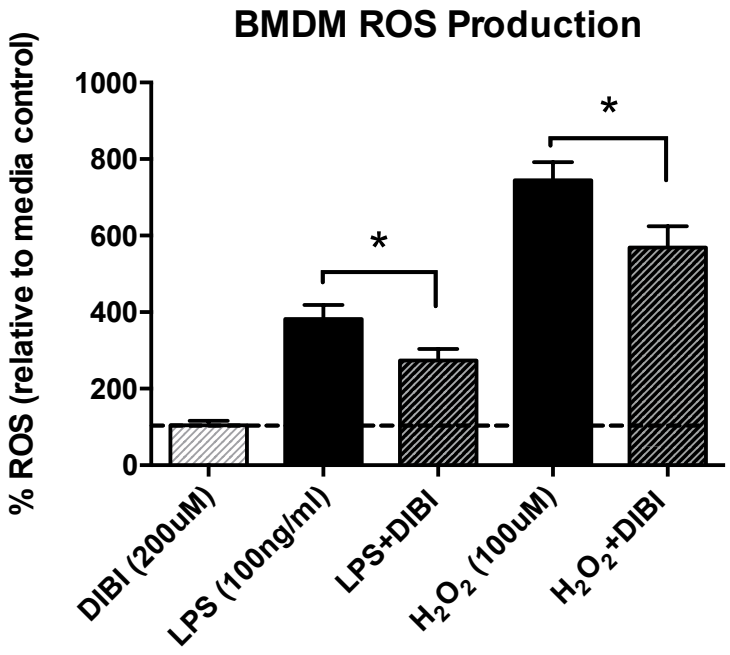

Figure 10. Intracellular reactive oxygen species production in BMDMs. BMDMs were treated with DCFDA, stimulated with LPS (100 ng/ml) or H_2O_2 (100 μM) and treated with DIBI (200 μM). Flow cytometry was used to assess levels of intracellular ROS in BMDMs. The dashed line denotes control cells. Data are a mean of 3 independent experiments ± SEM; * denotes $p < 0.05$.

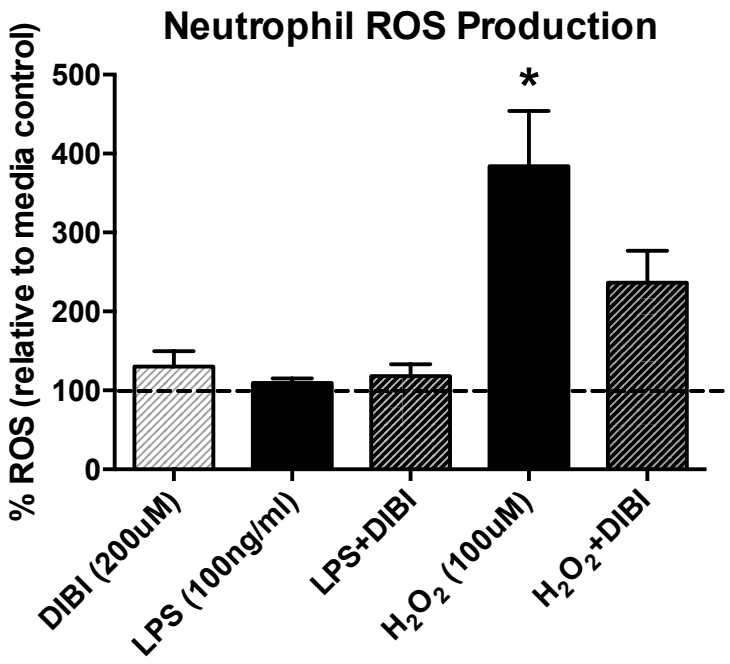

Figure 11. Intracellular reactive oxygen species production by neutrophils. Neutrophils were treated with DCFDA, stimulated with LPS (100 ng/ml) or H_2O_2 (100 μM) and treated with DIBI (200 μM). Flow cytometry was used to assess levels of intracellular ROS in neutrophils. The dashed line denotes control cells. Data are a mean of three independent experiments ± SEM; * denotes $p < 0.05$ vs. media control.

3.1.2 Amplex Red Assay

The Amplex Red assay was used to assess extracellular ROS production by neutrophils in response to LPS (100 ng/ml, 200 ng/ml) or H_2O_2 (100 μM) stimulation. In this assay, when Amplex Red reagent is in the presence of H_2O_2, it is reduced to a highly fluorescent resorufin compound (104); fluorescence is measured by a plate reader. When neutrophils were stimulated with the low dose (100 ng/ml) and high dose (200 ng/ml) of LPS, there was a statistically significant increase ($p < 0.05$) in extracellular ROS production compared to the medium control (Figure 12), but there were no significant differences between the two dosages of LPS. Administration of DIBI in combination with low and high dose LPS stimulation, caused a significant decrease ($p < 0.05$) in ROS production. H_2O_2 stimulation also significantly increased ($p < 0.05$) extracellular ROS production from the medium control. Administration of DIBI in combination with H_2O_2 decreased mean ROS production from 281% to 225%, but it was not significant. In line with what was found in other assays measuring ROS production, administration of DIBI alone did not significantly alter ROS production. These results indicate that DIBI has anti-oxidative effects on extracellular ROS *in vitro*.

3.1.3 Griess Assay

The Griess assay was used to assess the production of extracellular NO by neutrophils. NO is another component of the ROS/RNS family and is a major player in the cascade that leads to the development of oxidative stress (33). In this assay, LPS (100 ng/ml) was used to stimulate neutrophils, which resulted in a significant increase in nitric oxide production from 25 ng/ml (medium control) to 59 ng/ml (LPS) (Figure 13). The

combination of LPS stimulation with DIBI treatment resulted in 32% less NO production (59 ng/ml (LPS) to 40 ng/ml (LPS+DIBI)), but this was not significant. DIBI treatment alone resulted in an average 32% decrease in NO production, but this was not significant.

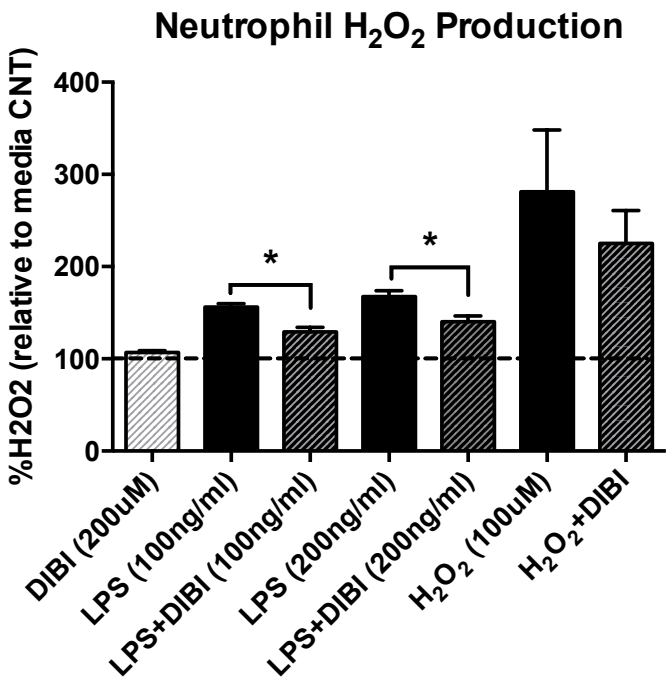

Figure 12. Production of extracellular H_2O_2 by neutrophils. Neutrophils were stimulated with LPS (100 ng/ml or 200 ng/ml) or H_2O_2 (100 μm) and treated with DIBI (200 μM). Cells were then used in the Amplex Red assay to measure extracellular H_2O_2 production. The dashed line denotes control cells. Data are a mean of three independent experiments ± SEM; * denotes $p < 0.05$.

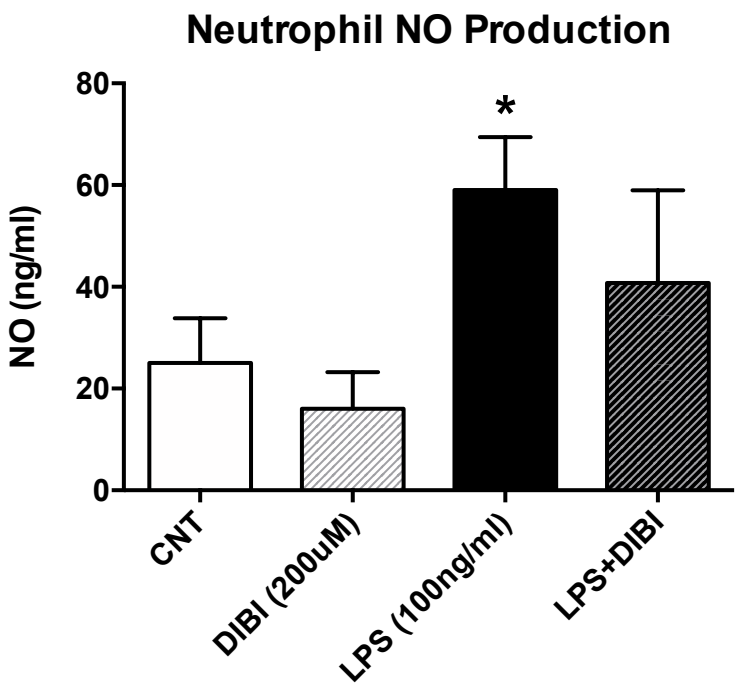

Figure 13. Extracellular NO production by neutrophils. Neutrophils were stimulated by LPS (100 ng/ml) and treated with DIBI (200 μM). Cell supernatants were collected and used in the Griess assay to measure NO production. Data are a mean of three independent experiments ± SEM; * denotes $p < 0.05$ vs. (CNT).

3.1.4 Chemokinesis Assay

Macrophages are one of the first cells on site during inflammation or infection. With intravital microscopy we are unable to look at migration of immune cells, which is the last step in the leukocyte activation cascade. Therefore, the undirected migration and coordinated movement of population of BMDMs was assessed with the chemokinesis assay.

In the chemokinesis assay, cells are allowed to adhere to either side of a cell culture insert, which is then removed leaving a gap between the cells (Figure 14A). The amount of cells present in the gap after 24 hours is assessed using imaging software and quantified. After 24 hours, it was found that vehicle treatment (PBS; 20 μl/ml) did not inhibit BMDM migration compared to control cells. DIBI (200 μM) treatment and untreated LPS (100 ng/ml) significantly ($p < 0.05$) reduced BMDM motility from vehicle control levels. Interestingly, the combination of LPS stimulation and DIBI treatment caused an additive effect, further reducing BMDM movement ($p < 0.05$) (Figure 14B). These results suggest that iron deprivation by DIBI has anti-inflammatory effects, reducing the movement of BMDMs.

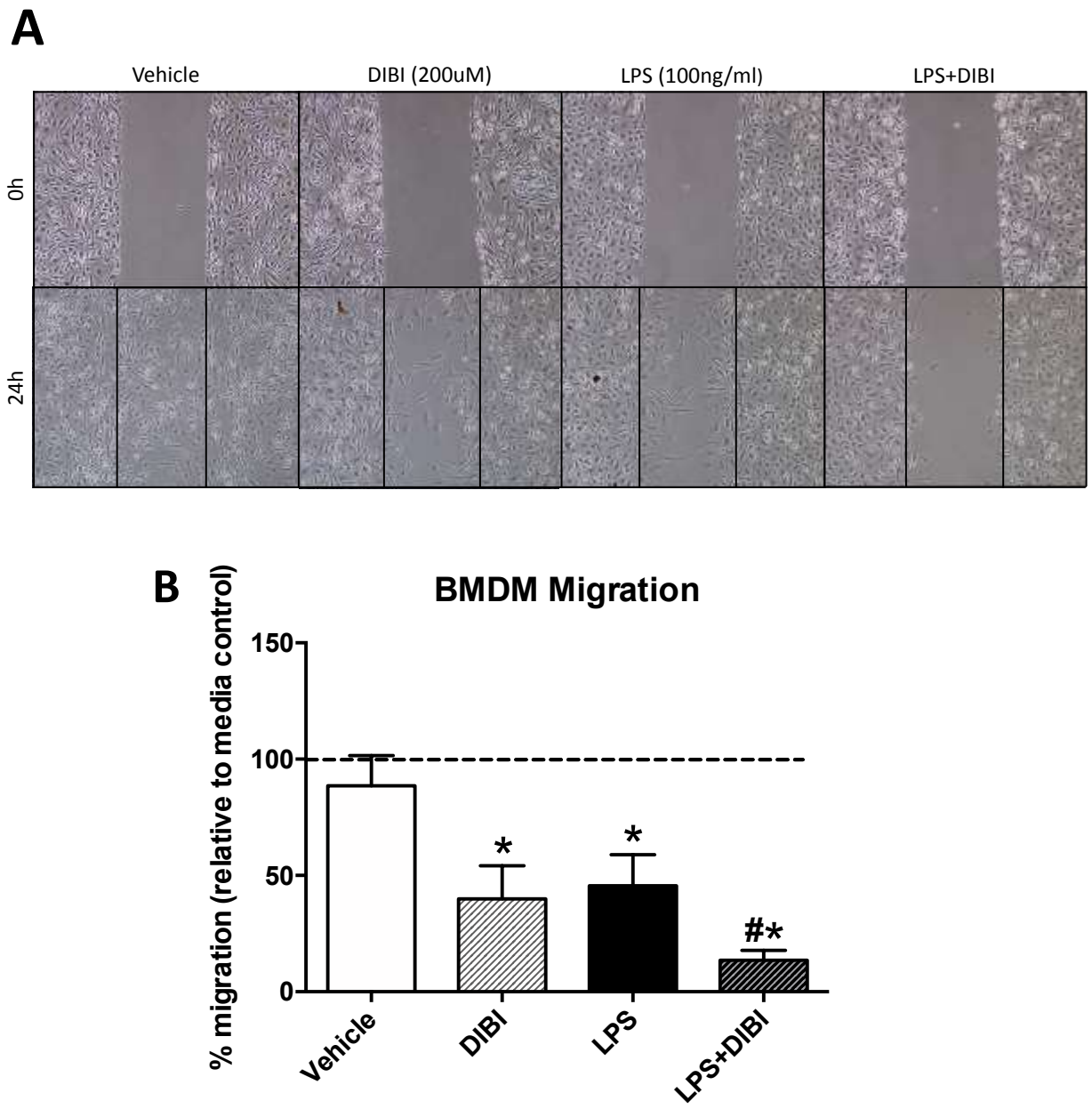

Figure 14. Chemokinesis assay showing the effect of DIBI on undirected, coordinated movement of BMDMs. (A) Representative images of the progress of cell movement at time 0 (top row) and 24 hours (bottom row) with four treatment groups. (B) Numerical representation of BMDM migration. The dashed line represents migration of control cells. Data are a represented as a mean of four independent experiments ± SEM; * denotes $p < 0.05$ vs. vehicle, # denotes $p < 0.05$ vs. LPS.

3.2 *In vivo* studies

3.2.1 Experimental Endotoxemia Model

The endotoxemia model represents an experimental model of sepsis that causes immune hyper-activation in the absence of bacteria (58). Using this model, the effect of iron chelation could be evaluated in a hyper-inflammatory state, but since LPS is only a component of the Gram-negative bacterial cell wall, this embodied a more controlled model because there was not an active bacterial infection.

3.2.1.1 Leukocyte Adherence

Previous studies in our lab that examined the effects of iron chelation in an murine endotoxemia model with an older formulation of DIBI found that LPS stimulation in combination with DIBI resulted in reduced leukocyte activation (97). The endotoxemia model was then used to assess the effects of the newer formulation of DIBI on leukocyte activation, as well as determine an optimal dosing strategy for DIBI administration. Finally, PVP - the polymer backbone of DIBI - was administered in combination with LPS to determine whether the molecule of DIBI itself had effects on leukocyte activation aside from iron-chelating effects. Mice were administered with LPS (5 mg/kg) followed 15 minutes later by administration of DIBI (10 mg/kg, 5 mg/kg, or 2.5 mg/kg) or PVP (10 mg/kg). The outcome of endotoxin challenge was assessed by intravital microscopy.

Leukocyte adhesion was the primary endpoint to assess leukocyte activation and inflammation because in order for leukocytes to firmly adhere to the endothelium, they have gone through 2 stages of activation. In the V1 venules, endotoxin challenge

significantly increased ($p < 0.05$) leukocyte adhesion compared to control mice (Figure 15). Notably, there is a baseline level of leukocyte activation in control groups as these mice underwent catheterization and laparotomy. DIBI (2.5 mg/kg) did not significantly alter the number of adherent leukocytes compared to untreated LPS and levels of adherent leukocytes remained significantly increased ($p < 0.05$) from control animals. DIBI (10 mg/kg), DIBI (5 mg/kg), and PVP (10 mg/kg) significantly reduced ($p < 0.05$) leukocyte adhesion from untreated LPS animals, with the greatest reduction seen in DIBI (10 mg/kg). Of note, the most variable effects were seen with DIBI (5 mg/kg) and PVP (10 mg/kg).

Similar results were seen in the post capillary V3 venules. Endotoxin challenge significantly increased ($p < 0.05$) leukocyte adhesion compared to control animals (Figure 16). Administration of DIBI 10mg/kg reduced leukocyte adhesion from untreated LPS by 25%, which was greater than other DIBI doses, but it was not a statistically significant decrease. Interestingly, DIBI (2.5 mg/kg) significantly increased ($p < 0.05$) leukocyte adhesion in V3 compared to untreated LPS animals.

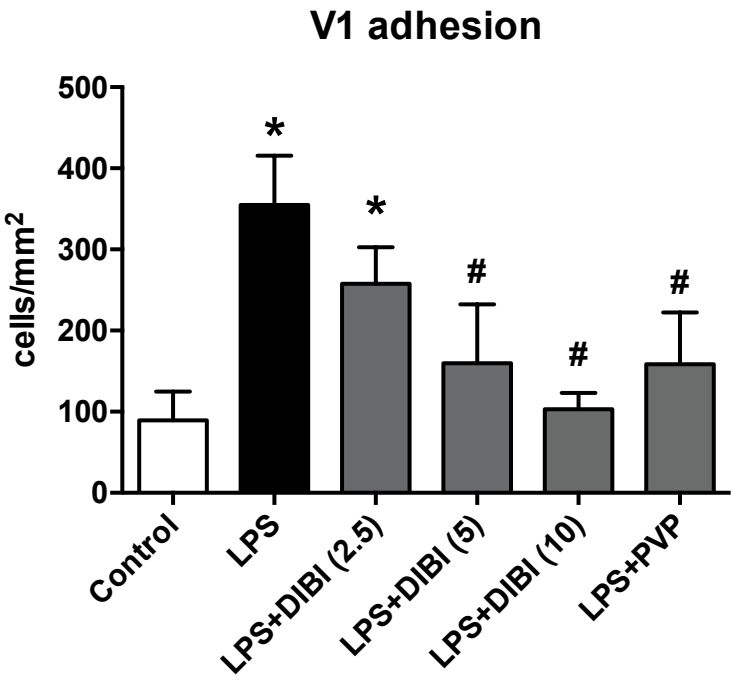

Figure 15. Effect of iron chelation on leukocyte adhesion in intestinal submucosal collecting venules after systemic administration of LPS. Bar graphs represent firmly adherent leukocytes in the submucosal collecting venules (V1; 50-100 μm vessel diameter) (cells/mm^2). Data represented as mean ± SEM (n= 5-7 per group); * $p < 0.05$ compared to control group, # $p < 0.05$ compared to LPS group.

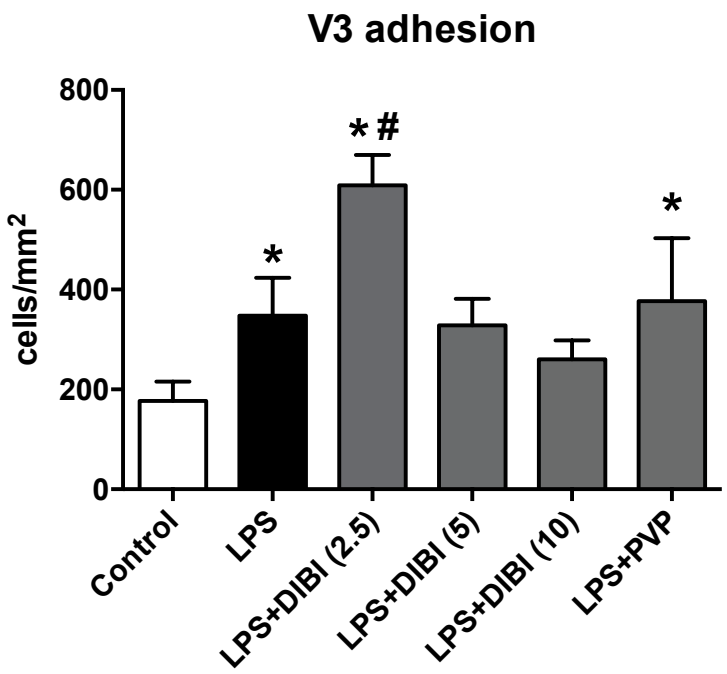

Figure 16. Effect of iron chelation on leukocyte adhesion in intestinal postcapillary venules after systemic administration of LPS. Bar graphs represent firmly adherent leukocytes in the postcapillary venules (V3; < 40 μm vessel diameter) (cells/mm^2). Data represented as mean ± SEM (n= 5-7 per group), * $p < 0.05$ compared to control group.

3.2.1.2 Leukocyte Rolling

The step before leukocyte firm adhesion is rolling. During this stage, leukocytes become lightly tethered onto selectins expressed on the surface of endothelial cells; however, the integrins that cause firm adhesion are not yet in their high affinity. This provides another measurement of leukocyte activation. In both the V1 and V3 venules, endotoxin challenge resulted in a significant decrease ($p < 0.05$) in the number of rolling leukocytes compared to control animals (Figure 17). Administration of all doses of DIBI and PVP also resulted in a significant decrease ($p < 0.05$) of rolling leukocytes in V1 and V3 venules compared to control mice, with no groups significantly different from the untreated LPS group.

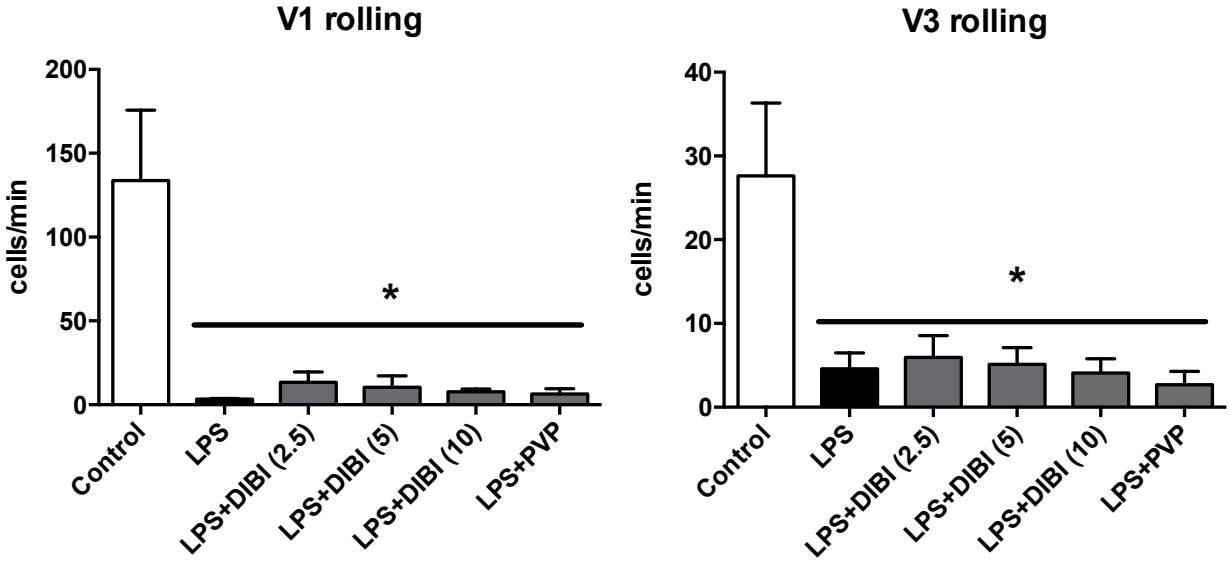

Figure 17. Effect of iron chelation on leukocyte rolling in intestinal submucosal venules after systemic administration of LPS. Bar graphs represent leukocyte rolling in the submucosal collecting venules (V1; 50-100 μm vessel diameter) and postcapillary venules (V3; <40 μm vessel diameter) (cells/min). Data represented as mean ± SEM (n= 5-7 per group); * $p < 0.05$ compared to control group for endotoxin challenged groups.

3.2.1.3 Functional Capillary Density

Microcirculatory dysfunctions during sepsis, such as reduced capillary perfusion, represents a major event in the pathophysiology of sepsis and progression toward multiple organ dysfunction (105). In the endotoxemia model, capillary perfusion was measured in the intestinal muscle layer and mucosal villi as a measurement of total perfused capillaries in a pre-determined area (functional capillary density (FCD)). A reduction in FCD is common in sepsis, and as expected, in our endotoxemia model, LPS administration caused a significant decrease ($p < 0.05$) in functionally perfused capillaries in both the intestinal muscle layer and mucosal villi (Figure 18 and Figure 19). In the intestinal muscle layer, PVP and all doses of DIBI improved FCD significantly ($p < 0.05$) compared to LPS, to levels that were similar to control levels. Of note, DIBI (5 mg/kg) had the most variable effects in the intestinal muscle layer.

Similar effects were seen in the mucosal villi where all doses of iron chelators (and PVP) significantly improved ($p < 0.05$) FCD from untreated LPS animals, back to levels comparable to control animals (Figure 19).

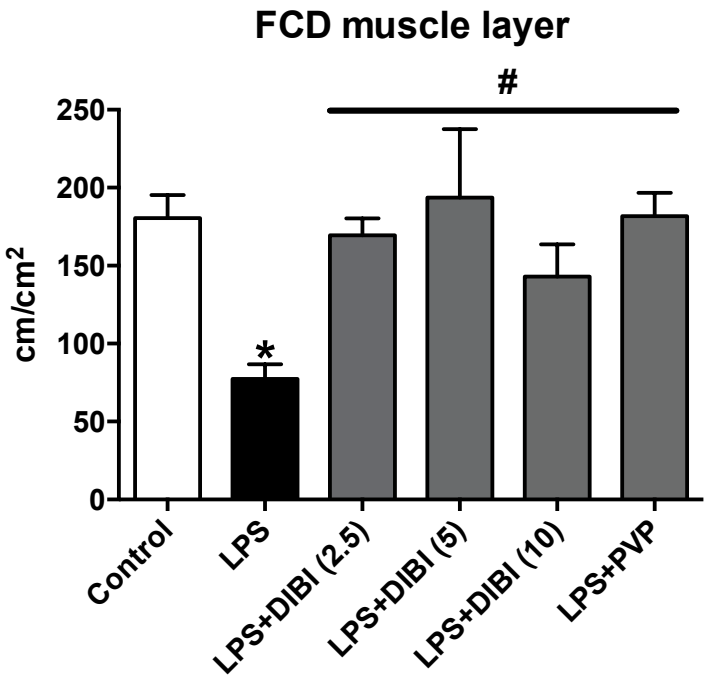

Figure 18. Effect of iron chelation on capillary perfusion in intestinal muscle layer after systemic administration of LPS. Bar graphs represent functional capillary density (FCD), quantified as the total length of perfused capillaries in a pre-determined area (cm/cm^2). Data represented as mean ± SEM (n= 5-7 per group); * $p < 0.05$ compared to control group, # $p < 0.05$ compared to LPS for all endotoxemia animals with treatment.

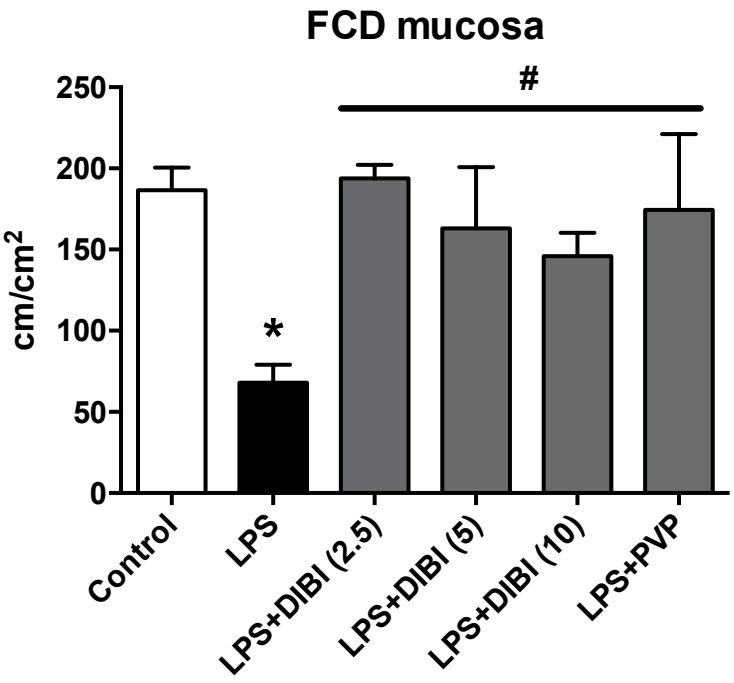

Figure 19. Effect of iron chelation on capillary perfusion in intestinal mucosal villi after systemic administration of LPS. Bar graphs represent functional capillary density (FCD), quantified as the total length of perfused capillaries in a pre-determined area (cm/cm^2). Data represented as mean ± SEM (n= 5-7 per group); * $p < 0.05$ compared to control group, # $p < 0.05$ compared to LPS for all endotoxemia animals with treatment.

3.2.2 Colon Ascendens Stent Peritonitis

The CASP model was used to study the effects of iron chelation by DIBI in a poly-bacterial peritonitis induced sepsis model. Multiple dosing strategies were used to determine the most appropriate dosing strategy. The inflammatory state of the mice was evaluated by intravital microscopy on the microcirculation of the intestine and the expression of an array of pro and anti-inflammatory cytokine molecules. The bacterial burden of the mice was also assessed by measuring bacterial growth in the peritoneal fluid and blood.

3.2.2.1 Leukocyte adherence

The active leakage of fecal contents into the peritoneum caused by the CASP surgery resulted in a significant increase ($p < 0.05$) in the number of adherent leukocytes in the V1 venules compared to SHAM operated mice in the 8 hour time course of the experiment (Figure 20). Although the surgical intervention the SHAM mice underwent did not result in peritonitis, they did present with a baseline level of leukocyte activation because they still experienced the trauma of surgery. Administration of DIBI (40 mg/kg i.p.) did not result in a significant reduction ($p < 0.05$) in adherent leukocytes from CASP in the V1 venules, but administration of DIBI (80 mg/kg i.p.) did significantly reduce ($p < 0.05$) the number of adherent leukocytes compared to CASP. This dosing strategy was also no longer significantly different from SHAM animals.

Additional doses of DIBI given 4 hours after initial CASP completion did not further improve the number of adherent leukocytes from CASP in the V1 venules. Administration of DIBI (80 mg/kg i.p. x 2) significantly reduced ($p < 0.05$) leukocyte

adherence from CASP, but the number of adherent leukocytes were still significantly higher than SHAM levels (Figure 20). Administration of DIBI (80 mg/kg i.p. + 80 mg/kg i.v.) did not result in any significant improvements from CASP levels and levels remained significantly increased from SHAM operated animals.

In the V3 venules, CASP intervention resulted in a 55% increase in the number of adherent leukocytes compared to SHAM animals (n.s.) (Figure 21). Administration of DIBI (80 mg/kg i.p.) reduced the number of adherent leukocytes by 48% compared to untreated CASP (n.s.) and was the only dosing strategy that reduced the number of adherent leukocytes from CASP to levels comparable to SHAM controls.

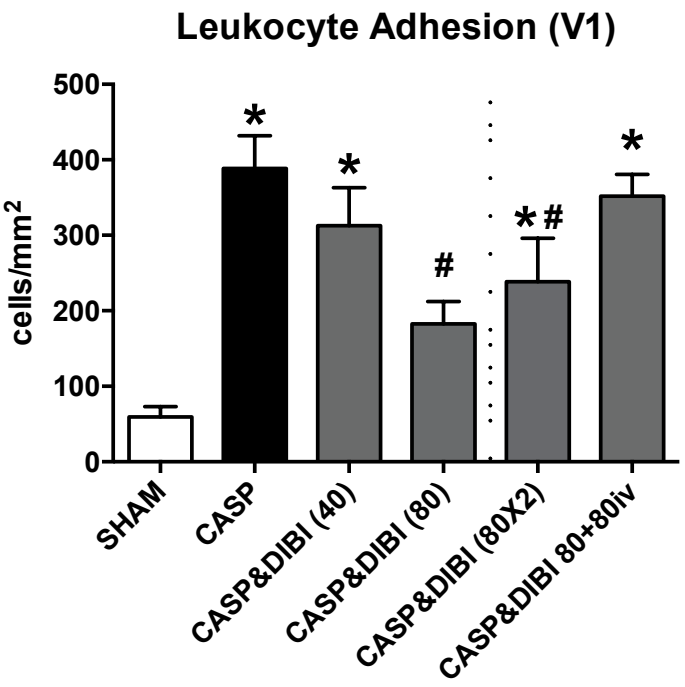

Figure 20. Effect of iron chelation on leukocyte adhesion in intestinal submucosal collecting venules 8 hours after CASP surgery. Bar graphs represent firmly adherent leukocytes in the submucosal collecting venules (V1; 50-100 μm vessel diameter) (cells/mm^2). Data represented as mean ± SEM (n= 5-7 per group); * $p < 0.05$ compared to SHAM group, # $p < 0.05$ compared to CASP group.

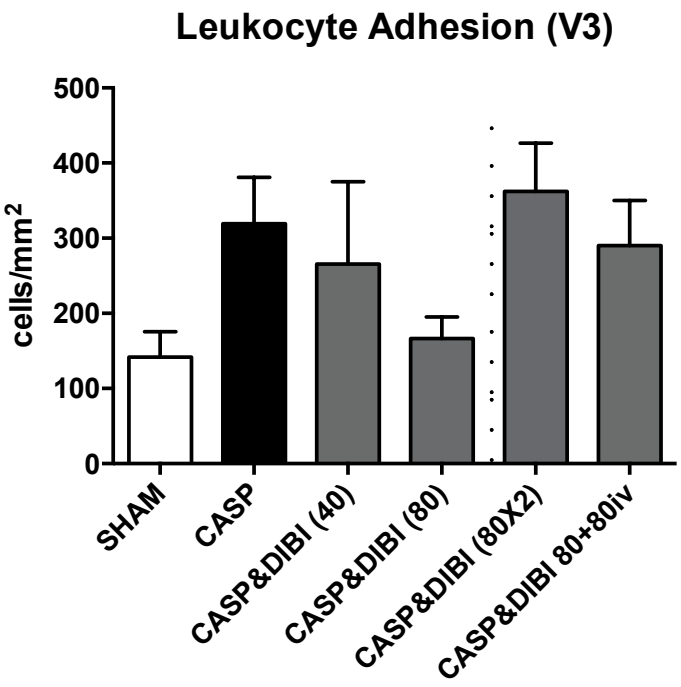

Figure 21. Effect of iron chelation on leukocyte adhesion in intestinal postcapillary venules 8 hours after CASP surgery. Bar graphs represent firmly adherent leukocytes in the postcapillary venules (V3; < 40 μm vessel diameter) (cells/mm^2). Data represented as mean ± SEM (n= 5-7 per group).

3.2.2.2 Leukocyte Rolling

CASP intervention significantly reduced ($p < 0.05$) the number of rolling leukocytes in both the V1 and V3 venules compared to SHAM operated mice (Figure 22). None of the DIBI dosing strategies significantly altered the number of rolling leukocytes in the V1 or V3 venules compared to untreated CASP; all dosing strategies remained significantly reduced ($p < 0.05$) from SHAM operated mice.

3.2.2.3 Functional Capillary Density

Within the submucosal intestinal muscle layer, successful completion of the CASP operation resulted in a significant decrease ($p < 0.05$) in functionally perfused capillaries compared to SHAM operated mice (Figure 23). Administration of DIBI (40 mg/kg i.p.) produced no significant alterations in capillary perfusion compared to untreated CASP animals; however, DIBI (80 mg/kg i.p.) increased FCD by 36% to levels comparable to SHAM treated animals, but this was non-significant. DIBI (80 mg/kg i.p. x2) and DIBI (80 mg/kg i.p. + 80 mg/kg i.v.) also increased capillary perfusion from untreated CASP by 23% and 26%, respectively; however, these increases were also not significant.

In the intestinal mucosal villi, CASP operation resulted in a significant decrease ($p < 0.05$) in the amount of functionally perfused capillaries compared to SHAM animals (Figure 23). Administration of DIBI (40 mg/kg) did not significantly alter the capillary perfusion in the mucosal villi and remained significantly reduced ($p < 0.05$) from SHAM levels. The remaining DIBI dosing strategies did not significantly improve FCD from untreated CASP; however, the FCD of remaining dosing strategies was no longer significantly decreased from SHAM animals.

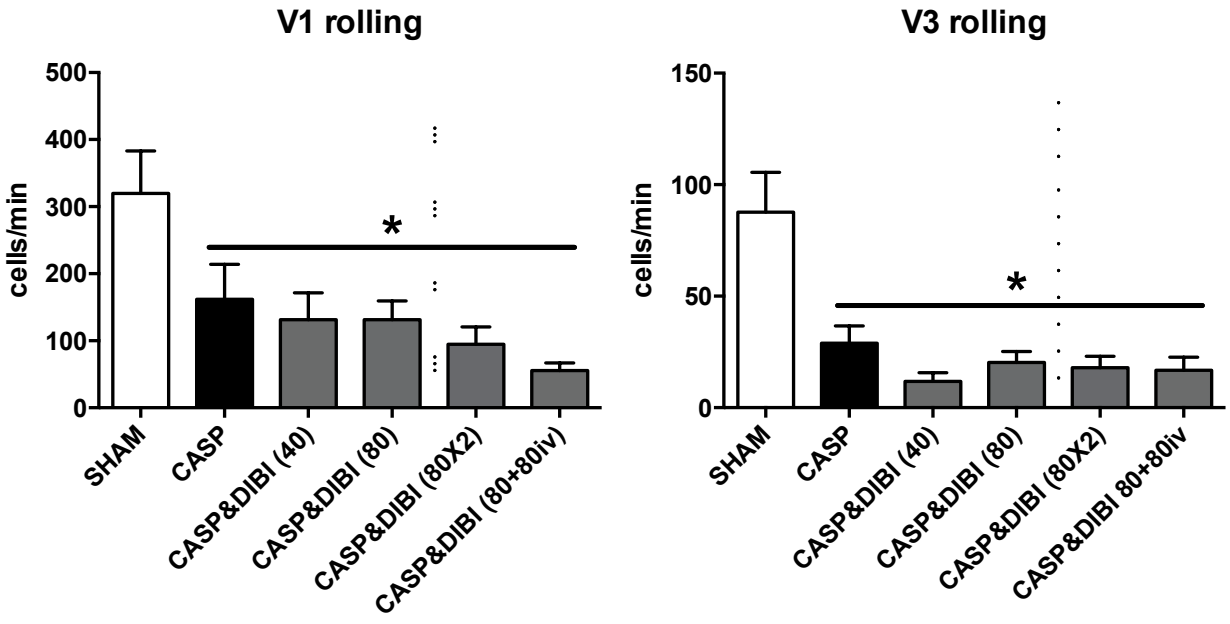

Figure 22. Effect of iron chelation on leukocyte rolling in intestinal submucosal venules 8 hours after CASP surgery. Bar graphs represent leukocyte rolling in the submucosal collecting venules (V1; 50-100 μm vessel diameter) and postcapillary venules (V3; <40 μm vessel diameter) (cells/min). Data represented as mean ± SEM (n= 5-7 per group); * $p < 0.05$ compared to SHAM group in all CASP operated groups.

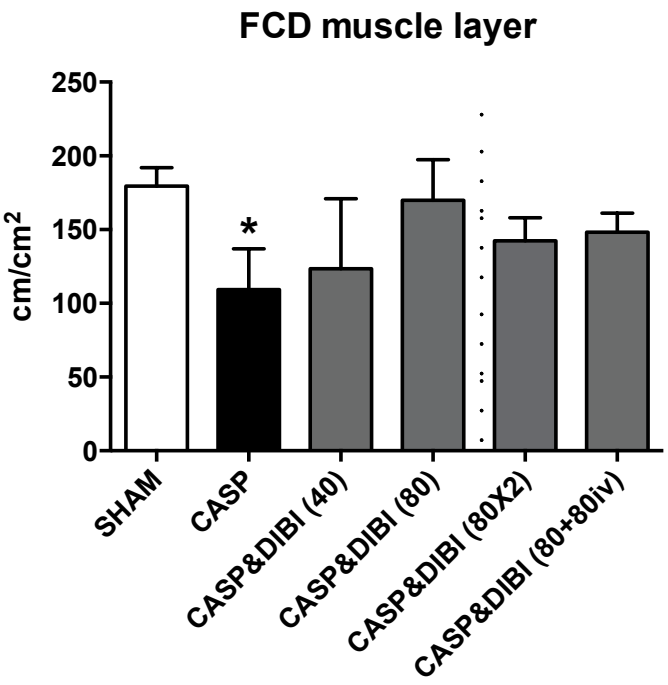

Figure 23. Effect of iron chelation on capillary perfusion in intestinal muscle layer 8 hours after CASP surgery. Bar graphs represent functional capillary density (FCD), quantified as the total length of perfused capillaries in a pre-determined area (cm/cm^2). Data represented as mean ± SEM (n= 5-7 per group); * $p < 0.05$ compared to SHAM group.

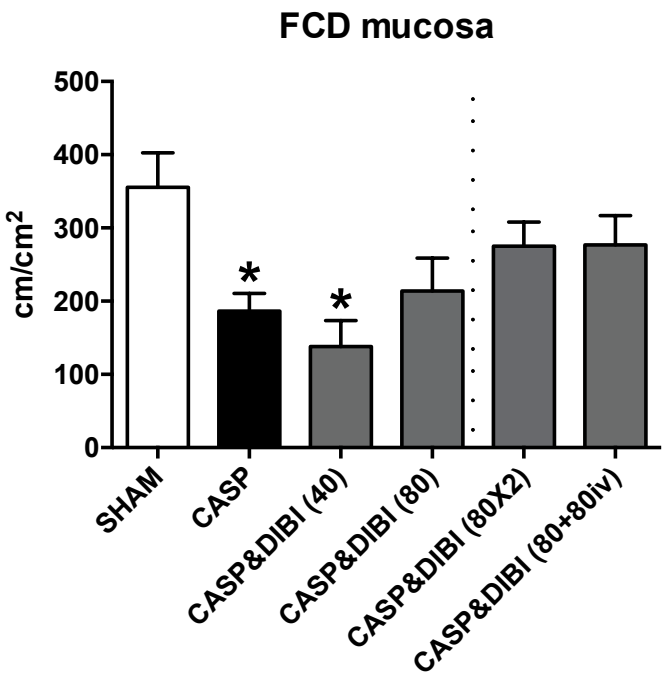

Figure 24. Effect of iron chelation on capillary perfusion within the mucosal villi of the intestinal lumen 8 hours after CASP surgery. Bar graphs represent functional capillary density (FCD), quantified as the total length of perfused capillaries in a pre-determined area (cm/cm^2). Data represented as mean ± SEM (n= 5-7 per group), * $p < 0.05$ compared to SHAM group.

3.2.3 Bacteria Enumeration

The CASP model causes peritonitis and bacteremia due to an active leakage of fecal matter into the peritoneum. In order to assess the bacterial burden in the peritoneum and blood, samples of peritoneal lavage fluid (PLF) and blood were plated on TSA plates to count bacterial colonies present in samples (CFU/ml). The bacterial burden in the PLF of SHAM animals was very low compared to CASP operated animals; however, bacteria were still present in some animals (Figure 25). As expected, CASP operation caused a significant increase ($p < 0.05$) of bacteria in the PLF samples compared to SHAM animals ($2.72x10^6$ CFU/ml vs. 179.7 CFU/ml, respectively). Administration of DIBI (40 mg/kg i.p.) increased the bacterial burden in PLF by 54% compared to untreated CASP (n.s.). DIBI (80 mg/kg i.p.) and DIBI (80 mg/kg i.p. x 2) reduced bacterial burden by 59% and 57%, respectively, compared to untreated CASP (n.s.), while DIBI (80 mg/kg i.p. + 80 mg/kg i.v.) did not alter the bacterial burden in PLF.

The 8 hour CASP experiment resulted in bacteremia measured by CFU in the blood. Samples from SHAM operated animals possessed very small amounts of bacteria, mean= 8.65 CFU/ml (Figure 26), which could have been due to contamination/human error. Untreated CASP animals had a mean bacterial load of $2.5x10^4$ CFU/ml, but this was not significantly increased from SHAM operated animals. Administration of DIBI (40 mg/kg i.p.), (80 mg/kg i.p.), and (80mg/kg i.p. + 80mg/kg i.v.) increased bacterial burden to $5x10^5$ CFU/ml, $1.7x10^5$ CFU/ml, and $1.04x10^5$ CFU/ml respectively (n.s.).

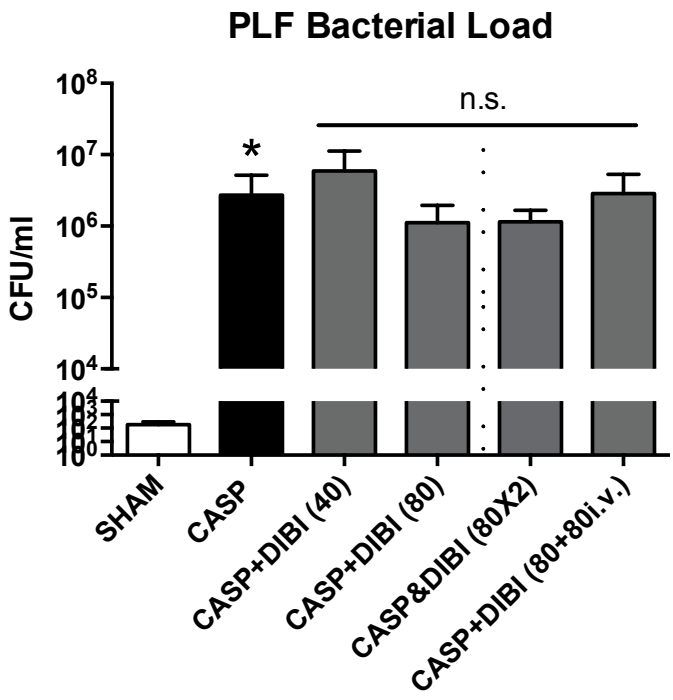

Figure 25. Bacterial load in the PLF of mice 8 hours after CASP completion. Bacterial burden was assessed by plating PLF samples in tryptic soy agar plates and counting bacterial colonies 16-24 hours later (CFU/ml). Data are represented as mean ± SEM (n= 5-7 per group); * $p < 0.05$ compared to SHAM group.

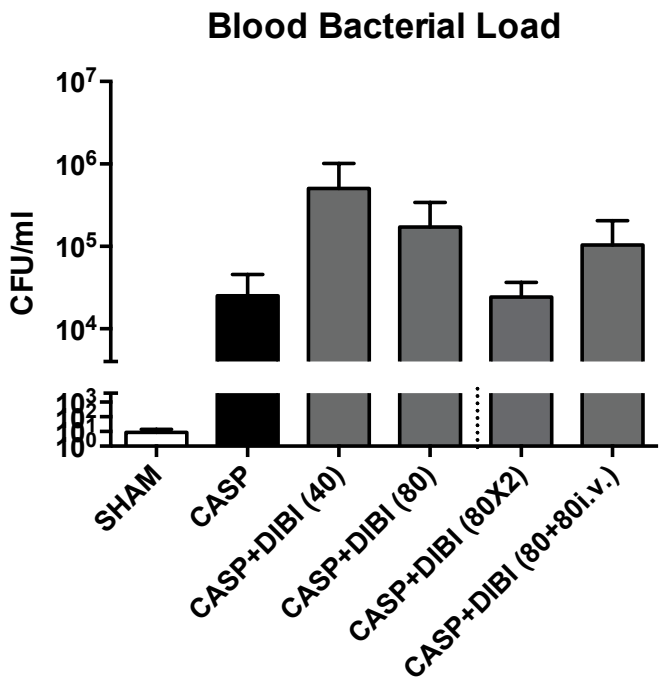

Figure 26. Bacterial load in the blood of mice 8 hours after CASP completion. Bacterial burden was assessed by plating blood samples in tryptic soy agar plates and counting bacterial colonies 16-24 hours later (CFU/ml). Data are represented as mean ± SEM (n= 3-5 per group).

3.2.4 Microbiome Sequencing

The DNA in PLF samples were sent for microbiome sequencing to determine the proportions of bacterial species in the sample and how DIBI affected the growth of bacterial populations. PLF samples from SHAM animals did not contain an adequate amount of DNA to obtain sequencing results, as determined by the alpha-diversity rarefaction plot (Figure 27). In untreated CASP animals, the class Bacteroidia comprised the majority of the samples with Bacilli, Clostridia and Gammaproteobacteria also being major components (Figure 28). Administration of DIBI (40 mg/kg i.p.), (80 mg/kg i.p.), and (80 mg/kg x 2 i.p.) did not consistently change the composition of the PLF samples; however, administration of DIBI (80 mg/kg i.p.+ 80 mg/kg i.v.) eliminated populations of Bacteroidia, Clostridia, and Bacilli that were present in other CASP operated groups. The major populations of bacteria making up samples treated with DIBI (80 mg/kg i.p.+ 80 mg/kg i.v.) consisted of Gammaproteobacteria and Betaproteobacteria.

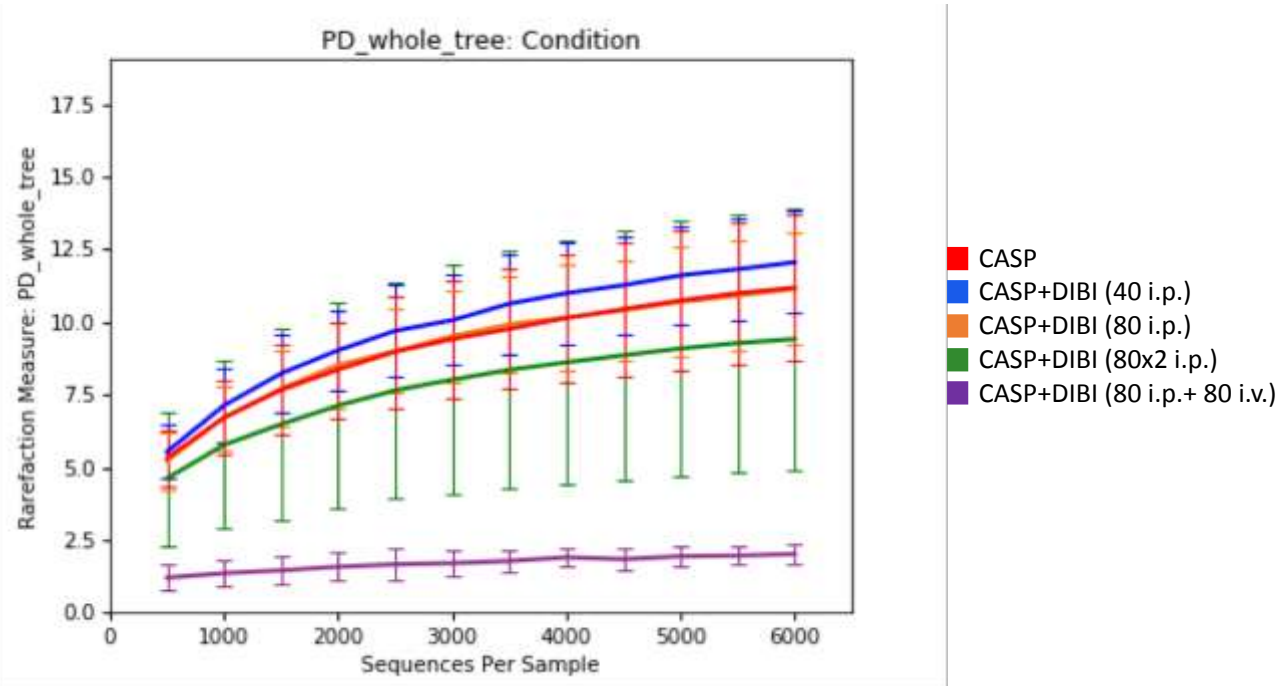

Figure 27. Alpha rarefaction curve representing the phylogenetic diversity for each group of samples. A rarefaction is a random collection of sequences from a sample, with a specified depth (number of sequences). This plot represents the expected diversity of a sample. n= 4-5 per group.

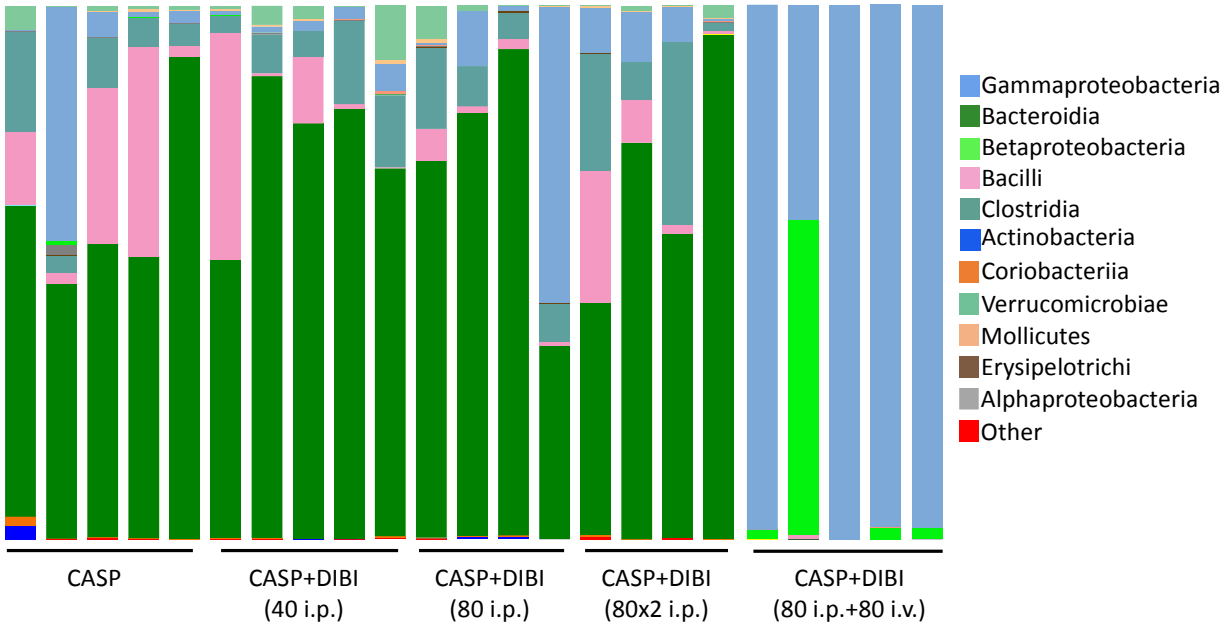

Figure 28. Taxonomic summary of microbiome sequencing at the class level. Bar graph plot of the taxonomic composition of bacteria in PLF samples. SHAM animals had an insufficient amount of DNA in samples to analyze. n= 4-5 per group.

3.2.5 Plasma Cytokines and Adhesion Molecules

To further assess the inflammatory state of SHAM and CASP operated animals, levels of cytokines and adhesion molecules were assessed in plasma samples obtained 9 hours after initial completion of CASP/SHAM surgeries.

Analysis of TNF-α levels indicated a significant increase ($p < 0.05$) in CASP animals compared to SHAM operated animals, in whom plasma TNF-α was undetectable (Figure 29). Plasma TNF-α levels were significantly increased ($p < 0.05$) from SHAM levels with administration of DIBI (80 mg/kg i.p. + i.v.), but no significant effects were found in other DIBI treatment groups. Plasma IL-6 levels were only significantly increased ($p < 0.05$) from SHAM levels with administration of DIBI (80 mg/kg i.p. + i.v.) (Figure 29). Plasma IFN-γ levels were significantly decreased ($p < 0.05$) with CASP surgery compared to SHAM operated animals (Figure 30). Administration of DIBI (80 mg/kg i.p. x 2) significantly increased ($p = 0.0036$) plasma IFN-γ levels, but no significant differences were found in the other DIBI dosing strategies. Plasma levels of IL-12p70 were undetectable in SHAM operated animals, and CASP surgery did not significantly alter levels (Figure 30). Administration of DIBI (80 mg/kg i.p. + 80 mg/kg i.v.) significantly increased ($p < 0.05$) IL-12p70 levels compared to SHAM and CASP operated animals. The anti-inflammatory cytokine IL-10 was significantly increased ($p < 0.05$) after CASP operation and all DIBI dosing strategies, excluding DIBI (80 mg/kg i.p.) (Figure 31). Concentrations of IL-17A were not significantly increased with untreated CASP compared to SHAM. In addition, none of the DIBI dosing strategies significantly altered IL-17A levels from CASP or SHAM, except DIBI (80 mg/kg i.p. + 80 mg/kg i.v.), which was significantly increased ($p < 0.05$) compared to SHAM (Figure

31). Concentrations of IL-4 significantly decreased ($p < 0.05$) with CASP surgery compared to SHAM operated animals (Figure 32). All DIBI dosing strategies increased plasma IL-4 levels significantly ($p < 0.05$) compared to untreated CASP. Plasma IL-13 levels were not significantly altered after untreated CASP or DIBI treatments (Figure 32).

The levels of soluble plasma adhesion molecules P-selectin and ICAM-1 were also assessed 9 hours following CASP surgery. Plasma levels of ICAM-1 were significantly increased ($p < 0.05$) with CASP, DIBI (80 mg/kg i.p.), DIBI (80 mg/kg i.p. x 2), and DIBI (80 mg/kg i.p. + 80 mg/kg i.v.) compared to SHAM operated animals (Figure 33). Administration of DIBI (80 mg/kg i.p. x 2) resulted in a significant increase ($p < 0.05$) compared to untreated CASP. Concentrations of soluble P-selectin were not significantly altered after CASP surgery or DIBI treatments (Figure 33).

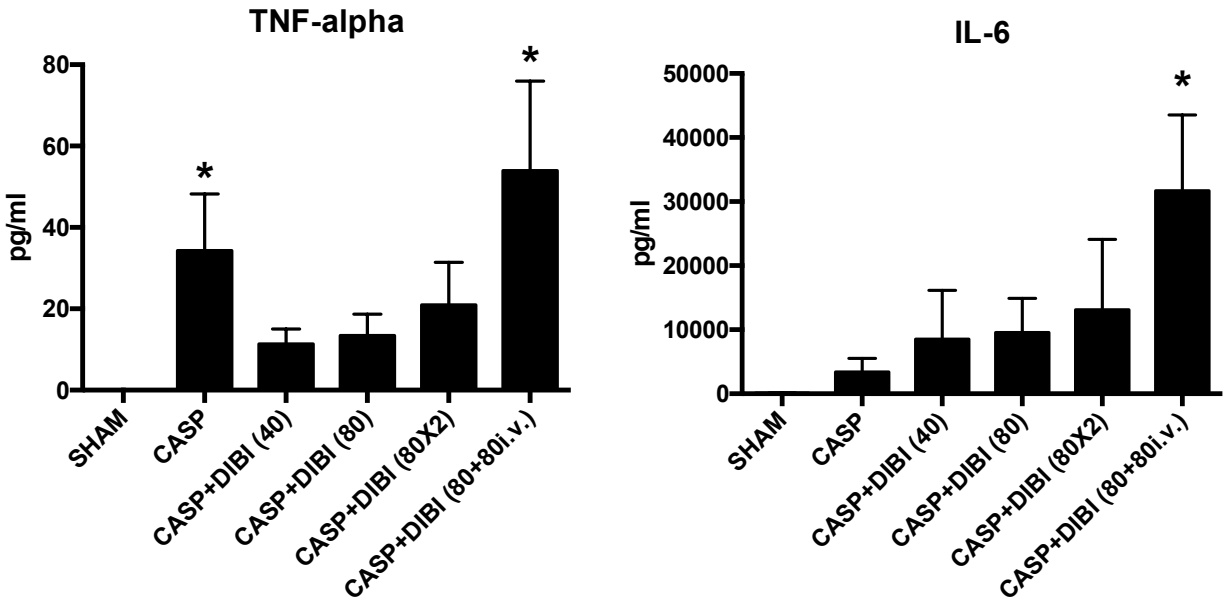

Figure 29. Plasma cytokine levels of TNF-α and IL-6. Samples were taken nine hours after initial CASP/SHAM procedure. Bar graphs represent mean cytokine values ± SEM (n = 3-5 per group); * $p < 0.05$ compared to SHAM group.

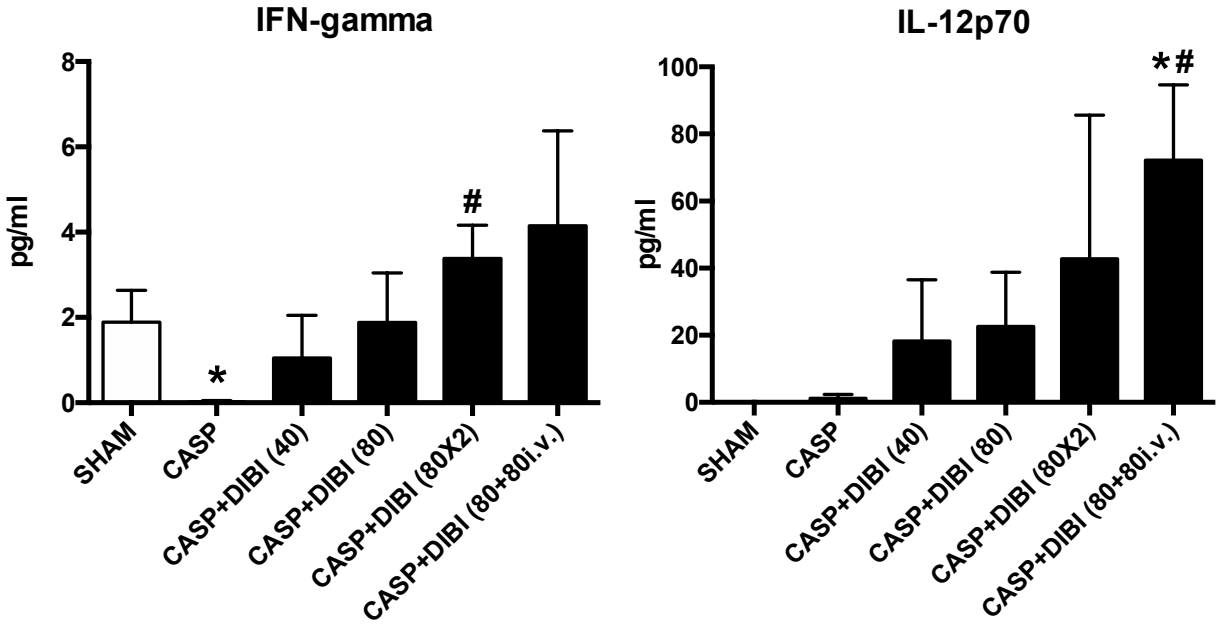

Figure 30. Plasma cytokine levels of IFN-gamma and IL-12p70. Samples were taken nine hours after initial CASP/SHAM procedure. Bar graphs represent mean cytokine values ± SEM (n = 3-5 per group); * $p < 0.05$ compared to SHAM group, # $p < 0.05$ compared to CASP group.

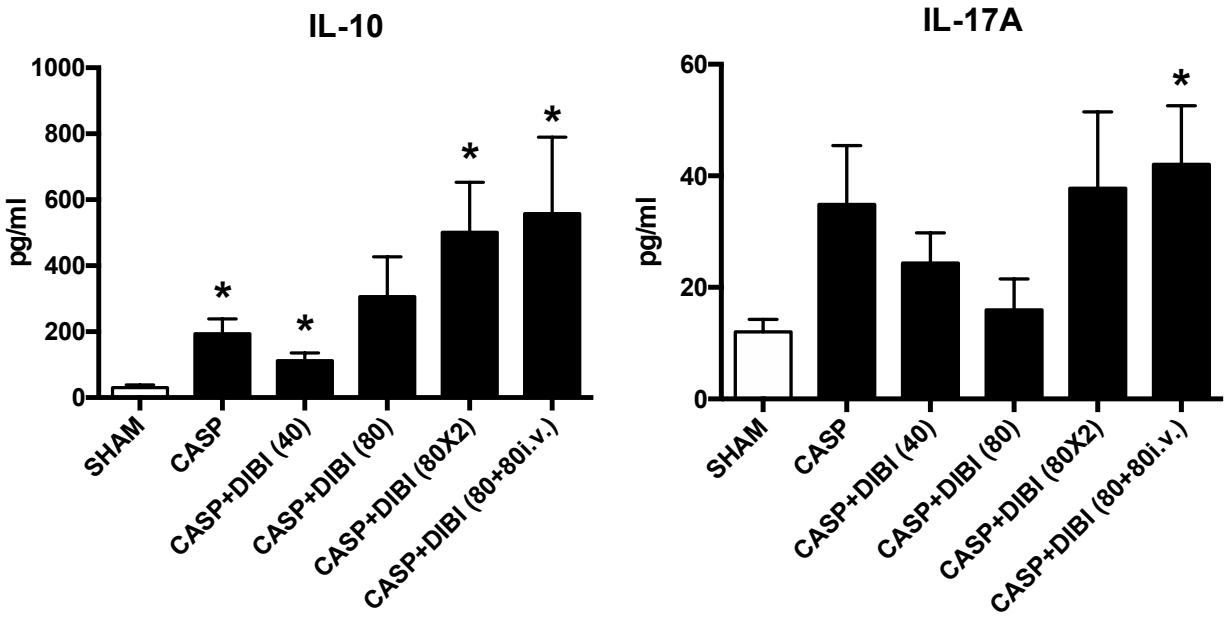

Figure 31. Plasma cytokine levels of IL-10 and IL-17A. Samples were taken nine hours after initial CASP/SHAM procedure. Bar graphs represent mean cytokine values ± SEM (n = 3-5 per group); * $p < 0.05$ compared to SHAM group, # $p < 0.05$ compared to CASP group.

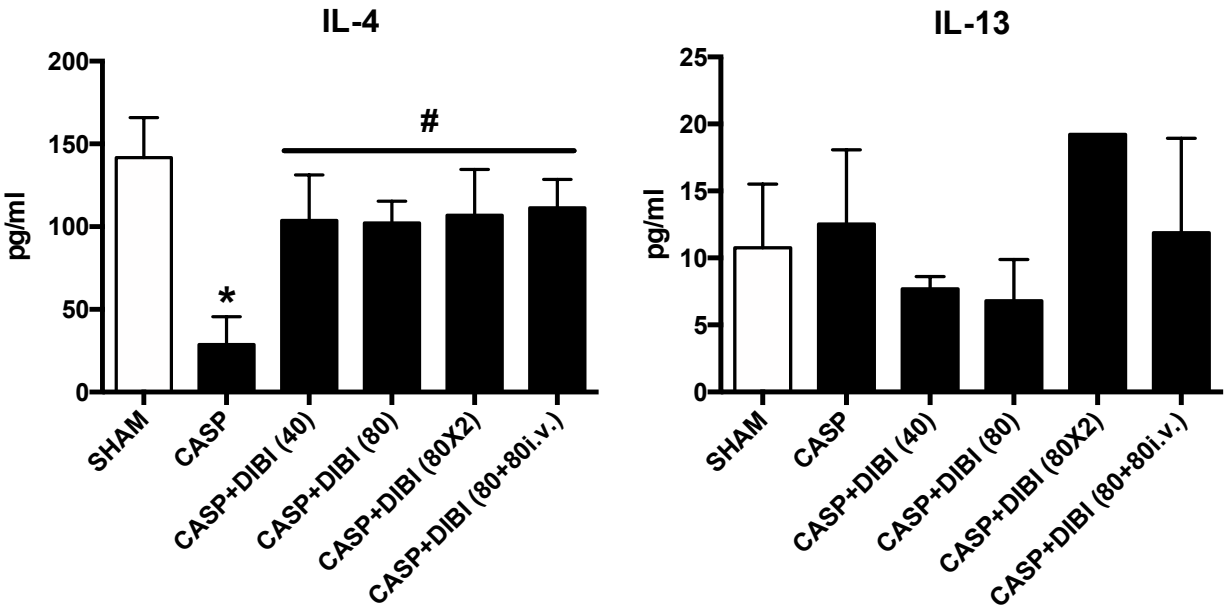

Figure 32. Plasma cytokine levels of IL-4 and IL-13. Samples were taken nine hours after initial CASP/SHAM procedure. Bar graphs represent mean cytokine values ± SEM (n = 3-5 per group); * $p < 0.05$ compared to SHAM group, # $p < 0.05$ compared to CASP group.

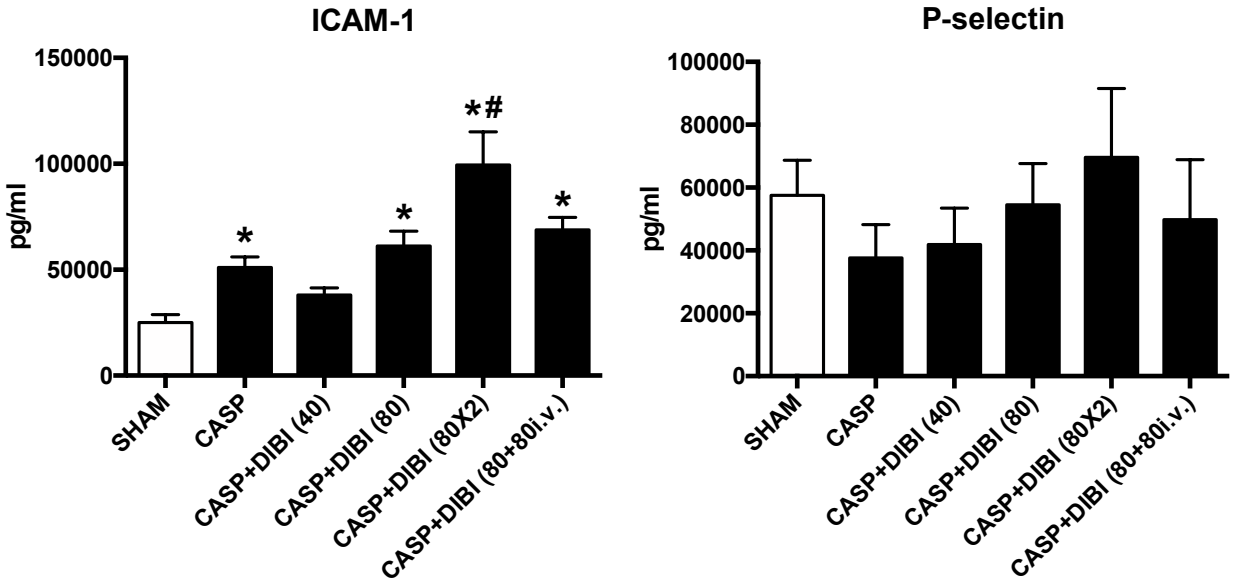

Figure 33. Plasma adhesion molecule levels of ICAM-1 and P-selectin. Samples were taken nine hours after initial CASP/SHAM procedure. Bar graphs represent mean cytokine values ± SEM (n = 3-5 per group); * $p < 0.05$ compared to SHAM group, # $p < 0.05$ compared to CASP group.

CHAPTER 4: DISCUSSION

The rising incidence rates of sepsis, coupled with its unacceptably high mortality rate, calls for an effective treatment that targets the exaggerated immune responses during sepsis. Multiple anti-inflammatory therapeutic interventions targeting the hyper-inflammatory response have been studied, including, but not limited to TNF-α and IL-1β antagonists, TLR4-antagonists, endotoxin antibodies, and anti-coagulants (6,106–108). Ultimately, none of these interventions showed significant benefits in humans (109). Sepsis therapies that target oxidative stress have also been an attractive option due to the role oxidative stress plays in sepsis pathologies. Antioxidant therapies have shown beneficial effects in experimental sepsis models (110), but antioxidants can also have adverse effects if consumed at levels significantly above the recommended dietary intake (111). Therapeutic interventions with iron chelators have an impact on the oxidant status by reducing ROS levels contributing to oxidative stress. The iron chelator deferoxamine has been tested in experimental sepsis models, with reported beneficial effects such as improved survival, decreased oxidative stress and reduced leukocyte infiltration (112,113). This is the first study to demonstrate anti-oxidant functions of a novel iron chelator, DIBI, and its anti-inflammatory effects in experimental sepsis with regard to changes in the intestinal microcirculation.

4.1 ROS Measuring Assays

In order to confirm the anti-oxidative effects of DIBI, *in vitro* studies were performed on macrophages and neutrophils. In the ROS measuring assays, DIBI reduced

intracellular ROS production in LPS-stimulated macrophages (Figure 10) and reduced extracellular ROS production in LPS-stimulated neutrophils (Figure 12 & Figure 13).

During infection, immune cells hold iron within intracellular compartments to reduce its bioavailability to microorganisms. DIBI is a large molecule and its ability to chelate intracellular iron is unclear. The DCFDA assay is a commonly performed method to detect intracellular levels of ROS by a single measurement of fluorescence and was used to evaluate DIBI's intracellular effects on ROS production in LPS-stimulated neutrophils and macrophages. LPS is a potent inducer of ROS by interacting with TLRs to trigger inflammatory responses, including the activation of Nox, and subsequently the respiratory burst (58,79). In this assay, as expected, LPS stimulation induced ROS production in macrophages, which was significantly reduced when LPS-stimulated cells were treated with DIBI. Although we anticipated that DIBI would reduce ROS formation by limiting extracellular iron availability, the intracellular effects of DIBI have not been characterized. According to current literature, the clinically used iron chelators DFX, DFP, and DFO have been found to work intracellularly or extracellularly depending, on characteristics such as size, charge and lipid solubility (114). Low molecular weight chelators, such as DFP, can act on intracellular compartments and rapidly access iron pools, allowing them to "shuttle" iron out of cells; however, DFP has a weak affinity for iron; therefore, much of the bound iron will be lost before it is excreted (115). Larger chelators, such as DFO, have slower kinetic access to iron, but once bound they act as an iron "sink", accepting iron with high stability (114). Some studies have tried combining "shuttle" and "sink" chelators to optimize iron removal (114,115): this would also be an option to maximize the effects of DIBI.

In the DCFDA assay on neutrophils, LPS-stimulation did not induce intracellular ROS generation, but there was a significant increase in ROS when cells were stimulated with the positive control (H_2O_2) (Figure 11). This confirms these results were not due to a problem with the assay, such as the cells not taking up the DCFDA compound. To determine whether these findings were consistent with other studies that tried to detect intracellular ROS production by LPS-stimulated neutrophils, the literature revealed mixed results. Some studies are in line with our findings, reporting that LPS was not able to significantly increase ROS accumulation (116). However, a study by Ren *et al*. (117) measured intracellular ROS production in human neutrophils stimulated with 1 μg/ml LPS. In our studies, neutrophils were stimulated with 100ng/ml LPS, so perhaps adjustments in the LPS dosage could have generated a significant increase in ROS production. Additionally, the size of the encountered microbe can influence the location of ROS release, with larger molecules stimulating extracellular release of ROS (117). Perhaps, due to the high molecular weight of LPS (~100 kDa), the NADPH oxidase was assembled on the plasma membrane, generating ROS that was extracellular.

To delve deeper into DIBI's anti-oxidant effects on neutrophils, the Amplex Red and Griess assays were used to assess extracellular ROS production. Neutrophils are well known for their potent antimicrobial defense actions, releasing ROS and other pro-inflammatory mediators upon activation by inflammatory stimuli, such LPS (48,118). As expected, in the Amplex Red and Griess assays, LPS stimulation induced extracellular H_2O_2 and NO production, respectively. In the Amplex red assay, DIBI treatment significantly reduced H_2O_2 production in LPS-stimulated neutrophils (Figure 12).

However, in the Griess assay, NO levels were not significantly reduced upon DIBI treatment in LPS-stimulated neutrophils (Figure 13).

Upon neutrophil activation by LPS, H_2O_2 is generated during the respiratory burst via Nox (119). Iron is not directly linked to H_2O_2 generation; however, when iron is present with H_2O_2, it will catalyze the formation of hydroxyl radicals. These radicals are extremely potent and will indiscriminately damage tissues, propagating inflammation and triggering a feed forward mechanism of increased ROS production. DIBI administration may break this cycle by restricting iron's availability to catalyze hydroxyl radical formation, thereby diminishing further inflammation and immune cell recruitment and limiting the pro-inflammatory stimuli that drives additional H_2O_2 generation.

Similarly to H_2O_2, iron is not directly involved in NO production. Rather, neutrophil stimulation by bacterial products or inflammatory mediators induces *de novo* synthesis of inducible nitric oxide synthase (iNOS), producing NO (86,120). Reducing the cycle of ROS production by DIBI may also reduce the inflammatory stimuli that leads to NO production. However, in our findings, DIBI did not significantly reduce NO generation. In our experiments, NO production was measured two hours after LPS stimulation. Due to the relatively low levels of NO detected in our studies, perhaps this incubation time was inadequate for a strong induction of NO. In a study by Kaplan *et al*. (121), NO production was measured in human neutrophils 6 and 12 hours after LPS stimulation, with significant differences found between groups. Perhaps, in our studies, if neutrophils had a longer incubation period, DIBI could have more time to exert a significant effect.

Overall, these findings provide evidence of an anti-oxidant effect of DIBI by reducing intracellular levels of ROS in macrophages, and extracellular levels of ROS in neutrophils. Although iron is not directly involved in generating all species of ROS, by limiting the production of the most potent ROS species, the hydroxyl radical, DIBI may break the cycle of ROS generation, immune stimulation and damage, and more ROS generation.

4.2 Chemokinesis Assay

Leukocyte transmigration through endothelial cells to the inflammatory stimulus represents the next step in the leukocyte activation cascade after firm adhesion to the endothelium (43). *In vitro,* LPS-stimulation has been found to induce macrophage polarization and elongation, contributing to their accelerated movement to an inflammatory stimulus (122). Unexpectedly, our findings show migration was reduced in LPS-stimulated macrophages, and naïve macrophages treated with DIBI (Figure 14). Furthermore, DIBI in combination with LPS-stimulation produced an apparent enhanced effect, further reducing macrophage migration. It was expected that LPS stimulation would increase migration, and DIBI may reduce, or have no effect on macrophage migration. However, the obtained results may be explained by the nature of the assay and the cell line chosen.

The chemokinesis assay, also known as the scratch assay, is used to study cell-cell interactions and the undirected migration of cells. During leukocyte transmigration, cells migrate along a chemical gradient in response to a stimulus, but because there is no chemical gradient with the chemokinesis assay, the migration observed is not mimicking

leukocyte transmigration. A more appropriate assay to study leukocyte transmigration would be a transwell assay (also known as Boyden Chamber assay). These assays are used frequently to assess the directed migration of cells to a stimulus (44,123,124). Additionally, macrophages were chosen for this assay because they are adherent cells and function well in this assay; however, macrophages make up a small component of circulating leukocytes (about 3%) (125), making them a less relevant cell line for what we sought to study. Neutrophils would have been a more relevant cell to use because they are the primary cells observed during IVM and make up the majority of leukocytes in the blood (126).

After identifying the limitations of the assay, the findings could be interpreted as follows. Firstly, although LPS-stimulation of macrophages has been observed to increase migration in transwell migration assays (124,127,128), we likely did not see an increase in migration because in our assay, macrophages were not provided with a chemoattractant. Also, upon activation and arrival to an infection, macrophages will stay at the site, producing cytokines and chemoattractants to recruit additional leukocytes (125,129). This may account for the decreased migration observed in our findings. Secondly, the reduced migration of macrophages with DIBI treatment, and the enhanced effects of LPS and DIBI, could be explained by an interruption in cell signaling. Beyond ROS's microbial killing functions, ROS have also been found to act as secondary messengers, performing functions that include activating signaling pathways (76). Kastl *et al*. (130) found that induction of ROS in murine hepatocytes enhanced cell migration in a wound healing assay, and the effects were reversed upon addition of N-acetylcystein, a ROS scavenger. The observed decreased migration in our studies could represent

additional anti-inflammatory effects of DIBI, potentially reducing hyper-activation of immune cells during sepsis.

4.3 Endotoxemia

Endotoxemia experiments reproduce many pathophysiologic features of sepsis without an infectious focus. The endotoxemia model is a highly controlled and standardized model, inducing endotoxemia in mice by systemic administration of LPS, an endotoxin of Gram-negative bacteria. LPS is used as a substitute for live bacteria, activating pro-inflammatory pathways, and causing an exaggerated systemic host response to the presence of bacterial antigens (131). The endotoxemia model has multiple advantages including its ease of administration, high reproducibility, and the pathological changes induced by LPS are similar to clinical changes observed in sepsis patients (131). Therefore, this model was first used to evaluate the effects of iron chelation during an acute hyper-inflammatory state of sepsis.

4.3.1 Intravital Microscopy

Intravital microscopy allowed us to observe live leukocyte endothelial interactions in the microvasculature of the intestine while maintaining physiologic conditions. This technique has been well-established in our lab, and can be used to study microcirculatory changes at various sites including the intestine, eye, and brain (96,132–134).

Leukocyte adherence in the submucosal V1 venules was our primary endpoint for assessing immune activation in the endotoxemia model because leukocytes adhering to the endothelium are highly activated and ready to transmigrate. In our control group, we

observed basal levels of leukocyte adhesion and high amounts of rolling leukocytes in both the V1 and V3 venules. This was expected due to the surgical trauma induced by jugular vein catherization and laparotomy. Intravenous administration of LPS (5 mg/kg) has previously been reported to increase leukocyte adherence to endothelial cells, which is in line with our findings where a significant increase in the number of adhering leukocytes was observed in the V1 and V3 venules after LPS stimulation compared to control groups (Figure 15 and Figure 16). The increase in leukocyte activation is due to the up-regulation of adhesion molecules by endothelial cells and leukocytes upon activation by bacterial antigens such as LPS (39). Administration of DIBI was successful in attenuating the number of adherent leukocytes in doses of 10 mg/kg and 5 mg/kg, while DIBI (2.5 mg/kg) had no significant effects. These results were expected based on the anti-oxidative actions of DIBI observed in our *in vitro* findings, and the link between high levels of ROS exacerbating inflammatory responses (135,136). Due to the novelty of DIBI, its anti-inflammatory actions are not well characterized; however, reducing oxidative stress by iron chelation has been found to be successful in attenuating immune hyper-activation, and improving survival in other models of endotoxemia (137,138).

As part of these studies, the effects of PVP were also tested in the endotoxemia model. PVP represents the backbone of DIBI without iron binding capabilities. We found here that PVP significantly reduced leukocyte adhesion in the V1 venules compared to untreated LPS animals, but the number of adhering leukocytes in the V3 venules remained significantly higher than control animals (Figure 16). PVP is one of the most widely used polymers in medicine because it is water soluble and non-toxic (139). In the past, PVP has been used as plasma volume expander due to its ability to act as a colloid.

Synthetic colloids, such as hydroxyethyl starch (HES), have been found to have protective effects against reperfusion injury by inhibiting adhesive interactions between neutrophils and endothelial cells (140–144). Therefore, PVP's observed effects could be a result of volume expanding effects, whereby PVP disrupts adhesive interactions between neutrophils and endothelial cells. On its own, PVP has not been found to possess direct antibacterial effects *in vitro*; however, when complexed with other compounds such as iodine or silver, it increases their antimicrobial actions by dispersing the compounds in solution, and increasing the surface-to-volume ratio (145,146).

Accompanying the LPS-induced increase in leukocyte adherence was a significant reduction in the number of rolling leukocytes in the V1 and V3 venules, indicating that the inflammatory stimulus caused most of the rolling leukocytes to adhere to the endothelium (Figure 17). We expected the reduction of adherent leukocytes to cause a concomitant increase in rolling leukocytes; however, none of our treatments restored leukocyte rolling to normal levels, even when leukocyte adherence was significantly reduced. In control groups, leukocyte rolling is controlled by the expression of selectins and their receptors on leukocytes and endothelial cells. If DIBI is attenuating the inflammatory environment as we expect, DIBI administration may cause a reduced expression of these selectin receptors, minimizing leukocyte rolling and adherence. Furthermore, if the PVP backbone of DIBI has volume expanding effects, this could also reduce leukocyte rolling and adherence.

As part of the endotoxemia experiments, capillary perfusion was observed in the intestinal microcirculation of endotoxemic mice because microcirculatory dysfunction represents a key feature in the pathophysiologic cascade of sepsis. Microcirculatory

disturbances in sepsis are multifactorial, arising from factors such as leukocyte activation, red blood cell activation, and edema externally compressing microvessels. As expected, LPS administration significantly reduced capillary perfusion in the muscle layer and mucosal villi of the intestine from control levels (Figure 18 and Figure 19). Administration of DIBI and PVP in endotoxemic mice were able to significantly prevent the LPS-induced reduction of FCD in the muscle layer and mucosal villi of the intestinal microcirculation. These results suggest that by limiting irons participation in ROS-generating reactions early during an inflammatory state, we can minimize microcirculatory disturbances that develop disease pathologies.

4.4 Colon Ascendens Stent Peritonitis

Although the LPS-induced endotoxemia model has many advantages, such as its simplicity and high reproducibility, it also has disadvantages. Firstly, the ability to tightly control the dose of the stimulating agent and induce similar physiological changes in each animal can be considered an advantage. However, it is also a major drawback because it is not representing the diverse physiological responses observed clinically. Also, the endotoxemia model lacks the presence of viable pathogens, therefore the complete pathophysiologic changes occurring during sepsis is not well represented in this model. Additionally, LPS administration in mice results in a very rapid release in systemic cytokines, differing from clinical sepsis, which shows a more gradual prolonged elevation of systemic cytokine levels (147). The significance of these differences can be recognized when treatments found to be beneficial in endotoxemia models, such as inhibiting

inflammatory mediators, fail to demonstrate substantial benefit in clinical trials (148,149).

In the development of therapeutic options for sepsis, a model needs to be used that more closely mimics the course of human disease. To overcome drawbacks of the endotoxemia model, specifically the lack of viable pathogens, host-barrier disruption models that induce sepsis by endogenous fecal contamination through organ barrier disruption have been employed. Of these models, CASP and cecal ligation and puncture (CLP) represent the most reliable and clinically relevant models to study human sepsis (150). Although both models have been used extensively and offer advantages for analyzing different aspects of sepsis, published data indicates that CASP creates a more reliable model than CLP (151,152). Stent insertion in the CASP model generates a consistent leakage of fecal matter into the peritoneum, inducing peritonitis and bacteremia. Whereas in the CLP model, bowel perforations created by cecal ligation and puncture can be blocked by the formation of abscesses over the perforations, preventing the progression of peritonitis (150). For these reasons, the CASP model was chosen to study the anti-inflammatory effects of DIBI in a clinically relevant sepsis model.

4.4.1 Intravital Microscopy

To complement our endotoxemia model, we decided to first use IVM to assess detrimental microcirculatory changes produced by CASP-induced peritonitis and the potential benefits of iron chelation therapy in attenuating these effects. In our SHAM operated animals, we observed basal levels of leukocyte adhesion and high amounts of rolling leukocytes in both the V1 and V3 venules, which are expected due to the trauma

induced by the laparotomy surgery (Figure 20 and Figure 21). The CASP surgery caused a significant increase in adhering leukocytes in the V1 venules of the intestinal microcirculation compared to the SHAM group. These findings are consistent with previous CASP studies that assessed leukocyte recruitment and infiltration in various organs (96,132,153,154). Also, as expected, the variability in the numbers of adhering leukocytes were far greater in the CASP studies than the endotoxemia experiments. This could account for a lack of statistical significance found in our results of leukocyte adhesion in the V3 venules. Furthermore, consistent with our results from endotoxemia experiments, CASP surgery caused a significant reduction in leukocyte rolling in the V1 and V3 venules, presumably because the majority of leukocytes were adhering to the endothelium.

When deciding a dosing strategy for DIBI, we turned to a previous CASP study by our lab that found significant reductions in leukocyte activation 16h after CASP when DIBI was administered i.p. at a dosage of 40 mg/kg (96); therefore, we decided to use this as a starting dose for our model. We found that DIBI (40 mg/kg i.p.) did not significantly reduce the number of adhering leukocytes, which was inconsistent with previous reports from Islam *et al.* (96). Due to the relatively short time frame (8h) until observation after stent implantation, it may have not been a sufficient amount of time for DIBI to have an effect. However, when we increased the DIBI dosage to 80 mg/kg given i.p., the number of adhering leukocytes were significantly decreased in the submucosal V1 venules compared to CASP operated animals. This reduction in leukocyte adherence by DIBI (80 mg/kg) was not a complete reversal to levels observed in SHAM operated animals, but a more modest reduction in leukocyte hyper-activation. We believe this is a favourable

response since an adequate level of immune cell activation is still needed to promote bacterial clearance, but the damage associated with exaggerated pro-inflammatory mediator production and immune infiltration is still reduced.

The half-life of DIBI has not been fully characterized, although initial reports suggest DIBI has a short half-life of less than two hours, similar to half-lives of other clinically used iron chelators (155). For this reason, additional doses of DIBI were given both i.p. and i.v. four hours after the initial CASP insult. We were most interested in the anti-bacterial effects additional doses would cause due to the limited effects of other doses, which will be discussed in more detail later. Surprisingly, additional doses did not further reduce the number of adherent leukocytes in the V1 venules, and the second dose of DIBI administered i.v. had less of an effect on reducing leukocyte adherence than a single dose administered i.p. In order to provide a possible explanation for these observations several issues need to be addressed. First, could high doses of DIBI be toxic? This is unlikely as the acute and chronic systemic toxicity of DIBI has been tested and no significant adverse effects were found in rats receiving daily i.v. administration of DIBI up to 200 mg/kg for 14 days (Holbein, unpublished). On the other hand, although DIBI itself is not toxic, reducing systemic iron levels to an exceptionally low level may cause adverse effects, particularly during a time of systemic infection. Iron deficiency has been found to influence the immune response to infection, but in a way that's characterized by reduced phagocytic activity, oxidative burst, and cytokine production (156). Therefore, low iron levels are less likely to explain the changes we observed. Our answer may lie in the effects DIBI had, not on the immune cells, but on the bacteria inducing the immune response. Although the total numbers of bacteria measured from the

peritoneal lavage fluid were not significantly altered with DIBI treatments, microbiome analysis of those samples found that the additional i.v. dose of DIBI caused a major change in the proportions of bacterial species colonizing the peritoneal cavity. The pathogenic consequences of bacterial colonization depend on the varying virulence factors of different bacteria species. Before DIBI 80 i.p.+ 80 i.v., the majority of the microbiome was composed of Bacteroidia species, which although Gram-negative, the endotoxins produced by some of the species that make up this class, such as *B. fragilis* (the most common cause of bacterial sepsis), are 10-1000 times less toxic than that of *E. coli* (157). The other major components were Gram-positive species (Bacilli, Clostridia), which are also less virulent than the Gram-negative bacteria (Gammaproteobacteria, Betaproteobacteria) that made up the microbiome composition after DIBI 80 i.p.+ 80 i.v. The high toxicity of the endotoxins produced by species of these bacterial classes, such as *E. coli,* could have accounted for the observed increase in leukocyte adherence by stimulating more pro-inflammatory mediators.

As part of our CASP studies we also measured functional capillary density in the muscle layer and mucosal villi within the intestinal microcirculation. Similar to our endotoxemia experiments, 8 hours after the CASP surgery there was a significant reduction in the amount of perfused capillaries in the mucosal villi and muscle layer in the terminal ileum (Figure 23 and Figure 24). Contrary to results from endotoxemia experiments, no DIBI dosing strategies significantly prevented CASP-induced reductions of FCD in the muscle layer or mucosal villi. The discrepancies between DIBI's effects in the endotoxemia model and CASP model is likely due to the more complex pathological changes induced by live bacteria in the CASP model. This highlights the importance of

using clinically relevant models to test drug therapies as more simple models may show greater significance than what may be observed clinically.

4.4.2 Bacterial Quantification and Microbiome Analysis

During the 8h time course of CASP, fecal matter diffuse from the intestine into the peritoneal cavity, closely mimicking the clinical course of diffuse fecal peritonitis. The active bacterial infection in the CASP model gave us to opportunity to assess anti-bacterial effects of DIBI *in vivo.* In the limited published studies using DIBI, it has been found to possess specific anti-microbial effects. In a study by Holbein and Orduna (98), DIBI, but not DFP or DFO, was found to limit the growth of *Candida albicans* and *Candida vini in vitro.* Similar results were found in a study by Savage *et al*. (158) in which DIBI, but not DFO or DFP, inhibited the growth of *C. albicans in vitro*. Additionally, as part of this study, the influence of iron withdrawal on the activity of antifungals was evaluated in an experimental mouse model of *C. albicans* vaginitis. DIBI in combination with fluconazole, an antifungal medication, enhanced the rate of clearance compared to fluconazole treatment alone. However, administration of DIBI alone had no effect on vaginal fungal burden. Furthermore, a CASP study by Islam *et al*. (96), showed a significant reduction of bacterial burden in the PLF and blood compared to untreated CASP with the combined administration of DIBI and imipenem, a Beta-lactam antibiotic. However, administration of DIBI alone had no significant effects on the bacterial burden in the blood or PLF compared to untreated CASP.

In our studies, the bacterial burden was extremely variable between mice, even between animals in the same group. As a result of this, no statistical significances could

be obtained in the bacterial counts from the blood or between treatment groups in the PLF. The extreme variability of bacterial counts in our model could be explained by the relatively short time frame of our study. The statistical significance reported by Islam *et al*. was obtained 16 hours after the initial stent implantation, whereas our samples were obtained only 8 hours after stent implantation. Consistent with other studies that assessed DIBI's antimicrobial properties *in vivo,* we did not observe any significant effects on total bacterial counts after administration of DIBI. Perhaps if the CASP-intervention model was used (where the stent is removed and the intestine leak is fixed), DIBI could have exhibited more of an effect because there would not be a continuous flow of fecal matter.

The bacterial counts allowed us to assess the total number of bacteria in the mice, but they did not tell us what species made up the samples. Microbiome sequencing of the PLF samples gave us insight to the species comprising the bacteria colonizing the peritoneal cavity after CASP surgery. Essentially all microbial cells require iron for their growth, making the competition for bioavailable iron fierce between microbes colonizing the gut, and between invading microbes and eukaryotic host cells. These pressures caused some bacteria to evolve iron acquiring mechanisms, such as siderophore secretion, to obtain iron from their environment, resulting in some bacterial species that are susceptible to iron withdrawal than others. To our knowledge, no other study has evaluated the microbiome composition of mice following poly-bacterial sepsis and iron chelation. Firstly, it was determined by alpha rarefaction, that SHAM animals did not contain enough bacterial DNA to accurately determine samples, which was expected due to the very low bacterial counts in those samples. When microbiome sequencing was performed on the CASP operated animals, only the DIBI group with a second dose of

DIBI administered i.v. resulted in a significant change in the bacterial composition of the samples. The composition of the main classes in the samples switched from Bacteroidia, Bacilli, and Clostridia, to Gammaproteobacteria and Betaproteobacteria.

To understand the significance of this change and how it could have affected other parameters measured in this study, we must first know some basic characteristics of these classes of bacteria. Making up the majority of the microbiome composition before i.v. DIBI administration was the class Bacteroidia. Species in this class are Gram-negative and normally have a mutualistic relationship with the host when retained in the gut, but if they escape, they can cause significant pathology, including intra-abdominal infection leading to sepsis (159,160). Bacteroidia species are reported to have the most antibiotic resistant mechanisms of all Gram-negative Bacilli, with each strain requiring a specific antibiotic therapy (157,161). Interestingly, DIBI administered i.v. completely eliminated Bacteroidia species in the peritoneal cavity without the help of antibiotics. There is no apparent evidence that Bacteroidia species possess iron-acquiring mechanisms, potentially making them particularly sensitive to iron-removal (157). To our knowledge, this is the only study that has observed the elimination of Bacterioidia species in the presence of iron-chelating agents, representing a promising role for DIBI in restoring antibiotic efficacy against Bacteroidia infections. The next class of bacteria that made up a major component of the microbiome were Bacilli species. Bacilli are almost exclusively Gram-positive bacteria with a wide range of physiologic abilities, allowing them to adapt to a wide range of environments (162). As part of the gut microbiome, Bacilli help maintain intestinal homeostasis by aiding in the metabolism of dietary components and drugs (163). However, Bacilli species, particularly *B. cereus*, have been associated as

causative agents of bacteremia and peritonitis in immunosuppressed patients (164–166). Several Bacilli species, including *B. cereus,* have been reported to secrete siderophores in an attempt to adapt to low iron conditions; however, they secrete bidentate ligands, which have lower affinity for iron than hexadentate ligands, such as DIBI (167). Therefore, DIBI may have outcompeted Bacillli species for iron, thereby preventing their growth. Clostridia species made up another major component of the microbiome before i.v. DIBI administration. Clostridia is a class of Gram-positive bacteria that includes several significant human pathogens such as *C. difficile*, an important cause of diarrhea and recently classified as an "urgent" antibiotic resistant threat by the CDC (168). Although sepsis caused by Clostridia is uncommon, it does occur, with reports of severe sepsis linking *C. perfringens* and *C. difficile* as the infectious etiology (169,170). *C. perfringens* and *C. difficile* infections can be difficult to treat because they require specific antibiotics which requires confirmation of infectious etiology, delaying treatment. The elimination of Clostridia species in our study presents a possible role for DIBI in treating Clostridia infections. Iron acquisition systems have been identified in Clostridia species (171); however, DIBI may have stronger iron chelating abilities than the mechanisms Clostridia species use.

Gammaproteobacteria and Betaproteobacteria were the major classes of bacteria making up the microbiome after i.v. DIBI administration. They are both Gram-negative bacteria and contain a number of important pathogens including *Escherichia coli, Pseudomonas aeruginosa, Yersinia pestis, Vibrio cholera, Salmonella spp.* (Gammaproteobacteria), *Neisseria gonorrhoeae, Neisseria meningitidis,* and *Bordetella pertussis* (Betaproteobacteria). Several species from these classes are common causes of

bacterial sepsis including *E. coli, P. aeruginosa,* and *N. meningitidis* (172). The persistence of these bacterial species in the presence of DIBI may be due to the many sophisticated iron acquiring mechanisms possessed by members of these classes. For instance, the siderophore produced by *Y. pestis* is able to remove iron directly from transferrin and lactoferrin (173). Also, *E.coli* and *P. aeruginosa* produce catecholate siderophores with hexadentate binding capabilities similar to DIBI (173). Additionally, the catecholate siderophore produced by *E. coli* has the highest affinity toward iron than any other known siderophore. Ma *et al.* (174) studied the growth inhibiting effects of DFP and DFX on *E. coli* alone and in combination with antibiotics and found that iron chelation alone had no effect on *E. coli'*s growth. Although, DIBI has been found to reduce microbial growth better than other clinically used iron chelators, its growth inhibiting effects on *E. coli,* and other Gammaproteobacteria and Betaproteobacteria species have not been assessed *in vitro*. This represents a future direction we can take to confirm the findings from our study.

With the bacterial counts, we observed that there were no significant differences in the total amount of bacterial from the PLF, but microbiome sequencing revealed that administration of DIBI 80 mg/kg i.p. + 80 mg/kg i.v. affected the composition of bacteria in the PLF. The major question that these findings raise is whether or not the changes observed in the microbiome composition are beneficial. From other parameters measured in this study it appears that the shift in the microbiome caused a more pro-inflammatory environment due to the presence of highly toxic endotoxins produced by the Gram-negative species of Gammaproteobacteria and Betaproteobacteria. However, many bacterial species associated with antibiotic resistance and particularly deadly sepsis cases

were eliminated during this change. In order to determine the consequences of these changes, further experimentation using survival studies is needed to establish if the microbiome shift affects the long term survival of mice. Nonetheless, the bacterial killing effects of DIBI are exciting and point to a potential role for iron chelation in restoring the efficacy of antibiotics. Another important question from this study is why only the second dose of DIBI i.v. changed the microbiome composition. Perhaps local doses of DIBI did not completely remove iron from systemic circulation before being degraded, allowing for bacteria with weaker iron acquisition systems to still access iron. However, systemic administration of DIBI removed all free iron, only allowing for the growth of bacterial species with strong iron acquiring mechanisms. This is just speculation and further experimentation, perhaps by measuring free iron in circulation after local and systemic DIBI administration, could help explain our findings.

4.4.3 Cytokine Measurements

Cytokines are signaling molecules released by various cell types, usually in response to an activating stimulus. They regulate a number of physiological and pathological functions, including innate immunity. During sepsis, the host immune system is highly stimulated, producing excessive levels of cytokines and other proinflammatory mediators, often described as the 'cytokine storm' (175). High levels of pro-inflammatory cytokines such as TNF-α, IL-1β, and IL-6 have been measured in septic patients; therefore, we wanted to assess cytokine levels in mice after CASP-induced peritonitis and observe how iron-chelation therapy impacted cytokine production.

Consistent with our expectations, the results from our CASP experiments showed low or negligible levels of pro-inflammatory molecules in SHAM-operated animals. On the other hand, some cytokine levels measured from CASP-operated animals were inconsistent with previous reports, showing low expression of pro-inflammatory mediators (IL-6, IFN-γ) that are typically high in CASP models. Our measurements were performed a relatively short time (9 hours) after initial stent implantation, which could explain the low levels observed. However, systemic levels of pro and anti-inflammatory cytokines associated with septic peritonitis have been found to be elevated a short time (three hours) after CASP stent implantation (176,177). Conversely, others have found low cytokine levels after 3 hours, with peak production reached 12 hours after stent implantation (178). Another possible explanation for the low levels of cytokines observed in CASP animals is that blood was not obtained for the sickest animals. Blood samples were obtained 9 hours after the initial completion of the CASP surgery and 2 hours after IVM setup began. During IVM setup, the animals were under anesthetia for 2 hours, and had their internal organs exposed to the outside environment for around 1 hour while IVM was performed. Many untreated CASP animals were too sick to make it to the end of the entire experiment; therefore, there are only a few blood samples for untreated CASP, and they are from the healthiest animals. Additional experimentation is needed to determine why some of the cytokine levels were low, which includes blood collection at earlier and later time points, and more animals per group to reduce the impact of potential outliers.

TNF-α is a pro-inflammatory cytokine that plays a key role in the progression of inflammatory pathologies and induces the production of other pro-inflammatory

cytokines. TNF-α can have protective effects when released locally, but systemic release can have damaging effects, including vasodilation, increased vascular permeability and eventually organ failure (179). Upon induction, TNF-α has many effects, including activating neutrophils to produce a respiratory burst, and inducing the expression of adhesion molecules and selectins on endothelial cells (105). The CASP operation caused a significant increase in TNF-α levels compared to SHAM animals, and upon administration of DIBI 40 mg/kg i.p., 80 mg/kg i.p., and 80 mg/kg i.p. X2, TNF-α levels were no longer significantly increased from SHAM. However, the same effects were not observed with the highest dose of DIBI (80 mg/kg i.p. + 80 mg/kg i.v.) and TNF-α levels remained significantly higher than SHAM animals. TNF-α is commonly elicited by macrophages in response to LPS-bearing pathogens. Therefore, the presence of more Gram-negative bacteria observed in the microbiome sequencing results could have caused the increased generation of TNF-α.

IL-6 has both pro- and anti-inflammatory activities, but generally, elevated IL-6 levels correlate with a higher chance of mortality in human sepsis patients (180). Contrary to our expectations, plasma levels of IL-6 were low nine hours after stent implantation in the untreated CASP group. Compared to the quick release of TNF-α, IL-6 production is delayed. Traeger *et al*. (178) observed peak levels of IL-6 12 hours after CASP induction; therefore, our short observation period may have been insufficient to elicit a strong IL-6 response. Additionally, among DIBI treated groups, there was a trend of increased expression of IL-6 as the dose of DIBI increased, with a significant increase observed after administration of the highest DIBI dose, (80 mg/kg i.p. + 80 mg/kg i.v.). Markel *et al*. (181) found that iron chelation by DFO increased IL-6 production, but not

TNF-α, in human fetal intestinal epithelial cells *in vitro.* Their rationale was that due to the capacity of bacteria to acquire iron from human cells, the presence of chelating agents may indicate there is a microbial invader, thereby initiating a proinflammatory response, specifically IL-6, which can go on to induce hepcidin synthesis.

The production of IL-12 and IFN-γ are closely interconnected. IL-12 is a immunoregulatory cytokine produced by antigen presenting cells and drives the differentiation of adaptive immune responses to a type 1 phenotype (182). Additionally, IL-12 induces IFN-γ production, a potent antimicrobial cytokine. IL-12 and IFN-γ have been found to be essential for the survival in mouse peritonitis models due to their antibacterial effector mechanisms (183). Deficiencies in IL-12 and IFN-γ have been found to increase susceptibility in the CASP model, due to a delay in immune responses without these cytokines (184). In our study, plasma levels of IFN-γ and IL-12 were negligible in untreated CASP animals. Ono *et al*. (185) measured IFN-γ, IL-12, and IL-10 levels in mice with mild and severe sepsis induced by CLP and found that IFN-γ and IL-12 levels in severe sepsis were significantly lower than those in mild sepsis at 6 and 12 hours after the procedure. Additionally, Zantl *et al*. (183) found that 3, 6, 12, and 24 hours after CASP surgery, systemic IFN-γ levels were undetectable. Ono *et al*. propose that low IL-12 and IFN-γ levels results could be due an imbalance of type 1 and type 2 cytokines, resulting from the general dysregulated immune response during sepsis. In line with this theory and consistent with reports from Ono *et al*., in untreated CASP animals the levels of IL-10, a type 2 cytokine, were significantly increased from SHAM levels. However, the levels of another type 2 cytokine, IL-4, were significantly reduced compared to SHAM animals. Upon administration of DIBI in CASP animals, there was a

trend of increased plasma levels of IFN-γ, IL-12, and IL-10 as the dose of DIBI increased. It appears that DIBI administration regained the balance between type 1 and type 2 cytokines. Additionally, IL-4 levels increased significantly from untreated CASP animals to levels similar to SHAM operated animals. It is unclear how DIBI restored the production of these protective cytokines and further experimentation must be done with cytokine measurements performed at multiple time points to determine the kinetics of cytokine production in our CASP model and better understand how DIBI is working.

IL-17A is another proinflammatory cytokine produced mainly by Th17 cells, but also innate cell populations such as neutrophils, and natural killer cells. IL-17A is important during early immune responses against extracellular bacteria with significantly increased levels reported as few as four hours after inoculation of bacteria in a murine sepsis model (186). In our study, CASP without treatment did not significantly increase IL-17A levels; however subsequent administration of DIBI (80 mg/kg i.p. + 80 mg/kg i.v.) caused a significant increase in plasma IL-17A levels compared to SHAM. The role of IL-17A during infection has been studied with local and systemic models with conflicting results on the consequences of IL-17A release in different disease models. During *Streptococcus pneumoniae* or *Klebsiella pneumoniae,* production of IL-17A protected mice through the rapid recruitment of neutrophils that aid bacterial clearance (187). Additionally, during *Escherichia coli* infection, depletion of IL-17A decreased neutrophil recruitment, resulting in impaired microbial clearance and increased bacterial burden (188). On the other hand, in a poly-bacterial model of sepsis induced by CLP, depletion of IL-17A led to a decrease in bacteremia and reduced production of systemic pro-inflammatory cytokines (189). Due to the pathological consequence of immune

hyper-activation in sepsis, reducing neutrophil recruitment by limiting IL-17A production is a beneficial outcome. Although our data was largely non-significant, there is a trend that IL-17A levels are reduced after administration of DIBI 80 mg/kg i.p., which was also the most successful dose in reducing leukocyte adherence. Since IL-17A can be induced by tissue damage, DIBI may reduce tissue damage through attenuating oxidative stress, and consequently IL-17A expression.

ICAM-1 is a adhesion molecule highly expressed on the surface of endothelial cells and is a key molecule mediating neutrophil migration and infiltration during sepsis (190). Blockage of ICAM-1 has been found to improve outcomes in CLP-induced sepsis models by attenuating injuries associated with immune cell infiltration, but still allowing efficient bacterial clearance (191). In our study, SHAM animals showed basal levels of soluble ICAM-1, which was expected because ICAM-1 is constitutively expressed on endothelial cells. Activation of endothelial cells can further upregulate ICAM-1 expression, consistent with our observations after CASP surgery. A significant increase in plasma ICAM-1 levels from SHAM was measured in all groups, except after administration of DIBI 40 mg/kg i.p. (Figure 33). DIBI administration did not reduce ICAM-1 expression, even in groups where leukocyte adherence was significantly reduced. This represents a disconnect between circulating (shed) ICAM-1 levels and leukocyte adherence. Although ICAM-1's role when present on endothelial cells is known, the pathological significance of soluble ICAM-1 is not yet elucidated. Therefore, the connection between soluble adhesion molecules relative to leukocyte adherence and migration is needed to understand the significance of our results.

Overall, the cytokine measurements obtained in our study had mixed consistencies with previous reports and additional experimentation is needed to determine why. We provided some theories with supporting documents to explain findings from specific cytokines. More generally, the main limitation of these findings that could provide an explanation for many of our findings is that the measurements were only performed at a single time point. Therefore, it is possible that when blood samples were taken, cytokine levels had already peaked and had decreased, resulting in the low levels of some cytokines in untreated CASP animals. Furthermore, DIBI administration could have changed the kinetics of cytokine production, delaying the peak, and resulting in the progressively higher levels observed in our findings. Additionally, as mentioned before, blood samples were not obtained for many untreated CASP animals that were too weak to make it through the entire procedure; therefore, cytokines measurements represent healthier animals. For these reasons, our cytokine measurements from this study should be taken with reservations as they may not depict the full picture.

4.5 Limitations and Future Directions

A few limitations can be identified in our study, starting with what the relevance of this data is? Since the majority of past anti-inflammatory sepsis treatments found to be successful in mouse models were not beneficial, or worsened outcomes in human trials, why would iron chelation be different? Human and mouse physiology is far from identical and a perfect model does not exist. However, animal models are necessary to gain a preliminary understanding of how a drug may function to determine which should move on to human trials. After observing the effects of iron chelation in a controlled

model of hyper-inflammation induced by LPS, we moved on to the CASP model, which is the most clinically relevant model of sepsis available.

Another limitation with our model is that it focused on resolving the hyper-inflammatory conditions of sepsis, but sepsis can also present with an immunosuppressive state. These immune responses in septic patients are heterogenous and do not follow a specific timeline. Therefore, characterizing the condition of the patients' immune status is crucial for successful implementation of therapeutics.

Furthermore, an additional factor to consider when interpreting this data is that not all data are as substantiated as others. For instance, the IVM method is well practiced in our lab and the results obtained in these studies are comparable with past experiments. In contrast, the data collected from the microbiome analysis should be regarded as a pilot experiment since it was the first time this method was used in our lab, and all the data is from one run. Until these results are confirmed with additional experiments, the data should still be considered as preliminary.

The possibility of experimenter bias represents another limitation of this study. The same experimenter performed all data collection, video analysis, and quantification of results. Although measures were taken to minimize sources of bias where possible, blinding all analyses and eliminating all sources of bias was not possible in this study. To reduce bias, videos were analyzed in a blinded fashion and each video was analyzed in the exact same way. Despite analyzing videos in a blinded fashion, since they were recorded by the same experimenter analyzing them, they could sometimes be recognized as belonging to a certain treatment group. To overcome this, six videos were obtained for

each parameter producing six unique values which were averaged to reduce the impact of possible bias.

In this study we reasoned that reducing levels of free iron is a useful therapeutic approach because it reduces levels of ROS production contributing to oxidative stress, thereby attenuating the overall pro-inflammatory environment contributing to sepsis pathologies. However, iron and ROS play an important role in regulating immune cell function and fighting pathogens during infection. Since this study was conducted over a short time frame we cannot conclude that the effects that we identified as beneficial would actually improve the long-term survival of mice. To overcome this, we already have plans to perform survival studies with this model to determine if early administration of iron chelators can improve the long-term survival of septic mice by resolving hyper-inflammation. Additionally, intestinal samples were recovered from each mouse in this study for histologic analysis, giving us the ability to visualize pathologic changes between groups and insight into whether the beneficial effects we observed protected mice at the cellular level.

4.6 Conclusions

The present study investigated the effects of iron chelation by a novel iron chelator, DIBI, *in vitro* and in two acute models of sepsis *in vivo*. Due to iron's participation in catalyzing harmful ROS generating reactions, we reasoned that by removing excess iron, ROS production would be reduced. In our *in vitro* assays we found this to be true in macrophages and neutrophils, two main players in innate immune responses. Translating these results to *in vivo* models, since ROS is associated with

excessive immune stimulation, we expected that reducing its generation with DIBI would decrease immune hyper-activation in acute models of sepsis characterized by excessive pro-inflammatory responses. In the LPS-induced endotoxemia model, DIBI administration reduced excessive immune activation measured by interactions between leukocytes and endothelial cells in the intestinal microcirculation. DIBI also preserved the microcirculatory perfusion in the intestinal layers, which was significantly impacted by LPS challenge. Similar anti-inflammatory effects by DIBI were observed in the CASP model, but unexpectedly, an additional i.v. dose of DIBI seemed to eliminate some of the anti-inflammatory effects of lower doses of DIBI, according to the parameters we observed. However, these results could be explained after the bacterial species colonizing the peritoneal cavity were identified by microbiome sequencing. Overall, this study has provided evidence that iron chelation can play a role in modulating innate immune responses during sepsis, and possibly improve patient outcomes. In addition, iron chelators may have a role in restoring the efficacy of antibiotics, which is particularly exciting during a time where antibiotic resistance is a major concern for patients and healthcare professionals.

REFERENCES

1. G. S. Martin. Sepsis, severe sepsis and septic shock: changes in incidence, pathogens and outcomes. *Expert Rev. Anti. Infect. Ther.* 10**,** 701–706 (2012).

2. L. Epstein, R. Dantes, S. Magill, and A. Fiore. Varying estimates of sepsis mortality using death certificates and administrative codes — United States, 1999–2014. *MMWR. Morb. Mortal. Wkly. Rep.* 65**,** 342–345 (2016).

3. T. Navaneelan, S. Alam, P. A. Peters, and O. Phillips. Deaths involving sepsis in Canada. *Health at a Glance. Stats Canada*. (2016).

4. T. Lagu, M. B. Rothberg, M.-S. Shieh, P. S. Pekow, J. S. Steingrub, and P. K. Lindenauer. Hospitalizations, costs, and outcomes of severe sepsis in the United States 2003 to 2007. *Crit. Care Med.* 40**,** 754–761 (2012).

5. C. M. Torio, and B. J. Moore. National Inpatient Hospital Costs: The most expensive conditions by payer, 2011. HCUP Statistical Breif #160. *Agency for Healthcare Research and Quality, Rockville, MD.* 1-12 (2016).

6. C. S. Deutschman, and K. J. Tracey. Sepsis: Current dogma and new perspectives. *Immunity* 40**,** 463–475 (2014).

7. K. M. DeMerle, S. C. Royer, M. E. Mikkelsen, and H. C. Prescott. Readmissions for recurrent sepsis. *Crit. Care Med.* 45**,** 1702–1708 (2017).

8. S. Geroulanos, and E. T. Douka. Historical perspective of the word "sepsis" *Intensive Care Med* 32**,** 2077 (2006).

9. K. Yuki, and N. Murakami. Sepsis pathophysiology and anesthetic consideration. *Cardiovasc. Hematol. Disord. Drug Targets* 15**,** 57–69 (2015).

10. A. Suarez De La Rica, F. Gilsanz, and E. Maseda. Epidemiologic trends of sepsis in western countries. *Ann. Transl. Med.* 4**,** 325-331 (2016).

11. R. C. Bone, W. J. Sibbald, and C. L. Sprung. The ACCP-SCCM consensus conference on sepsis and organ failure. *Chest* 101**,** 1481–1483 (1992).

12. M. Singer, C. S. Deutschman, C. W. Seymour, M. Shankar-Hari, D. Annane, M. Bauer, R. Bellomo, G. R. Bernard, J.-D. Chiche, C. M. Coopersmith, R. S. Hotchkiss, M. M. Levy, J. C. Marshall, G. S. Martin, S. M. Opal, G. D. Rubenfeld, T. van der Poll, J.-L. Vincent, and D. C. Angus. The Third International Consensus Definitions for Sepsis and Septic Shock (Sepsis-3). *JAMA* 315**,** 801–810 (2016).

13. M. M. Levy, M. P. Fink, J. C. Marshall, E. Abraham, D. Angus, D. Cook, J. Cohen, S. M. Opal, J.-L. Vincent, and G. Ramsay. 2001 SCCM/ESICM/ACCP/ATS/SIS International Sepsis Definitions Conference. *Crit. Care Med.* 31**,** 1250–1256 (2003).

14. J.-L. Vincent, R. Moreno, J. Takala, S. Willatts, A. De Mendonça, H. Bruining, C. K. Reinhart, P. M. Suter, and L. G. Thijs. The SOFA (Sepsis-related Organ Failure Assessment) score to describe organ dysfunction/failure. *Intensive Care Med.* 22**,** 707–710 (1996).

15. J. L. Vincent, A. de Mendonça, F. Cantraine, R. Moreno, J. Takala, P. M. Suter, C. L. Sprung, F. Colardyn, and S. Blecher. Use of the SOFA score to assess the incidence of organ dysfunction/failure in intensive care units: results of a multicenter, prospective study. Working group on "sepsis-related problems" of the European Society of Intensive Care Medicine. *Crit. Care Med.* 26**,** 1793–1800 (1998).

16. A. Kumar, D. Roberts, K. E. Wood, B. Light, J. E. Parrillo, S. Sharma, R. Suppes, D. Feinstein, S. Zanotti, L. Taiberg, D. Gurka, A. Kumar, and M. Cheang. Duration of hypotension before initiation of effective antimicrobial therapy is the critical determinant of survival in human septic shock. *Crit. Care Med.* 34**,** 1589–1596 (2006).

17. C. W. Seymour, V. X. Liu, T. J. Iwashyna, F. M. Brunkhorst, T. D. Rea, A. Scherag, G. Rubenfeld, J. M. Kahn, M. Shankar-Hari, M. Singer, C. S. Deutschman, G. J. Escobar, and D. C. Angus. Assessment of clinical criteria for sepsis. *JAMA* 315**,** 762-774 (2016).

18. E. K. Stevenson, A. R. Rubenstein, G. T. Radin, R. S. Wiener, and A. J. Walkey. Two decades of mortality trends among patients with severe sepsis: a comparative meta-analysis. *Crit. Care Med.* 42**,** 625–631 (2014).

19. C. W. Seymour, F. Gesten, H. C. Prescott, M. E. Friedrich, T. J. Iwashyna, G. S. Phillips, S. Lemeshow, T. Osborn, K. M. Terry, and M. M. Levy. Time to treatment and mortality during mandated emergency care for sepsis. *N. Engl. J. Med.* 376**,** 2235–2244 (2017).

20. J. Cohen. The immunopathogenesis of sepsis. *Nature* 420**,** 885–891 (2002).

21. R. R. Ehrman, A. N. Sullivan, M. J. Favot, R. L. Sherwin, C. A. Reynolds, A. Abidov, and P. D. Levy. Pathophysiology, echocardiographic evaluation, biomarker findings, and prognostic implications of septic cardiomyopathy: a review of the literature. *Crit. Care* 22**,** 112-126 (2018).

22. S. C. Cheng, B. P. Scicluna, R. J. W. Arts, M. S. Gresnigt, E. Lachmandas, E. J. Giamarellos-Bourboulis, M. Kox, G. R. Manjeri, J. A. L. Wagenaars, O. L. Cremer, J. Leentjens, A. J. Van Der Meer, F. L. Van De Veerdonk, M. J. Bonten, M. J. Schultz, P. H. G. M. Willems, P. Pickkers, L. A. B. Joosten, T. Van Der Poll, and M. G. Netea. Broad defects in the energy metabolism of leukocytes underlie immunoparalysis in sepsis. *Nat. Immunol.* 17, 406-413 (2016).

23. A. Linnér. Clinical and pathophysiological aspects of sepsis. *Karolinska Institute, Stockholm, Sweden.* (2014).

24. M. Gatt. The role of the gut in sepsis. *Surg.* 33**,** 534–541 (2015).

25. J. S. Boomer, J. M. Green, and R. S. Hotchkiss. The changing immune system in sepsis: is individualized immuno-modulatory therapy the answer? *Virulence* 5**,** 45–56 (2014).

26. Y.-M. Yao, Y.-Y. Luan, Q.-H. Zhang, and Z.-Y. Sheng. Pathophysiological aspects of sepsis: An overview. *Humana Press, New York, NY.* 5–15 (2015).

27. K. N. Iskander, M. F. Osuchowski, D. J. Stearns-Kurosawa, S. Kurosawa, D. Stepien, C. Valentine, and D. G. Remick. Sepsis: Multiple abnormalities, heterogeneous responses, and evolving understanding. *Physiol. Rev.* 93**,** 1247–1288 (2013).

28. R. S. Hotchkiss, and I. E. Karl. The pathophysiology and treatment of sepsis. *N. Engl. J. Med.* 348**,** 138–150 (2003).

29. P. A. Danai, M. Moss, D. M. Mannino, and G. S. Martin. The epidemiology of sepsis in patients with malignancy. *Chest* 129**,** 1432–1440 (2006).

30. M. A. Kinnebrew, and E. G. Pamer. Innate immune signaling in defense against intestinal microbes. *Immunol. Rev.* 245**,** 113–131 (2012).

31. E. Christaki, P. Anyfanti, and S. M. Opal. Immunomodulatory therapy for sepsis: an update. *Expert Rev. Anti. Infect. Ther.* 9**,** 1013–1033 (2011).

32. A. W. Girotti. Lipid hydroperoxide generation, turnover, and effector action in biological systems. *J. Lipid Res.* 39**,** 1529–1542 (1998).

33. H. F. Galley. Oxidative stress and mitochondrial dysfunction in sepsis. *Br. J. Anaesth.* 107**,** 57–64 (2011).

34. K. Brown, S. Brain, J. Pearson, J. Edgeworth, S. Lewis, and D. Treacher. Neutrophils in development of multiple organ failure in sepsis. *Lancet* 368**,** 157–169 (2006).

35. J. A. Smith. Neutrophils, host defense, and inflammation: a double-edged sword. *J. Leukoc. Biol.* 56**,** 672–686 (1994).

36. W. A. Muller. How endothelial cells regulate transmigration of leukocytes in the inflammatory response. *Am. J. Pathol.* 184**,** 886–896 (2014).

37. H. F. Langer, and T. Chavakis. Leukocyte-endothelial interactions in inflammation. *J. Cell. Mol. Med.* 13**,** 1211–1220 (2009).

38. R. P. Mcever, R. D. Cummings, and W. K. Warren. Perspectives series: Cell adhesion in vascular biology role of PSGL-1 binding to selectins in leukocyte recruitment. *J. Clin. Invest* 100**,** 485–492 (1997).

39. J. C. Brazil, and C. A. Parkos. Pathobiology of neutrophil-epithelial interactions. *Immunol. Rev.* 273**,** 94–111 (2016).

40. N. Hogg, R. Henderson, B. Leitinger, A. McDowall, J. Porter, and P. Stanley. Mechanisms contributing to the activity of integrins on leukocytes. *Immunol. Rev.* 186**,** 164–171 (2002).

41. A. Basit, J. Reutershan, M. A. Morris, M. Solga, C. E. Rose, and K. Ley. ICAM-1 and LFA-1 play critical roles in LPS-induced neutrophil recruitment into the alveolar space. *AJP Lung Cell. Mol. Physiol.* 291**,** 200–207 (2006).

42. M. J. Elices, L. Osborn, Y. Takada, C. Crouse, S. Luhowskyj, M. E. Hemler, and R. R. Lobb. VCAM-1 on activated endothelium interacts with the leukocyte integrin VLA-4 at a site distinct from the VLA-4/fibronectin binding site. *Cell* 60**,** 577–584 (1990).

43. W. A. Muller. Mechanisms of leukocyte transendothelial migration. *Annu. Rev. Pathol.* 6**,** 323–344 (2011).

44. T. Chavakis, T. Keiper, R. Matz-Westphal, K. Hersemeyer, U. J. Sachs, P. P. Nawroth, K. T. Preissner, and S. Santoso. The junctional adhesion molecule-C promotes neutrophil transendothelial migration in vitro and in vivo. *J. Biol. Chem.* 279**,** 55602–55608 (2004).

45. T. Thorburn, M. Aali, and C. Lehmann. Immune response to systemic inflammation in the intestinal microcirculation. *Front. Biosci. (Landmark Ed.)* 23**,** 782–795 (2018).

46. J. Zhou, M. Soltow, K. Zimmermann, D. Pavlovic, B. Johnston, and C. Lehmann. Experimental TLR4 inhibition improves intestinal microcirculation in endotoxemic rats. *Microvasc. Res.* 101**,** 33–37 (2015).

47. Y.C. Yeh, M.J. Wang, C.P. Lin, S.Z. Fan, J.C. Tsai, W.Z. Sun, and W.J. Ko. Enoxaparin sodium prevents intestinal microcirculatory dysfunction in endotoxemic rats. *Crit. Care* 16**,** 59-69 (2012).

48. K. Tanaka, Y. Koike, T. Shimura, M. Okigami, S. Ide, Y. Toiyama, Y. Okugawa, Y. Inoue, T. Araki, K. Uchida, Y. Mohri, A. Mizoguchi, and M. Kusunoki. In vivo characterization of neutrophil extracellular traps in various organs of a murine sepsis model. *PLoS One* 9**,** 1-14 (2014).

49. Y. Sakr, M. J. Dubois, D. De Backer, J. Creteur, and J. L. Vincent. Persistent microcirculatory alterations are associated with organ failure and death in patients with septic shock. *Crit Care Med* 32**,** 1825–1831 (2004).

50. D. De Backer, J. Creteur, J.C. Preiser, M.J. Dubois, and J.L. Vincent. Microvascular blood flow is altered in patients with sepsis. *Am. J. Respir. Crit. Care Med.* 166**,** 98–104 (2002).

51. S. Trzeciak, J. V. McCoy, R. Phillip Dellinger, R. C. Arnold, M. Rizzuto, N. L. Abate, N. I. Shapiro, J. E. Parrillo, S. M. Hollenberg, and on behalf of the M. A. in R. and S. (MARS) investigators. Early increases in microcirculatory perfusion during protocol-directed resuscitation are associated with reduced multi-organ failure at 24 h in patients with sepsis. *Intensive Care Med.* 34**,** 2210–2217 (2008).

52. T. Takiishi, C. I. M. Fenero, and N. O. S. Câmara. Intestinal barrier and gut microbiota: Shaping our immune responses throughout life. *Tissue Barriers* 5**,** 1-12 (2017).

53. R. Mittal, and C. M. Coopersmith. Redefining the gut as the motor of critical illness. *Trends Mol. Med.* 20**,** 214–223 (2014).

54. E. Tomasello, and S. Bedoui. Intestinal innate immune cells in gut homeostasis and immunosurveillance. *Immunol. Cell Biol.* 91**,** 201–203 (2013).

55. E. A. Deitch. Gut-origin sepsis: evolution of a concept. *Surgeon* 10**,** 350–356 (2012).

56. P. R. de Jong, J. M. González-Navajas, and N. J. G. Jansen. The digestive tract as the origin of systemic inflammation. *Crit. Care* 20**,** 279-291 (2016).

57. C. Lehmann, N. Sharawi, N. Al-Banna, N. Corbett, J. W. Kuethe, and C. C. Caldwell. Novel approaches to the development of anti-sepsis drugs. *Expert Opin. Drug Discov.* 441**,** 1–9 (2014).

58. P. A. Ward. New approaches to the study of sepsis. *EMBO Mol. Med.* 4**,** 1234–1243 (2012).

59. C. P. Hornik, D. K. Benjamin, K. C. Becker, D. K. Benjamin, J. Li, R. H. Clark, M. Cohen-Wolkowiez, and P. B. Smith. Use of the complete blood cell count in early-onset neonatal sepsis. *Pediatr. Infect. Dis. J.* 31**,** 799–802 (2012).

60. C. Meisel, J. C. Schefold, R. Pschowski, T. Baumann, K. Hetzger, J. Gregor, S. Weber-Carstens, D. Hasper, D. Keh, H. Zuckermann, P. Reinke, and H.-D. Volk. Granulocyte–macrophage colony-stimulating factor to reverse sepsis-associated immunosuppression. *Am. J. Respir. Crit. Care Med.* 180**,** 640–648 (2009).

61. B. M. Arneth, M. Ragaller, K. Hommel, O. Tiebel, M. Menschikowski, and G. Siegert. Novel parameters of extended complete blood cell count under fluorescence flow cytometry in patients with sepsis. *J. Clin. Lab. Anal.* 28**,** 130–135 (2014).

62. D. M. Frazer, and G. J. Anderson. The orchestration of body iron intake: how and where do enterocytes receive their cues? *Blood Cells, Mol. Dis.* 30**,** 288–297 (2003).

63. A. T. McKie, P. Marciani, A. Rolfs, K. Brennan, K. Wehr, D. Barrow, S. Miret, A. Bomford, T. J. Peters, F. Farzaneh, M. A. Hediger, M. W. Hentze, and R. J. Simpson. A novel duodenal iron-regulated transporter, IREG1, implicated in the basolateral transfer of iron to the circulation. *Mol. Cell* 5**,** 299–309 (2000).

64. J. E. Cassat, and E. P. Skaar. Iron in infection and immunity. *Cell Host Microbe* 13**,** 509–519 (2013).

65. J. Bullen, E. Griffiths, H. Rogers, and G. Ward. Sepsis: the critical role of iron. *Microbes Infect* 2**,** 409–415 (2000).

66. G. Papanikolaou, and K. Pantopoulos. Iron metabolism and toxicity. *Toxicol. Appl. Pharmacol.* 202**,** 199–211 (2005).

67. G. Weiss. Iron metabolism in the anemia of chronic disease. *Biochim. Biophys. Acta - Gen. Subj.* 1790**,** 682–693 (2009).

68. R. E. Fleming. Iron and inflammation: Cross-talk between pathways regulating hepcidin. *J. Mol. Med.* 86**,** 491–494 (2008).

69. M. K. Lawson, M. Valko, M. T. D. Cronin, and K. Jomová. Chelators in iron and copper toxicity. *Curr. Pharmacol. Reports* 271–280 (2016).

70. M. Franchini. Hereditary iron overload: Update on pathophysiology, diagnosis, and treatment. *Am. J. Hematol.* 81**,** 202–209 (2006).

71. R. E. Fleming, and P. Ponka. Iron overload in human disease. *N. Engl. J. Med.* 366**,** 348–359 (2012).

72. E. Nemeth, S. Rivera, V. Gabayan, C. Keller, S. Taudorf, B. K. Pedersen, and T. Ganz. IL-6 mediates hypoferremia of inflammation by inducing the synthesis of the iron regulatory hormone hepcidin. *J. Clin. Invest.* 113**,** 1271–1276 (2004).

73. M. Wessling-Resnick. Iron homeostasis and the inflammatory response. *Annu. Rev. Nutr.* 30**,** 105–122 (2010).

74. V. I. Lushchak. Free radicals, reactive oxygen species, oxidative stress and its classification. *Chem. Biol. Interact.* 224**,** 164–175 (2014).

75. B. Commoner, J. Townsend, and G. E. Pake. Free radicals in biological materials. *Nature* 174**,** 689–691 (1954).

76. K. Hensley, K. A. Robinson, S. P. Gabbita, S. Salsman, and R. A. Floyd. Reactive oxygen species, cell signaling, and cell injury. *Free Radic. Biol. Med.* 28**,** 1456–1462 (2000).

77. V. P. Skulachev. Mitochondria-targeted antioxidants as promising drugs for treatment of age-related brain diseases. *J. Alzheimer's Dis.* 28**,** 283–289 (2012).

78. A. J. Meyer, T. Brach, L. Marty, S. Kreye, N. Rouhier, J.-P. Jacquot, and R. Hell. Redox-sensitive GFP in *Arabidopsis thaliana* is a quantitative biosensor for the redox potential of the cellular glutathione redox buffer. *Plant J.* 52**,** 973–986 (2007).

79. G. T. Nguyen, E. R. Green, and J. Mecsas. Neutrophils to the ROScue: Mechanisms of NADPH oxidase activation and bacterial resistance. *Front. Cell. Infect. Microbiol.* 7**,** 373-397 (2017).

80. S. J. Klebanoff. Oxygen-dependent microbicidal mechanisms. *Encyclopedia of Immunology* 2, 1713–1718 (1998).

81. B. M. Babior. Oxygen-dependent microbial killing by phagocytes. *N. Engl. J. Med.* 298**,** 659–668 (1978).

82. I. Schimke, N. Richter, H. Wauer, U. Rohr, A.-S. Petersson, A. Wennmalm, H. Kuppe, and W. J. Kox. High and low response in relation to nitric oxide formation but not to lipid peroxidation in patients with sepsis. *Crit. Care Med.* 31**,** 65–72 (2003).

83. V. I. Lushchak. Glutathione homeostasis and functions: potential targets for medical interventions. *J. Amino Acids* 2012**,** 1-26 (2012).

84. C. S. Ceron, G. T. do Vale, J. A. Simplicio, S. T. Ricci, B. S. De Martinis, A. de Freitas, and C. R. Tirapelli. Chronic ethanol consumption increases vascular oxidative stress and the mortality induced by sub-lethal sepsis: Potential role of iNOS. *Eur. J. Pharmacol.* 825**,** 39–47 (2018).

85. D. Bar-Or, M. M. Carrick, C. W. Mains, L. T. Rael, D. Slone, and E. N. Brody. Sepsis, oxidative stress, and hypoxia: Are there clues to better treatment? *Redox Rep.* 20**,** 193–197 (2015).

86. C. Quoilin, A. Mouithys-Mickalad, S. Lécart, M.-P. Fontaine-Aupart, and M. Hoebeke. Evidence of oxidative stress and mitochondrial respiratory chain dysfunction in an in vitro model of sepsis-induced kidney injury. *Biochim. Biophys. Acta - Bioenerg.* 1837**,** 1790–1800 (2014).

87. C. Mylonas, and D. Kouretas. Lipid peroxidation and tissue damage. *In Vivo* 13**,** 295–309 (1999).

88. F. El Chaer, N. G. Holtzman, M. R. Baer, A. B. Zimrin, and J. Y. Law. Sickle Cell Disease complicated by iron overload: An under-recognized risk factor for V*ibrio vulnificus* infection. *Acta Haematol.* 139**,** 199–200 (2018).

89. H. K. Miller, L. Schwiesow, W. Au-Yeung, and V. Auerbuch. Hereditary hemochromatosis predisposes mice to *Yersinia pseudotuberculosis* infection even in the absence of the type III secretion system. *Front. Cell. Infect. Microbiol.* 6**,** 69-81 (2016).

90. L. E. Quenee, T. M. Hermanas, N. Ciletti, H. Louvel, N. C. Miller, D. Elli, B. Blaylock, A. Mitchell, J. Schroeder, T. Krausz, J. Kanabrocki, and O. Schneewind. Hereditary hemochromatosis restores the virulence of plague vaccine strains. *J. Infect. Dis.* 206**,** 1050–1058 (2012).

91. M. Nairz, A. Schroll, D. Haschka, S. Dichtl, P. Tymoszuk, E. Demetz, P. Moser, H. Haas, F. C. Fang, I. Theurl, and G. Weiss. Genetic and dietary iron overload differentially affect the course of *Salmonella typhimurium* Infection. *Front. Cell. Infect. Microbiol.* 7**,** 110-123 (2017).

92. R. J. Bergeron, N. Bharti, J. S. McManis, and J. Wiegand. Metabolically programmed iron chelators. *Bioorg. Med. Chem.* 23**,** 5954–5971 (2015).

93. N. Mobarra, M. Shanaki, H. Ehteram, H. Nasiri, M. Sahmani, M. Saeidi, M. Goudarzi, H. Pourkarim, and M. Azad. A review on iron chelators in treatment of iron overload syndromes. *Int. J. Hematol. stem cell Res.* 10**,** 239–247 (2016).

94. E. J. Neufeld. Update on iron chelators in thalassemia. *Hematology* 2010**,** 451–455 (2010).

95. M. R. Power Coombs, T. Grant, A. L. Greenshields, D. J. Arsenault, B. E. Holbein, and D. W. Hoskin. Inhibitory effect of iron withdrawal by chelation on the growth of human and murine mammary carcinoma and fibrosarcoma cells. *Exp. Mol. Pathol.* 99**,** 262–270 (2015).

96. S. Islam, S. Jarosch, J. Zhou, M. D. C. Parquet, J. T. Toguri, P. Colp, B. E. Holbein, and C. Lehmann. Anti-inflammatory and anti-bacterial effects of iron chelation in experimental sepsis. *J. Surg. Res.* 200**,** 266–273 (2015).

97. T. Thorburn, M. Aali, L. Kostek, C. LeTourneau-Paci, P. Colp, J. Zhou, B. Holbein, D. Hoskin, and C. Lehmann. Anti-inflammatory effects of a novel iron chelator, DIBI, in experimental sepsis. *Clin. Hemorheol. Microcirc.* 67**,** 241–250 (2017).

98. B. E. Holbein, and R. Mira de Orduña. Effect of trace iron levels and iron withdrawal by chelation on the growth of *Candida albicans* and *Candida vini*. *FEMS Microbiol. Lett.* 307**,** 19-24 (2010).

99. K. Wafa, C. Lehmann, L. Wagner, I. Drzymulski, A. Wegner, and D. Pavlovic. Desmopressin improves intestinal functional capillary density and decreases leukocyte activation in experimental endotoxemia. *Microvasc. Res.* 97**,** 98–104 (2015).

100. I. Burkovskiy, C. Lehmann, C. Jiang, and J. Zhou. Utilization of 3D printing for an intravital microscopy platform to study the intestinal microcirculation. *J. Microsc.* 1–3 (2016).

101. D. Pavlovic, H. Frieling, K.S. Lauer, V. H. Bac, J. Richter, M. Wendt, C. Lehmann, T. Usichenko, K. Meissner, and M. Gruendling. Thermostatic tissue platform for intravital microscopy: 'the hanging drop' model. *J. Microsc.* 224**,** 203–210 (2006).

102. A. M. Comeau, G. M. Douglas, and M. G. I. Langille. Microbiome helper: a custom and streamlined workflow for microbiome research. *mSystems* 2**,** 1-11 (2017).

103. D. Figueroa, M. Asaduzzaman, and F. Young. Real time monitoring and quantification of reactive oxygen species in breast cancer cell line MCF-7 by 2′,7′–dichlorofluorescin diacetate (DCFDA) assay. *J. Pharmacol. Toxicol. Methods* 94**,** 26–33 (2018).

104. V. G. Grivennikova, A. V. Kareyeva, and A. D. Vinogradov. Oxygen-dependence of mitochondrial ROS production as detected by Amplex Red assay. *Redox Biol.* 17**,** 192–199 (2018).

105. C. W. Lush, and P. R. Kvietys. Microvascular Dysfunction in Sepsis. *Microcirculation* 7**,** 83–101 (2000).

106. E. D. Crouser. Mitochondrial dysfunction in septic shock and multiple organ dysfunction syndrome. *Mitochondrion* 4**,** 729–741 (2004).

107. S. M. Opal, A. S. Cross, N. M. Kelly, J. C. Sadoff, M. W. Bodmer, J. E. Palardy, and G. H. Victor. Efficacy of a monoclonal antibody directed against tumor necrosis factor in protecting neutropenic rats from lethal infection with *Pseudomonas aeruginosa*. *J. Infect. Dis.* 161**,** 1148–1152 (1990).

108. T. Calandra, M. P. Glauser, J. Schellekens, and J. Verhoef. Treatment of Gram-negative septic shock with human IgG antibody to *Escherichia coli* J5: A prospective, double-blind, randomized trial. *J. Infect. Dis.* 158**,** 312–319 (1988).

109. B. D. Freeman, and C. Natanson. Anti-inflammatory therapies in sepsis and septic shock. *Expert Opin. Investig. Drugs* 9**,** 1651–1663 (2000).

110. A. M. Galvão, M. S. O. Wanderley, R. A. Silva, C. A. M. Filho, M. R. Melo-Junior, L. A. Silva, E. L. Streck, A. F. Dornelas de Andrade, M. B. Souza Maia, and C. M. M. Barbosa de Castro. Intratracheal co-administration of antioxidants and ceftriaxone reduces pulmonary injury and mortality rate in an experimental model of sepsis. *Respirology* 19**,** 1080–1087 (2014).

111. L. A. Pham-Huy, H. He, and C. Pham-Huy. Free radicals, antioxidants in disease and health. *Int. J. Biomed. Sci.* 4**,** 89–96 (2008).

112. E. Messaris, P. T. Antonakis, N. Memos, E. Chatzigianni, E. Leandros, and M. M. Konstadoulakis. Deferoxamine administration in septic animals: improved survival and altered apoptotic gene expression. *Int. Immunopharmacol.* 4**,** 455–459 (2004).

113. C. Ritter, M. E. Andrades, A. Reinke, S. Menna-Barreto, J. C. F. Moreira, and F. Dal-Pizzol. Treatment with N-acetylcysteine plus deferoxamine protects rats against oxidative stress and improves survival in sepsis. *Crit. Care Med.* 32**,** 342–349 (2004).

114. E. Vlachodimitropoulou Koumoutsea, M. Garbowski, and J. Porter. Synergistic intracellular iron chelation combinations: mechanisms and conditions for optimizing iron mobilization. *Br. J. Haematol.* 170**,** 874–883 (2015).

115. G. Link, A. M. Konijn, W. Breuer, Z. I. Cabantchik, and C. Hershko. Exploring the 'iron shuttle' hypothesis in chelation therapy: Effects of combined deferoxamine and deferiprone treatment in hypertransfused rats with labeled iron stores and in iron-loaded rat heart cells in culture. *J. Lab. Clin. Med.* 138**,** 130–138 (2001).

116. G. Li, Y. Liu, N. Tzeng, G. Cui, M. L. Block, B. Wilson, L. Qin, T. Wang, B. Liu, J. Liu, and J.-S. Hong. Protective effect of dextromethorphan against endotoxic shock in mice. *Biochem. Pharmacol.* 69**,** 233–240 (2005).

117. A. Warnatsch, T.-D. Tsourouktsoglou, N. Branzk, Q. Wang, S. Reincke, S. Herbst, M. Gutierrez, and V. Papayannopoulos. Reactive oxygen species localization programs inflammation to clear microbes of different size. *Immunity* 46**,** 421–432 (2017).

118. M. Saffarzadeh, C. Juenemann, M. A. Queisser, G. Lochnit, G. Barreto, S. P. Galuska, J. Lohmeyer, and K. T. Preissner. Neutrophil extracellular traps directly induce epithelial and endothelial cell death: A predominant role of histones. *PLoS One* 7**,** 1-14 (2012).

119. S. D. Kobayashi, J. M. Voyich, and F. R. Deleo. Regulation of the neutrophil-mediated inflammatory response to infection. *Microbes Infect.* 5, 1337-1344 (2003).

120. F. S. Mariano, A. P. Campanelli, F. H. Nociti Jr., R. O. Mattos-Graner, and R. B. Gonçalves. Antimicrobial peptides and nitric oxide production by neutrophils from periodontitis subjects. *Brazilian J. Med. Biol. Res.* 45**,** 1017–1024 (2012).

121. M. J. Kaplan, and M. Radic. Neutrophil extracellular traps: Double-edged swords of innate immunity. *J. Immunol.* 189**,** 2689-2895 (2012).

122. G. Kleveta, K. Borzęcka, M. Zdioruk, M. Czerkies, H. Kuberczyk, N. Sybirna, A. Sobota, and K. Kwiatkowska. LPS induces phosphorylation of actin-regulatory proteins leading to actin reassembly and macrophage motility. *J. Cell. Biochem.* 113**,** 80–92 (2012).

123. C. A. Parkos, C. Delp, M. A. Arnaout, and J. L. Madara. Neutrophil migration across a cultured intestinal epithelium. Dependence on a CD11b/CD18-mediated event and enhanced efficiency in physiological direction. *J. Clin. Invest.* 88**,** 1605–1612 (1991).

124. H. Bian, S. Gao, D. Zhang, Q. Zhao, F. Li, X. Li, S. Sun, S. Song, T. Li, Q. Zhu, W. Ren, C. Qin, and J. Qi. The E3 ubiquitin ligase MuRF2 attenuates LPS-induced macrophage activation by inhibiting production of inflammatory cytokines and migration. *FEBS Open Bio* 8**,** 234–243 (2018).

125. T. J. Koh, and L. A. DiPietro. Inflammation and wound healing: the role of the macrophage. *Expert Rev. Mol. Med.* 13**,** 23-37 (2011).

126. A. G. McBride, and G. C. Brown. Activated human neutrophils rapidly break down nitric oxide. *FEBS Lett.* 417**,** 231–234 (1997).

127. Y. Tu, L. Zhang, L. Tong, Y. Wang, S. Zhang, R. Wang, L. Li, and Z. Wang. EFhd2/swiprosin-1 regulates LPS-induced macrophage recruitment via enhancing actin polymerization and cell migration. *Int. Immunopharmacol.* 55**,** 263–271 (2018).

128. T. Tajima, T. Murata, K. Aritake, Y. Urade, H. Hirai, M. Nakamura, H. Ozaki, and M. Hori. Lipopolysaccharide induces macrophage migration via prostaglandin D(2) and prostaglandin E(2). *J. Pharmacol. Exp. Ther.* 326**,** 493–501 (2008).

129. L. A. DiPietro. Wound healing: the role of the macrophage and other immune cells. *Shock* 4**,** 233–240 (1995).

130. L. Kastl, S. W. Sauer, T. Ruppert, T. Beissbarth, M. S. Becker, D. Süss, P. H. Krammer, and K. Gülow. TNF-α mediates mitochondrial uncoupling and enhances ROS-dependent cell migration *via* NF-κB activation in liver cells. *FEBS Lett.* 588**,** 175–183 (2014).

131. D. G. Remick, and P. A. Ward. Evaluation of endotoxin models for the study of sepsis. *Shock* 24**,** 7–11 (2005).

132. C. Lehmann, M. Kianian, J. Zhou, I. Küster, R. Kuschnereit, S. Whynot, O. Hung, R. Shukla, B. Johnston, V. Cerny, D. Pavlovic, A. Spassov, and M. E. Kelly. Cannabinoid receptor 2 activation reduces intestinal leukocyte recruitment and systemic inflammatory mediator release in acute experimental sepsis. *Crit. Care* 16**,** 47-58 (2012).

133. J. Zhou, M. Schmidt, B. Johnston, F. Wilfart, S. Whynot, O. Hung, M. Murphy, V. Cerný, D. Pavlovic, and C. Lehmann. Experimental endotoxemia induces leukocyte adherence and plasma extravasation within the rat pial microcirculation. *Physiol. Res.* 60**,** 853–859 (2011).

134. N. Arora, S. Islam, K. Wafa, J. Zhou, J. T. Toguri, V. Cerny, and C. Lehmann. Evaluation of iris functional capillary density in experimental local and systemic inflammation. *J. Microsc.* 266**,** 55–59 (2017).

135. R. K. Thimmulappa, H. Lee, T. Rangasamy, S. P. Reddy, M. Yamamoto, T. W. Kensler, and S. Biswal. Nrf2 is a critical regulator of the innate immune response and survival during experimental sepsis. *J. Clin. Invest.* 116**,** 984–995 (2006).

136. M. Schieber, and N. S. Chandel. ROS Function in redox signaling and oxidative stress. *Curr. Biol.* 24**,** 453–462 (2014).

137. C. Ritter, A. A. da Cunha, I. C. Echer, M. Andrades, A. Reinke, N. Lucchiari, J. Rocha, E. L. Streck, S. Menna-Barreto, J. C. F. Moreira, and F. Dal-Pizzol. Effects of N-acetylcysteine plus deferoxamine in lipopolysaccharide-induced acute lung injury in the rat. *Crit. Care Med.* 34**,** 471–477 (2006).

138. J. Cermanova, Z. Kadova, E. Dolezelova, M. Zagorova, V. Safka, M. Hroch, T. Laho, M. Holeckova, J. Mokry, P. Kovarikova, J. Bures, M. Sterba, and S. Micuda. Deferoxamine but not dexrazoxane alleviates liver injury induced by endotoxemia in rats. *Shock* 42**,** 372–379 (2014).

139. H. Yu, X. Xu, X. Chen, T. Lu, P. Zhang, and X. Jing. Preparation and antibacterial effects of PVA-PVP hydrogels containing silver nanoparticles. *J. Appl. Polym. Sci.* 103**,** 125–133 (2007).

140. N. M. Matharu, L. M. Butler, G. E. Rainger, P. Gosling, R. K. Vohra, and G. B. Nash. Mechanisms of the anti-inflammatory effects of hydroxyethyl starch demonstrated in a flow-based model of neutrophil recruitment by endothelial cells. *Crit. Care Med.* 36**,** 1536–1542 (2008).

141. R. Hofbauer, D. Moser, S. Hornykewycz, M. Frass, and S. Kapiotis. Hydroxyethyl starch reduces the chemotaxis of white cells through endothelial cell monolayers. *Transfusion* 39**,** 289–294 (1999).

142. B. Nohé, T. Johannes, J. Reutershan, A. Rothmund, H. A. Haeberle, A. Ploppa, T. H. Schroeder, and H.-J. Dieterich. Synthetic colloids attenuate leukocyte-endothelial interactions by inhibition of integrin function. *Anesthesiology* 103**,** 759–767 (2005).

143. M. T. Handrigan, A. R. Burns, E. M. Donnachie, and R. A. Bowden. Hydroxyethyl starch inhibits neutrophil adhesion and transendothelial migration. *Shock* 24**,** 434–439 (2005).

144. J. L. Pascual, L. E. Ferri, P. Chaudhury, A. J. Seely, G. Campisi, B. Giannias, D. C. Evans, and N. V Christou. Hemorrhagic shock resuscitation with a low molecular weight starch reduces neutrophil-endothelial interactions and vessel leakage in vivo. *Surg. Infect. (Larchmt).* 2**,** 275-287 (2001).

145. E. Silva, S. M. Saraiva, S. P. Miguel, and I. J. Correia. PVP-coated silver nanoparticles showing antifungal improved activity against dermatophytes. *J. Nanoparticle Res.* 16**,** 2726 (2014).

146. M. Summa, D. Russo, I. Penna, N. Margaroli, I. S. Bayer, T. Bandiera, A. Athanassiou, and R. Bertorelli. A biocompatible sodium alginate/povidone iodine film enhances wound healing. *Eur. J. Pharm. Biopharm.* 122**,** 17–24 (2018).

147. E. A. Deitch. Animal models of sepsis and shock: a review and lessons learned. *Shock* 9**,** 1–11 (1998).

148. F. Zeni, B. Freeman, and C. Natanson. Anti-inflammatory therapies to treat sepsis and septic shock: a reassessment. *Crit. Care Med.* 25**,** 1095–1100 (1997).

149. G. Zanetti, D. Heumann, J. Gérain, J. Kohler, P. Abbet, C. Barras, R. Lucas, M. P. Glauser, and J. D. Baumgartner. Cytokine production after intravenous or peritoneal gram-negative bacterial challenge in mice. Comparative protective efficacy of antibodies to tumor necrosis factor-alpha and to lipopolysaccharide. *J. Immunol.* 148**,** 1890–1897 (1992).

150. G. Schabbauer. Polymicrobial sepsis models: CLP versus CASP. *Drug Discov. Today Dis. Model.* 9**,** 17–21 (2012).

151. S. Maier, T. Traeger, M. Entleutner, A. Westerholt, B. Kleist, N. Hüser, B. Holzmann, A. Stier, K. Pfeffer, and C.D. Heidecke. Cecal ligation and puncture versus colon ascendens stent peritonitis: two distinct animal models for polymicrobial sepsis. *Shock* 21**,** 505–511 (2004).

152. J. A. Buras, B. Holzmann, and M. Sitkovsky. Animal models of sepsis: setting the stage. *Nat. Rev. Drug Discov.* 4**,** 854–865 (2005).

153. C. Fuchs, E. Ladwig, J. Zhou, D. Pavlovic, K. Behrend, S. Whynot, O. Hung, M. Murphy, V. Cerny, and C. Lehmann. Argatroban administration reduces leukocyte adhesion and improves capillary perfusion within the intestinal microcirculation in experimental sepsis. *Thromb. Haemost.* 104**,** 1022–1028 (2010).

154. M. K. Lustig, V. H. Bac, D. Pavlovic, S. Maier, M. Gründling, O. Grisk, M. Wendt, C.-D. Heidecke, and C. Lehmann. Colon ascendens stent peritonitis--a model of sepsis adopted to the rat: physiological, microcirculatory and laboratory changes. *Shock* 28**,** 59–64 (2007).

155. M. J. Cunningham, and D. G. Nathan. New developments in iron chelators. *Curr. Opin. Hematol.* 12**,** 129–134 (2005).

156. T. H. Hassan, M. A. Badr, N. A. Karam, M. Zkaria, H. F. El Saadany, D. M. Abdel Rahman, D. A. Shahbah, S. M. Al Morshedy, M. Fathy, A. M. H. Esh, and A. M. Selim. Impact of iron deficiency anemia on the function of the immune system in children. *Medicine (Baltimore).* 95**,** 1-5 (2016).

157. H. M. Wexler. Bacteroides: the good, the bad, and the nitty-gritty. *Clin. Microbiol. Rev.* 20**,** 593–621 (2007).

158. K. A. Savage, M. del C. Parquet, D. S. Allan, R. J. Davidson, B. E. Holbein, E. A. Lilly, and P. L. Fidel. Iron restriction to clinical isolates of *Candida albicans* by the novel chelator DIBI inhibits growth and increases sensitivity to azoles *in vitro* and *in vivo* in a murine model of experimental vaginitis. *Antimicrob. Agents Chemother.* 17, 1-32 (2018).

159. I. Nakamura, K. Aoki, Y. Miura, T. Yamaguchi, and T. Matsumoto. Fatal sepsis caused by multidrug-resistant Bacteroides fragilis, harboring a cfiA gene and an upstream insertion sequence element, in Japan. *Anaerobe* 44**,** 36–39 (2017).

160. M. Garcia, P. Bouvet, F. Petitpas, C. Jayle, C. Legeay, J. Sautereau, A. Michaud, C. Burucoa, and C. Plouzeau. First case report of a human sepsis involving a recently identified anaerobic agent: *Bacteroides faecis*. *Anaerobe* 42**,** 74–77 (2016).

161. A. A. Medeiros. *Bacteroides Bacillemia*. *Arch. Surg.* 105**,** 819-820 (1972).

162. P. C. B. Turnbull. Bacillus. *Medical Microbiology. University of Texas Medical Branch at Galveston*. ISBN 978-0-9631172-1-2 (1996).

163. O. N. Ilinskaya, V. V Ulyanova, D. R. Yarullina, and I. G. Gataullin. Secretome of intestinal bacilli: A natural guard against pathologies. *Front. Microbiol.* 8**,** 1666-1681 (2017).

164. K. Hirabayashi, M. Shiohara, T. Suzuki, S. Saito, M. Tanaka, R. Yanagisawa, G. Tsuruta, T. Fukuyama, Y. Hidaka, Y. Nakazawa, T. Shimizu, K. Sakashita, and K. Koike. Critical illness polyneuropathy and myopathy caused by *Bacillus cereus* sepsis in acute lymphoblastic leukemia. *J. Pediatr. Hematol. Oncol.* 34**,** 110-113 (2012).

165. M. O. Musa, M. Al Douri, S. Khan, T. Shafi, A. Al Humaidh, and A. M. Al Rasheed. Fulminant septicaemic syndrome of *Bacillus cereus*: three case reports. *J. Infect.* 39**,** 154–156 (1999).

166. D. J. Cotton, V. J. Gill, D. J. Marshall, J. Gress, M. Thaler, and P. A. Pizzo. Clinical features and therapeutic interventions in 17 cases of *Bacillus bacteremia* in an immunosuppressed patient population. *J. Clin. Microbiol.* 25**,** 672–674 (1987).

167. A. M. Zawadzka, R. J. Abergel, R. Nichiporuk, U. N. Andersen, and K. N. Raymond. Siderophore-mediated iron acquisition systems in *Bacillus cereus*: Identification of receptors for anthrax virulence-associated petrobactin. *Biochemistry.* 48, 3645-3657 (2009).

168. Section 3: Current antibiotic resistance threats in the United States, by microorganism. *CDC*. (2013).

169. T. G. Simon, J. Bradley, A. Jones, and G. Carino. Massive intravascular hemolysis from *Clostridium perfringens* septicemia. *J. Intensive Care Med.* 29**,** 327–333 (2014).

170. S. E. Lowenkron, J. Waxner, P. Khullar, J. S. Ilowite, M. S. Niederman, and A. M. Fein. *Clostridium difficile* infection as a cause of severe sepsis. *Intensive Care Med.* 22**,** 990–994 (1996).

171. M. M. Awad, J. K. Cheung, J. E. Tan, A. G. McEwan, and J. I. Rood. Functional analysis of an feoB mutant in *Clostridium perfringens* strain 13. *Anaerobe* 41**,** 10–17 (2016).

172. F. B. Mayr, S. Yende, and D. C. Angus. Epidemiology of severe sepsis. *Virulence* 5**,** 4–11 (2014).

173. A. Khan, P. Singh, and A. Srivastava. Synthesis, nature and utility of universal iron chelator – Siderophore: A review. *Microbiol. Res.* 212–213**,** 103–111 (2018).

174. L. Ma, Y. Gao, and A. W. Maresso. *Escherichia coli* free radical-based killing mechanism driven by a unique combination of iron restriction and certain antibiotics. *J. Bacteriol.* 197**,** 3708–3719 (2015).

175. D. Rittirsch, M. A. Flierl, and P. A. Ward. Harmful molecular mechanisms in sepsis. *Nat. Rev. Immunol.* 8**,** 776–787 (2008).

176. G. Jusek, D. Reim, K. Tsujikawa, and B. Holzmann. Deficiency of the CGRP receptor component RAMP1 attenuates immunosuppression during the early phase of septic peritonitis. *Immunobiology* 217**,** 761–767 (2012).

177. K. Emmanuilidis, H. Weighardt, S. Maier, K. Gerauer, T. Fleischmann, X. X. Zheng, W. W. Hancock, B. Holzmann, and C. D. Heidecke. Critical role of Kupffer cell-derived IL-10 for host defense in septic peritonitis. *J. Immunol.* 167**,** 3919–3927 (2001).

178. T. Traeger, P. Koerner, W. Kessler, K. Cziupka, S. Diedrich, A. Busemann, C.-D. Heidecke, and S. Maier. Colon ascendens stent peritonitis (CASP)--a standardized model for polymicrobial abdominal sepsis. *J. Vis. Exp.* 46, 2299-2304 (2010).

179. K. Pfeffer. Biological functions of tumor necrosis factor cytokines and their receptors. *Cytokine Growth Factor Rev.* 14**,** 185–191 (2003).

180. A. Spittler, M. Razenberger, H. Kupper, M. Kaul, W. Hackl, G. Boltz-Nitulescu, R. Függer, and E. Roth. Relationship between interleukin-6 plasma concentration in patients with sepsis, monocyte phenotype, monocyte phagocytic properties, and cytokine production. *Clin. Infect. Dis.* 31**,** 1338–1342 (2000).

181. T. A. Markel, P. R. Crisostomo, M. Wang, C. M. Herring, T. Lahm, K. K. Meldrum, K. D. Lillemoe, F. J. Rescorla, and D. R. Meldrum. Iron chelation acutely stimulates fetal human intestinal cell production of IL-6 and VEGF while decreasing HGF: the roles of p38, ERK, and JNK MAPK signaling. *Am. J. Physiol. Gastrointest. Liver Physiol.* 292**,** 958-963 (2007).

182. T. Hamza, J. B. Barnett, and B. Li. Interleukin 12 a key immunoregulatory cytokine in infection applications. *Int. J. Mol. Sci.* 11**,** 789–806 (2010).

183. N. Zantl, A. Uebe, B. Neumann, H. Wagner, J. R. Siewert, B. Holzmann, C. D. Heidecke, and K. Pfeffer. Essential role of gamma interferon in survival of colon ascendens stent peritonitis, a novel murine model of abdominal sepsis. *Infect. Immun.* 66**,** 2300–2309 (1998).

184. M. Entleutner, T. Traeger, A. Westerholt, B. Holzmann, A. Stier, K. Pfeffer, S. Maier, and C.-D. Heidecke. Impact of interleukin-12, oxidative burst, and iNOS on the survival of murine fecal peritonitis. *Int. J. Colorectal Dis.* 21**,** 64–70 (2006).

185. S. Ono, C. Ueno, S. Aosasa, H. Tsujimoto, S. Seki, and H. Mochizuki. Severe sepsis induces deficient interferon-gamma and interleukin-12 production, but interleukin-12 therapy improves survival in peritonitis. *Am. J. Surg.* 182**,** 491–497 (2001).

186. D. L. W. Chong, R. J. Ingram, D. E. Lowther, R. Muir, S. Sriskandan, and D. M. Altmann. The nature of innate and adaptive interleukin-17A responses in sham or bacterial inoculation. *Immunology* 136**,** 325–333 (2012).

187. Z. Zhang, T. B. Clarke, and J. N. Weiser. Cellular effectors mediating Th17-dependent clearance of pneumococcal colonization in mice. *J. Clin. Invest.* 119**,** 1899–1909 (2009).

188. K. Shibata, H. Yamada, H. Hara, K. Kishihara, and Y. Yoshikai. Resident Vdelta1+ gammadelta T cells control early infiltration of neutrophils after *Escherichia coli* infection via IL-17 production. *J. Immunol.* 178**,** 4466–4472 (2007).

189. M. A. Flierl, D. Rittirsch, H. Gao, L. M. Hoesel, B. A. Nadeau, D. E. Day, F. S. Zetoune, J. V. Sarma, M. S. Huber-Lang, J. L. M. Ferrara, and P. A. Ward. Adverse functions of IL-17A in experimental sepsis. *FASEB J.* 22**,** 2198–2205 (2008).

190. H. F. Langer, and T. Chavakis. Leukocyte – endothelial interactions in inflammation. *J. Cell. Mol. Med* 13**,** 1211–1220 (2009).

191. Y. Zhao, W. Yi, X. Wan, J. Wang, T. Tao, J. Li, J. Wang, and X. Deng. Blockade of ICAM-1 improves the outcome of polymicrobial sepsis via modulating neutrophil migration and reversing immunosuppression. *Mediators Inflamm.* 2014**,** 1-10 (2014).